Critical Thinking in Aquifer Test Interpretation

Interpretation of pumping tests in aquifers with linear boundaries

Christopher J. Neville S.S. Papadopulos & Associates, Inc. Last update: April 28, 2025

- 1. Notes on the interpretation of pumping tests in aquifers with linear boundaries
- 2. Additional readings
 - Ferris et al. (1962) [except]
 - van der Kamp and Maathuis (2012)
 - Rafini, Chesnaux and Ferroud (2017)

Interpretation of pumping tests in aquifers with linear boundaries

Christopher J. Neville S.S. Papadopulos & Associates, Inc.

Last update: April 28, 2025

Overview

Although all aquifers are bounded, when we interpret the results of short-term pumping tests, we frequently ignore the presence of boundaries. In many cases of practical significance, neglecting the boundaries may be highly restrictive. It may limit our analysis to the consideration of drawdown from only the first few minutes or hours of pumping. Furthermore, such idealized analyses do not provide much insight into the effects that boundaries may have on the response to pumping.

These notes have been prepared to provide an introduction to the interpretation of pumping tests where boundaries are relatively close to the pumping well. To illustrate some basic concepts, we will consider three idealized cases that are amenable to treatment with an analytical approach:

- Aquifers with one linear constant-head boundary;
- Aguifers with one linear impermeable boundary; and
- Aquifers with two linear impermeable boundaries (channel aquifers).

We recognize from the outset that there may be cases in which complex boundary conditions may not be amenable to such simple analyses. Where boundaries and additional sources/sinks are located relatively close to the pumping well, the analyst may have to develop a numerical model to interpret the drawdown data.

Outline

- 1. Aquifers with a single linear constant-head boundary
- 2. Aquifers with a single impermeable boundary
- 3. Generalization of the results for a single linear boundary
- 4. Aquifers with two linear impermeable boundaries (channel aquifers)
- 5. Case study: Estevan, Saskatchewan
- 6. Key points
- 7. References

1. Aquifers with a single linear constant-head boundary

As with all pumping tests, the Theis model is the starting point for the interpretation of tests conducted in bounded aquifers. The Theis problem is linear; neither the coefficients appearing in the governing equation, nor the boundary conditions depend upon the drawdown. The property of linearity has important implications for the interpretation of pumping test data. For linear problems, we can derive solutions to complex problems by adding together solutions for simpler cases, a procedure referred to as *superposition*. Pumping tests conducted near a linear boundary (for example, a stream or a fault) can be interpreted by superposing Theis solutions in space, using what are referred to as *image wells*.

For the case of a linear constant-head boundary, the drawdown along the boundary is zero. As shown in Figure 1, a linear boundary with zero drawdown is simulated with an imaginary well placed an equal distance from the boundary, pumping at a rate equal in magnitude, but opposite in sign, to the actual well.

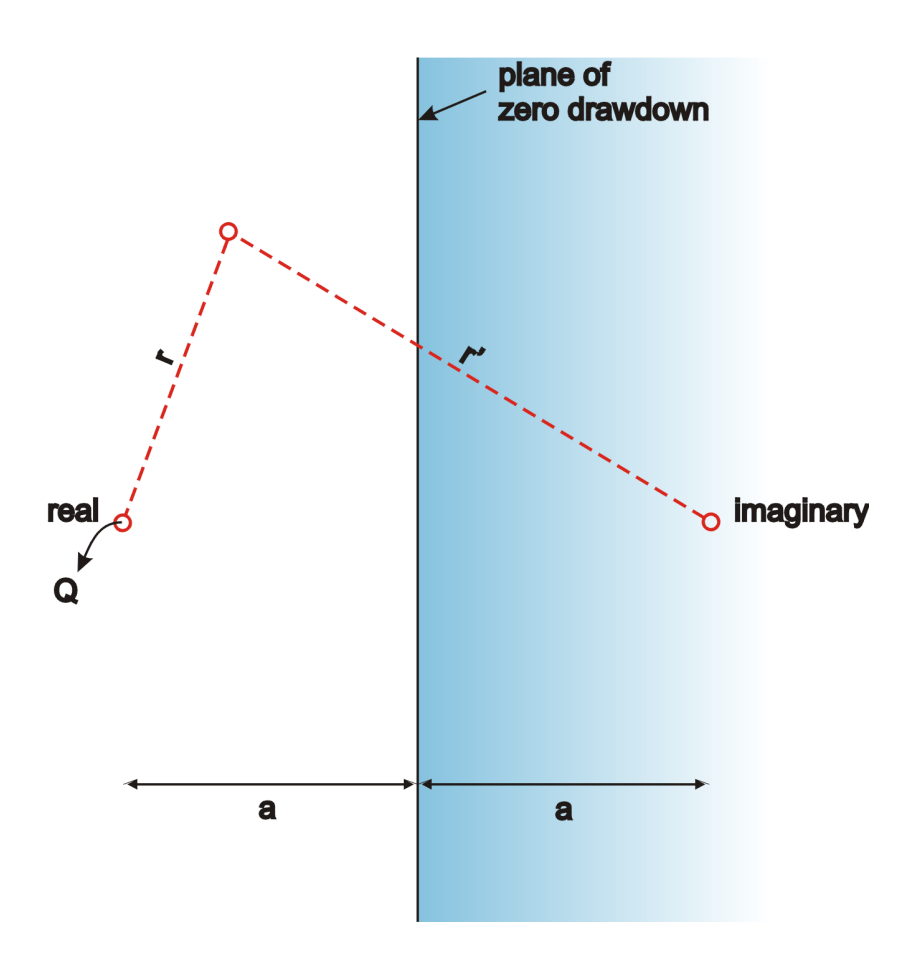


Figure 1. Application of image theory for a single linear constant-head boundary

The drawdown due to the pair of real and imaginary wells is:

$$S = \frac{Q}{4\pi T} W \left(\frac{r^2 S}{4Tt} \right) - \frac{Q}{4\pi T} W \left(\frac{r'^2 S}{4Tt} \right)$$

where r is the distance between the real well and the observation well, and r is the distance between the imaginary well and the observation well. Example calculations are shown in Figure 2. When a well is pumped near a constant head boundary, we observe two intervals of distinct response. During the early period, the observation well responds as if there were no boundary at all. The drawdown stabilizes after the effects of pumping propagate to the boundary.

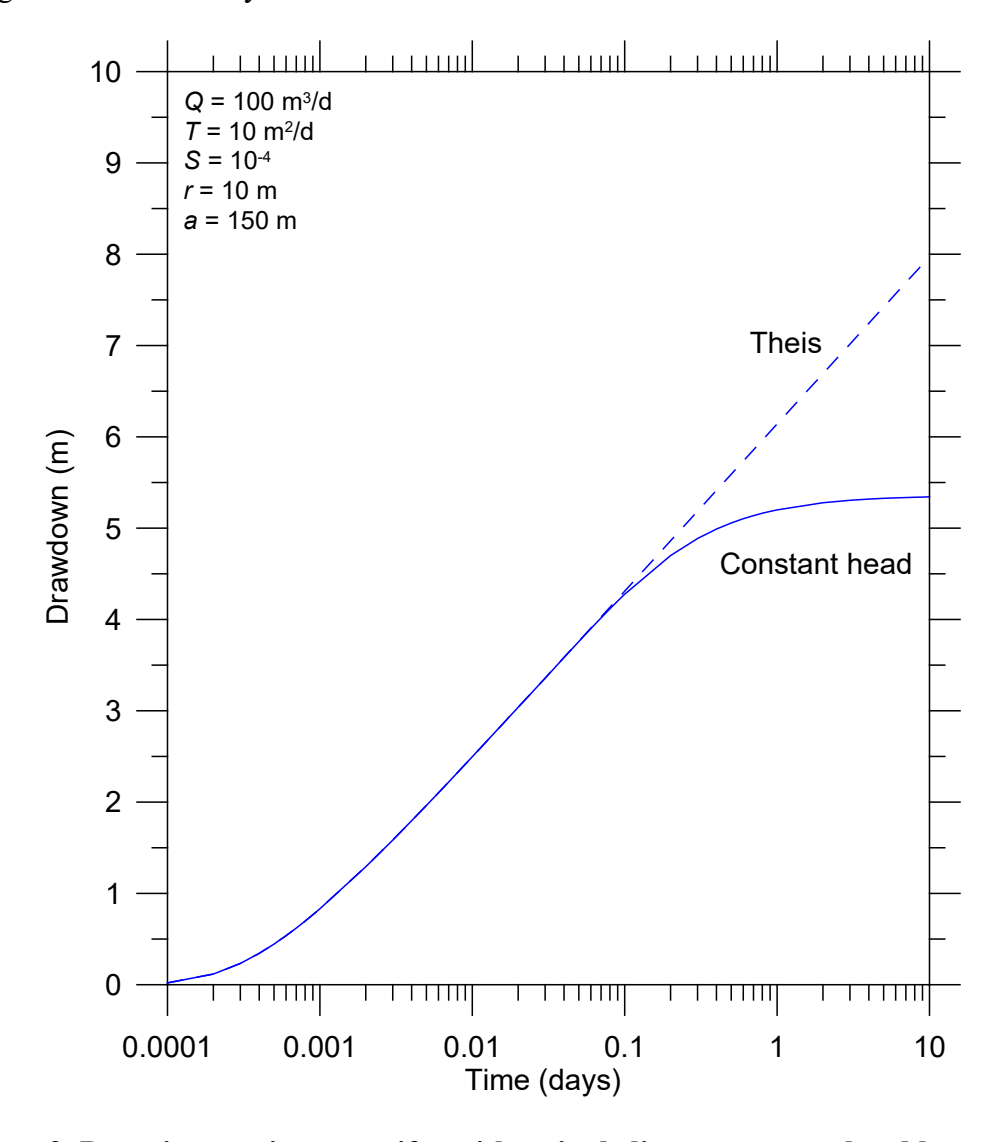


Figure 2. Pumping test in an aquifer with a single linear constant-head boundary

If we use the Cooper-Jacob approximation for the Theis well function, the drawdown is given by:

$$s = \frac{Q}{4\pi T} \left[-0.5772 - \ln \left\{ \frac{r^2 S}{4Tt} \right\} \right] - \frac{Q}{4\pi T} \left[-0.5772 - \ln \left\{ \frac{r^2 S}{4Tt} \right\} \right]$$

Using the properties of the log function, the expanded solution reduces to the simple expression:

$$s = \frac{Q}{4\pi T} \ln\left\{\frac{r^2}{r^2}\right\}$$
$$= \frac{Q}{2\pi T} \ln\left\{\frac{r'}{r}\right\} = \frac{Q}{2\pi T} 2.303 \log_{10}\left\{\frac{r'}{r}\right\}$$

The Cooper-Jacob approximation in this case is independent of time.

Late-time derivative

The derivative is defined as:

$$D_t(s) = \frac{\partial s}{\partial (\ln\{t\})}$$
$$= \frac{\partial}{\partial (\ln\{t\})} \left[\frac{Q}{2\pi T} \ln\left\{\frac{r}{r}\right\} \right] = 0$$

The presence of a constant-head boundary is indicated by a decline in the derivative to a value of zero.

$$D_t(s) \to 0$$

The decline in the derivative is diagnostic of recharge effects acting to attenuate drawdowns. The stabilization of the derivative for a single linear constant-head boundary is shown in Figure 3.

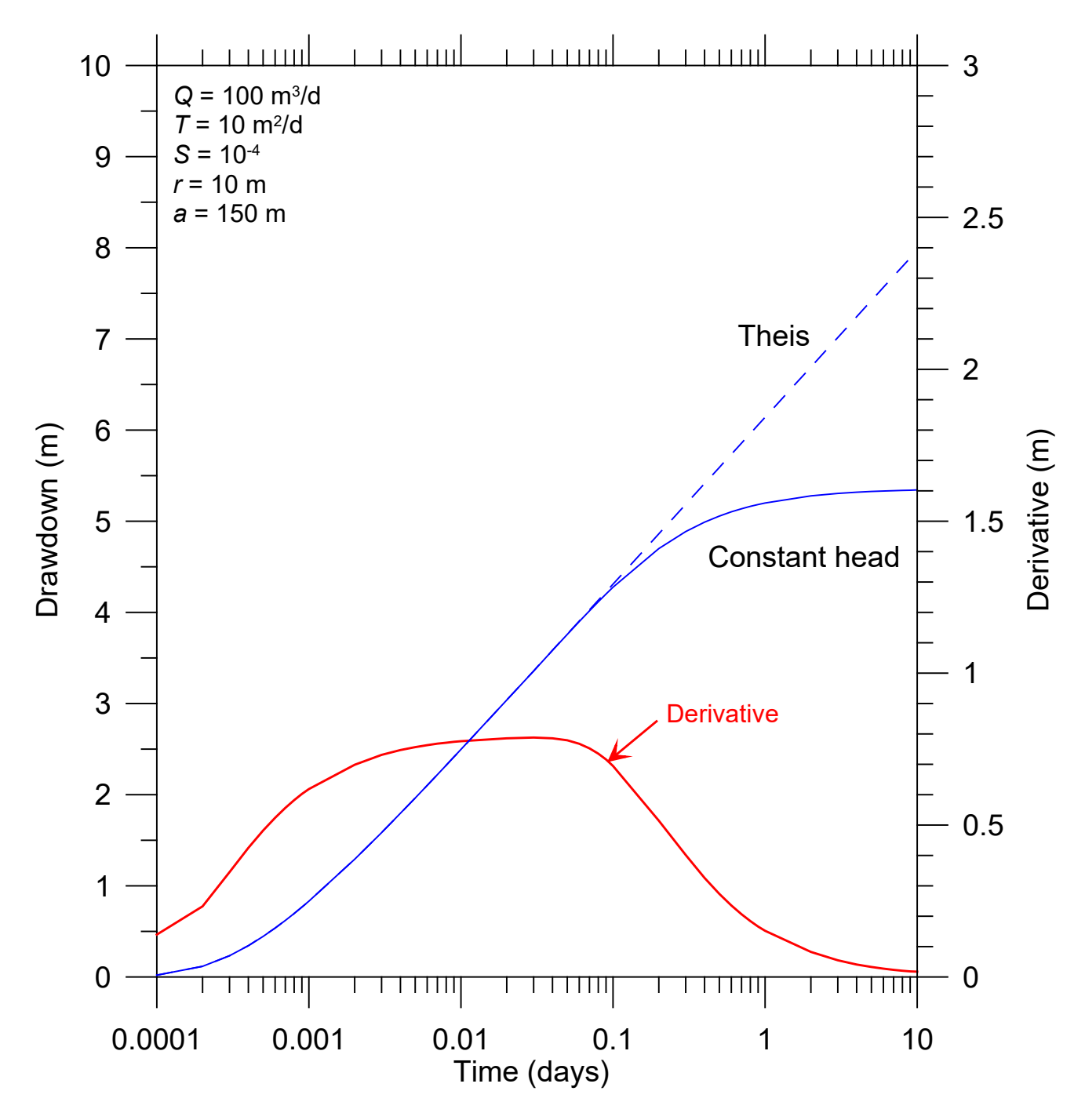


Figure 3. Pumping test in an aquifer with a single linear constant-head boundary

2. Aquifers with a single impermeable boundary

For the case of a linear no-flow boundary, the linear boundary is a line of symmetry. As shown in Figure 4, this is simulated with an imaginary well placed an equal distance from the boundary, pumping at the same rate as the real well.

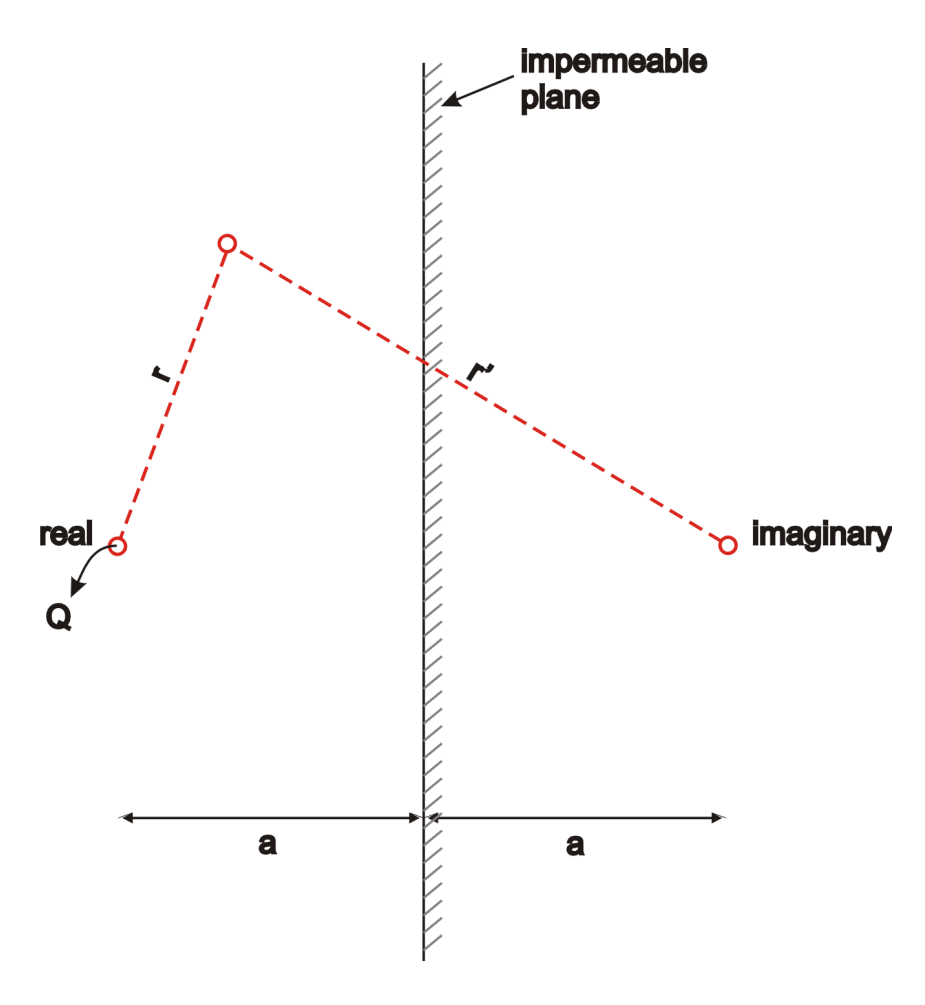


Figure 4. Application of image theory for a single linear impermeable boundary

The drawdown due to the pair of real and imaginary wells is:

$$s = \frac{Q}{4\pi T} W \left(\frac{r^2 S}{4Tt} \right) + \frac{Q}{4\pi T} W \left(\frac{r'^2 S}{4Tt} \right)$$

This solution differs from the solution for a constant-head boundary by the sign on the pumping rate for the imaginary well. Example calculations are shown in Figure 5. When a well is pumped near an impermeable boundary, we observe two intervals of distinct response. During the early period, the observation well responds as if there were no boundary at all. The drawdown steepens after the effects of pumping propagate to the boundary, and the slope on the semilog plot eventually doubles.

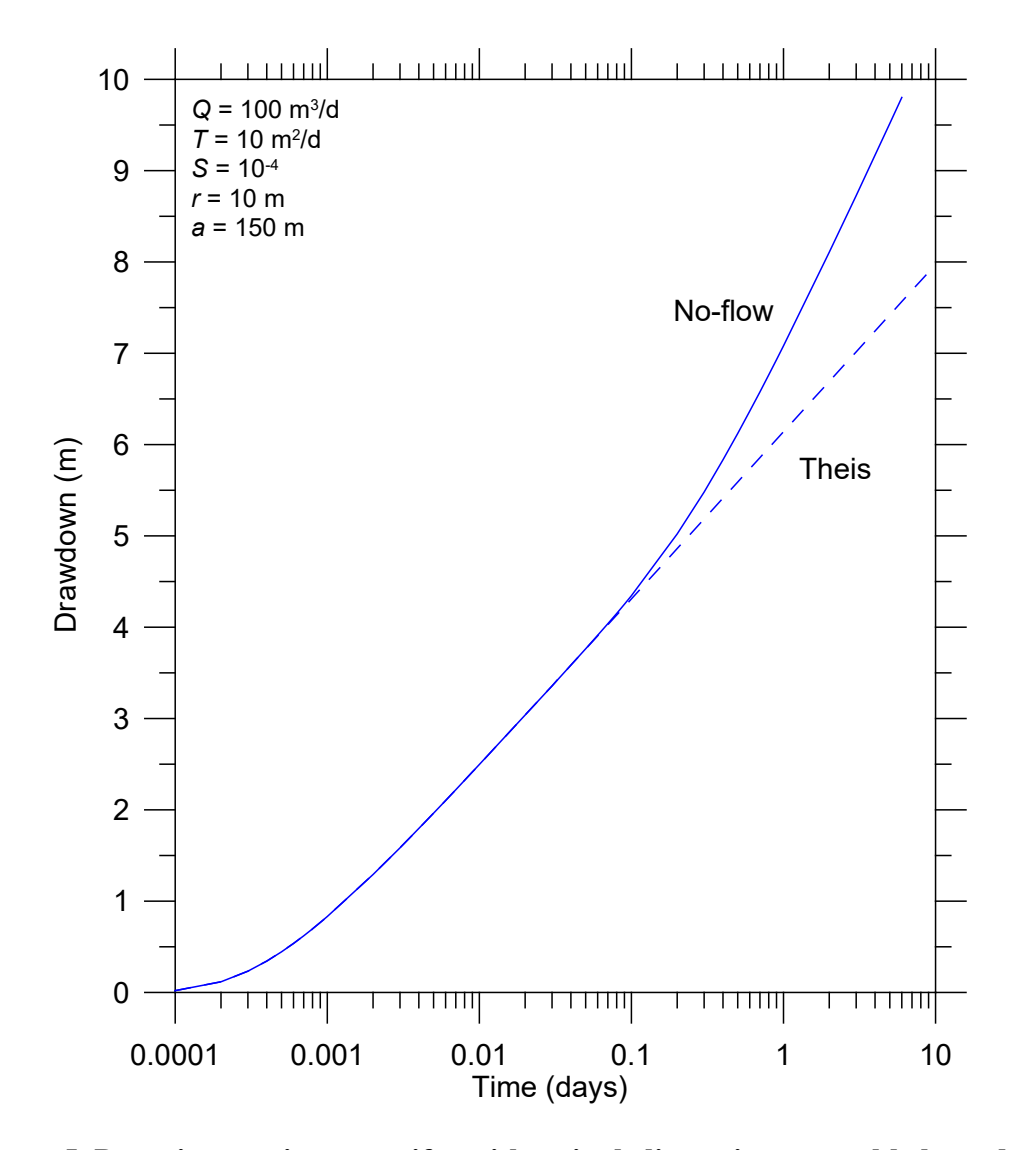


Figure 5. Pumping test in an aquifer with a single linear impermeable boundary

If we use the Cooper-and Jacob (1946) approximation for the Theis well function, the drawdown is given by:

$$s = \frac{Q}{4\pi T} \left[-0.5772 - \ln\left\{\frac{r^2 S}{4Tt}\right\} \right] + \frac{Q}{4\pi T} \left[-0.5772 - \ln\left\{\frac{r'^2 S}{4Tt}\right\} \right]$$

Using the properties of the log function, this reduces to:

$$s = \frac{Q}{4\pi T} \ln \left\{ \left[2.2459 \frac{Tt}{S} \right]^2 \frac{1}{r^2 r'^2} \right\}$$

$$= \frac{Q}{2\pi T} \ln \left\{ \left[2.2459 \frac{Tt}{S} \right] \frac{1}{rr'} \right\}$$

$$= \frac{Q}{2\pi T} 2.303 \log_{10} \left\{ \left[2.2459 \frac{Tt}{S} \right] \frac{t}{rr'} \right\}$$

Late-time derivative

The derivative of the Cooper-Jacob approximation is given by:

$$D_t(s) = \frac{\partial}{\partial (\ln\{t\})} \left[\frac{Q}{2\pi T} \ln\left\{ \left[2.2459 \frac{Tt}{S} \right] \frac{1}{rr'} \right\} \right]$$
$$= \frac{Q}{2\pi T}$$

The derivative of the Cooper-Jacob approximation for an infinite aquifer is given by:

$$D_t(s) = \frac{Q}{4\pi T}$$

We see that the later-time derivative for a linear impermeable boundary is double the derivative for an infinite aquifer.

The doubling of the derivative is diagnostic of the effect of a single linear impermeable boundary. The doubling of the derivative is illustrated in the example calculations shown in Figure 6.

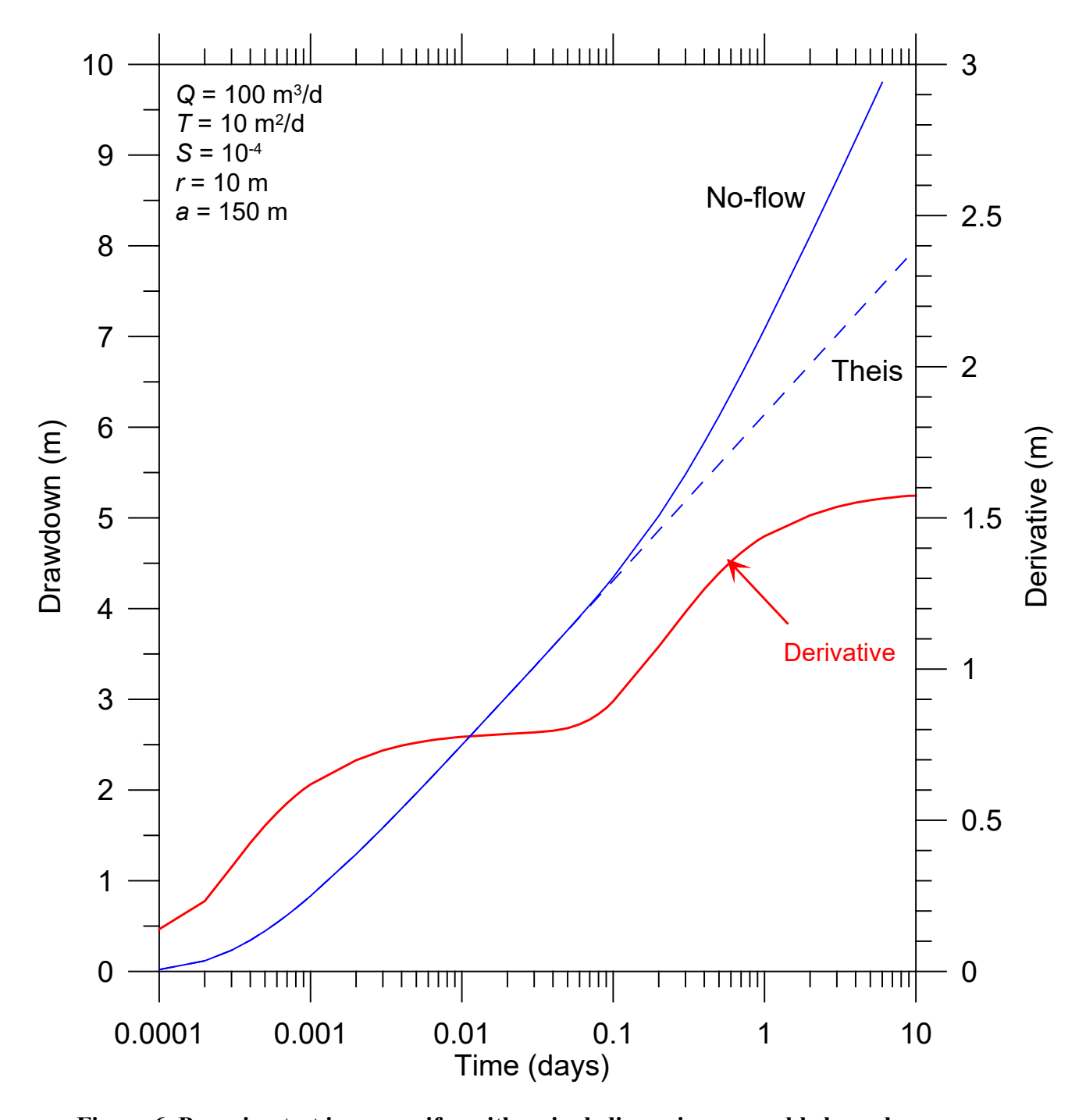


Figure 6. Pumping test in an aquifer with a single linear impermeable boundary

3. Generalization of the results for a single linear boundary

It is unlikely that the connection between a real aquifer and a constant-head feature is perfect or that real boundaries are truly impermeable. The boundaries that we may observe may actually be the interface between the aquifer and regions of relatively higher or lower transmissivity. With respect to interfaces with regions with different properties, the results from the two cases we have examined are important as they effectively bracket the range of responses that may be observed during a pumping test adjacent to a linear boundary:

- K-Zone 2 >> K-Zone $1 \rightarrow$ Linear constant-head condition; and
- K-Zone $2 \ll K$ -Zone $1 \to \text{Linear no-flow condition}$.

This concept is illustrated with the results of numerical model simulations. A two-dimensional confined aquifer that is 10 m thick is shown in Figure 7. The model contains two uniform zones. The pumping and observation wells are located in Zone 1 of the aquifer, which is assigned a hydraulic conductivity of 10 m/d. The well pumps at a constant rate of 50 m³/d. The observation well is located 100 m away, midway to interface with Zone 2.

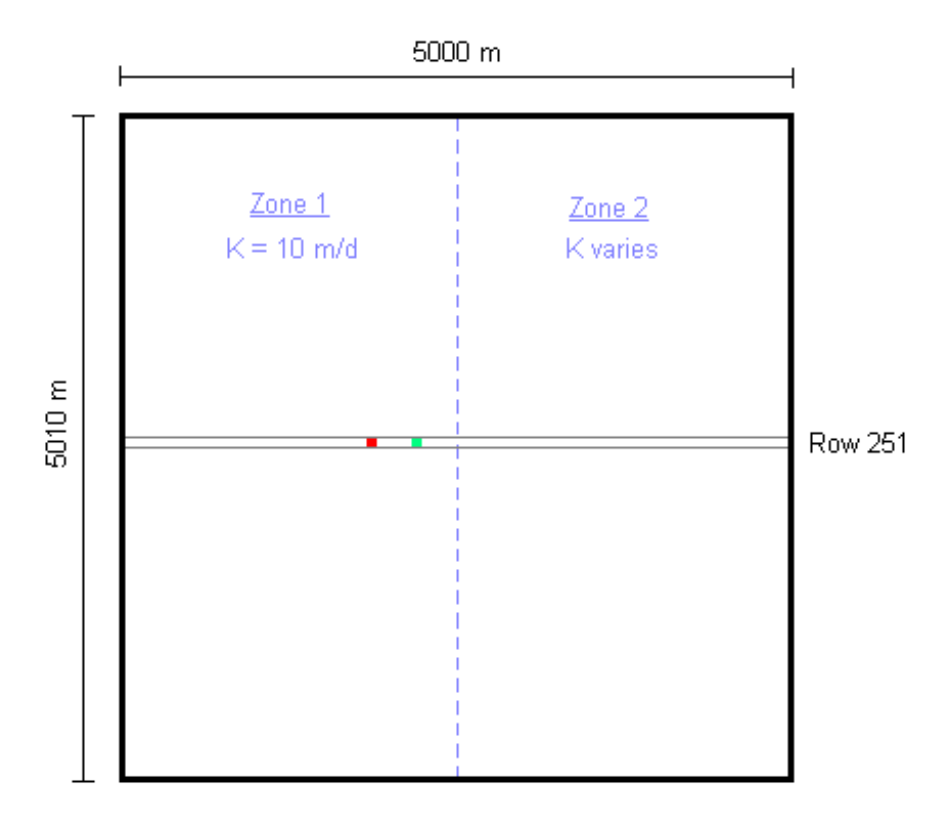


Figure 7. Conceptual model of pumping near a contrast in hydraulic conductivity

The drawdowns at the observation wells are plotted in Figure 8, for hydraulic conductivities of Zone 2 ranging from 1 m/d to 100 m/d. Up to about 0.01 days, the drawdowns are the same for all three cases. This reflects the fact that the effects of pumping are initially contained with Zone 1. After some time, the effects of pumping propagate from Zone 1 to Zone 2, encountering a region with different hydraulic conductivity. The results indicated for $K_H = 10$ m/d correspond to the "benchmark" results for an aquifer with uniform properties. For a Zone 2 hydraulic conductivity less than 10 m/d, the rate of drawdown increases relative to the benchmark, and for a Zone 2 hydraulic conductivity greater than 10 m/d the rate of drawdown is attenuated.

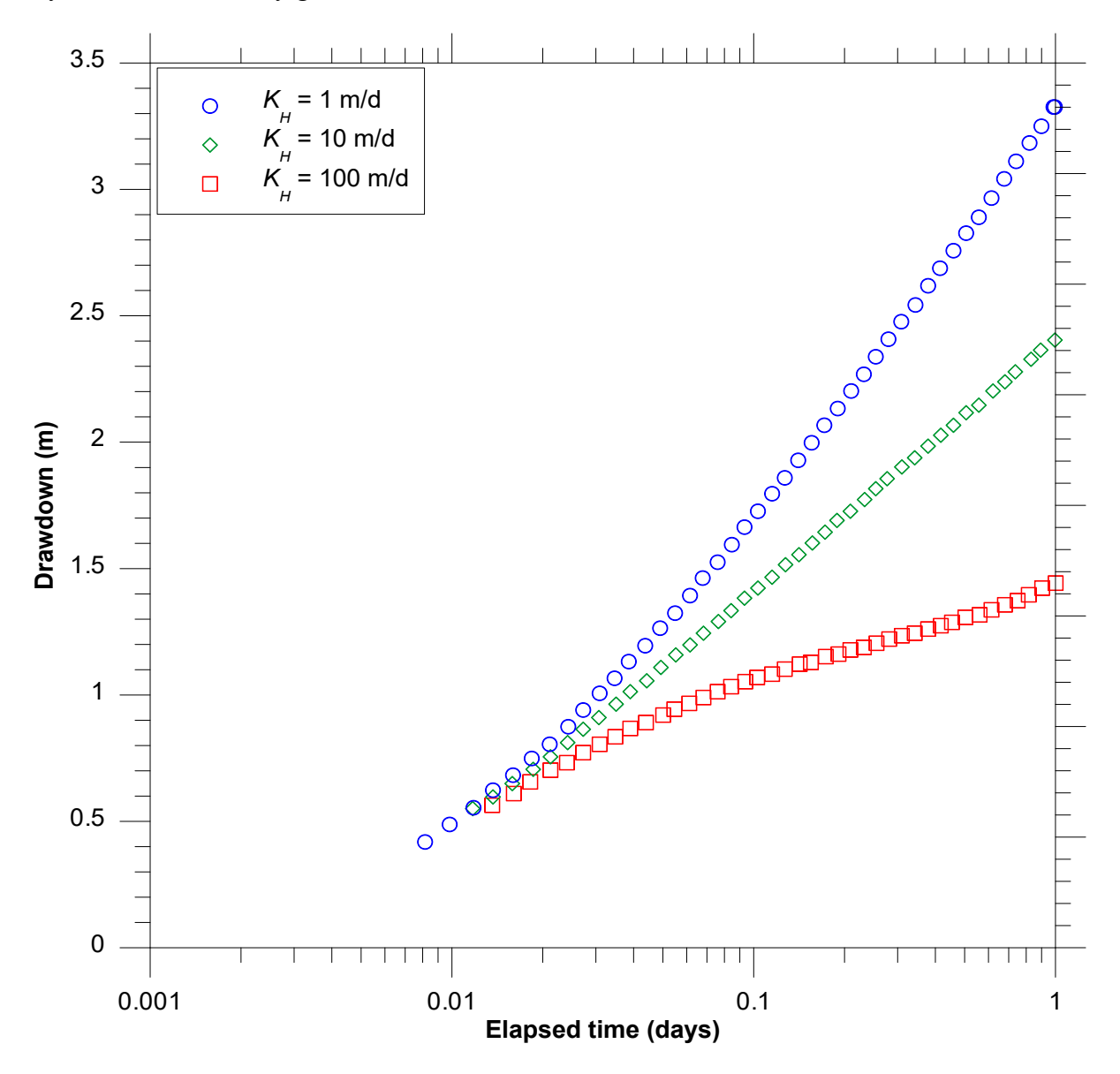


Figure 8. Drawdowns calculated for three values of K_H in Zone 2

To better understand the results of our simulations, we have added the results from analytical solutions with the Theis solution. As shown in Figure 9, the drawdowns for higher conductivities in Zone 2 approach the results obtained with the Theis solution with a single constant-head boundary. The drawdowns for lower conductivities in Zone 2 approach the results obtained with the Theis solution with a single no-flow boundary.

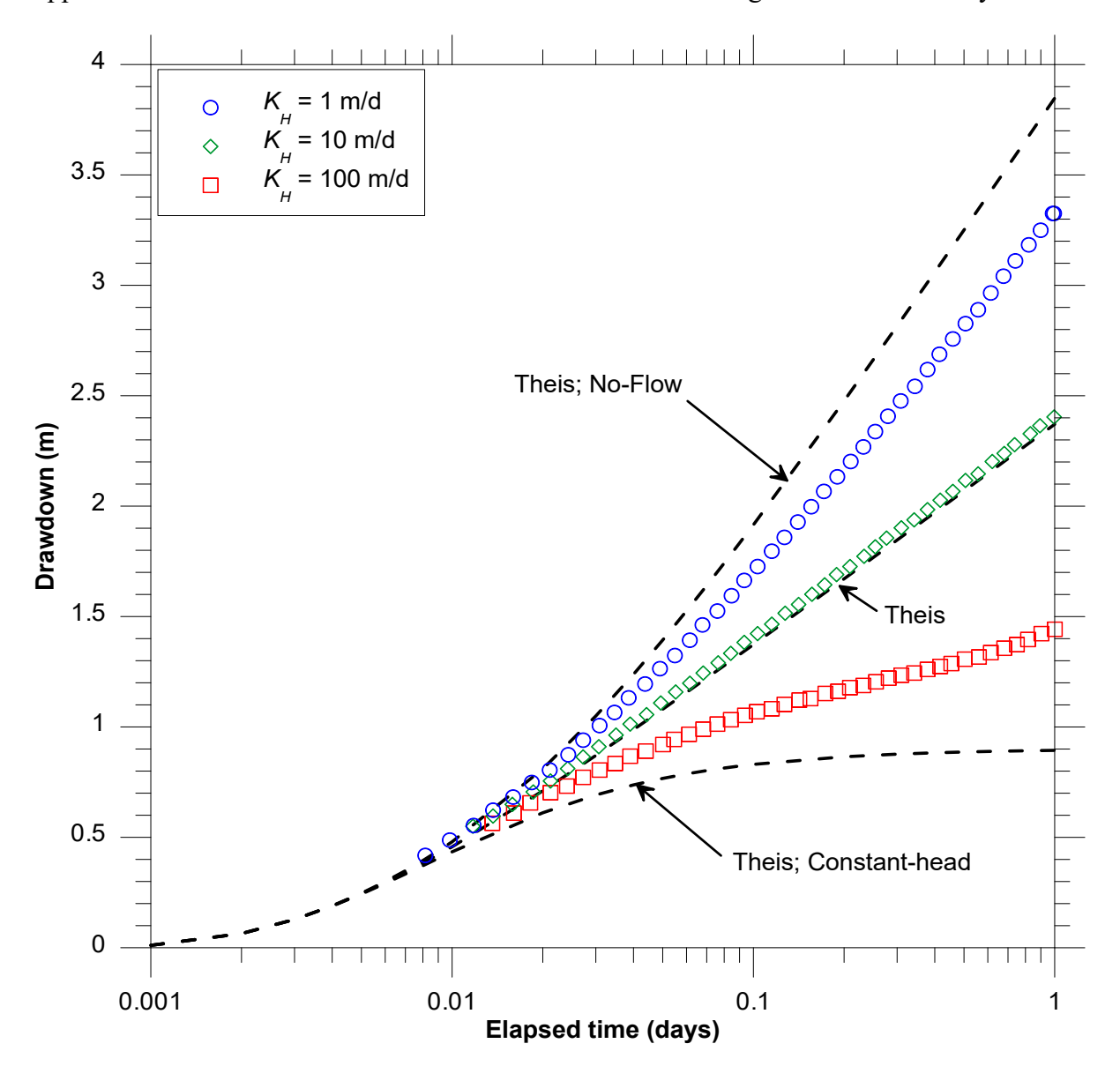


Figure 9. Drawdowns for contrasts in hydraulic conductivity

An expanded view of Figure 9 is shown in Figure 10 with the derivative plots added.

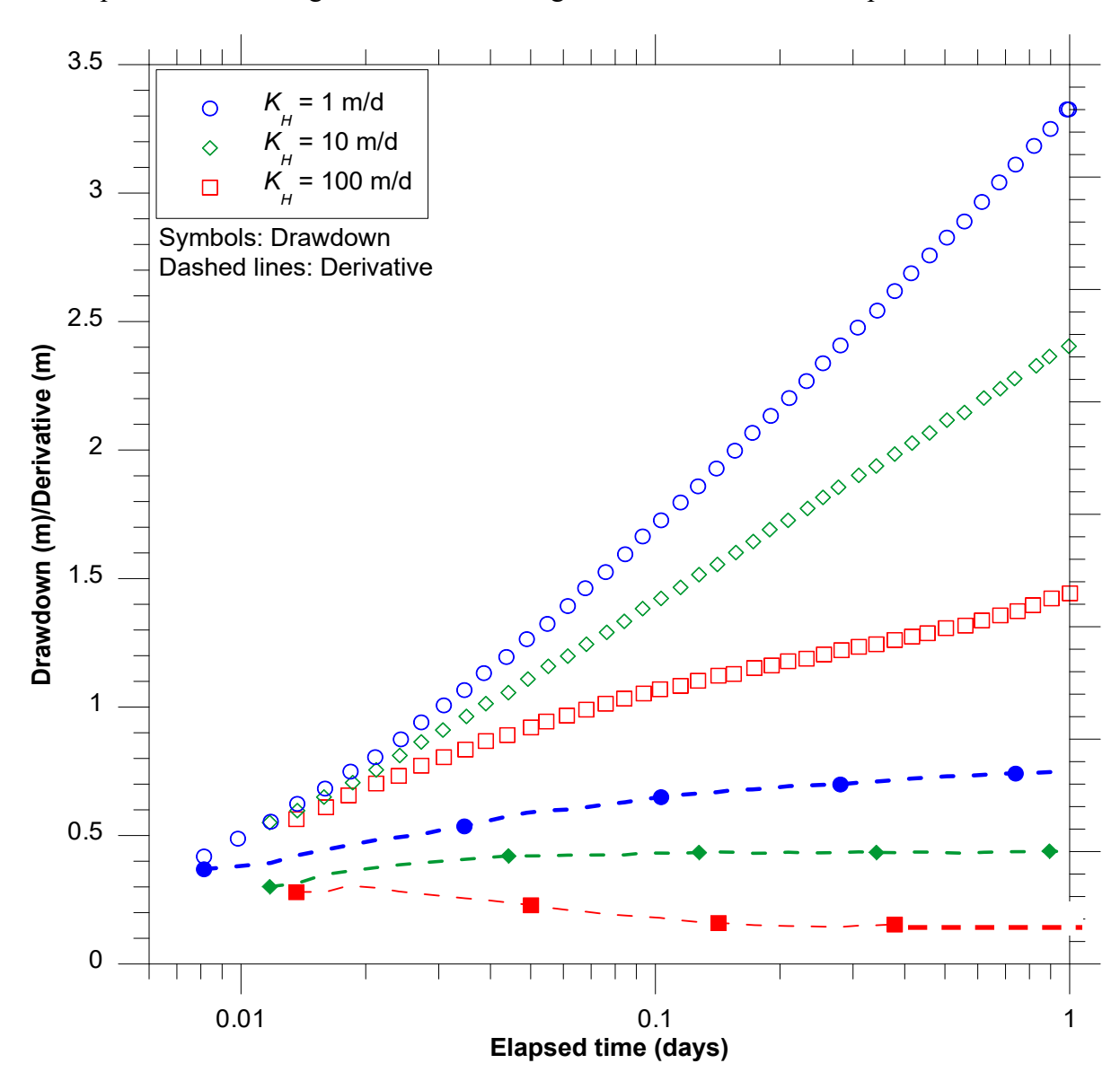


Figure 10. Drawdowns for extreme contrasts in hydraulic conductivity,

Derivative plots added

4. Aquifers with two linear impermeable boundaries (channel aquifers)

Buried channel aquifers are important conduits for groundwater in many areas of North America. Preliminary maps of delineated buried channel aquifers in Canada are shown in Figure 10. In western Canada, significant pre-glacial paleochannels have been filled with highly permeable sediments and subsequently overlain by low permeability glacial tills. Buried channel aquifers have been delineated in Alberta (see for example Farvolden, 1963) and Saskatchewan (see for example van der Kamp and Maathuis, 2002). Contrary to what is suggested in Figure 11, studies also suggest that there are buried channel aquifers in Manitoba (Betcher and others, 2005). Buried channel aquifers may also play a significant role in the hydrogeology of southern Ontario (Russell, Hinton, van der Kamp, and Sharpe, 2004).

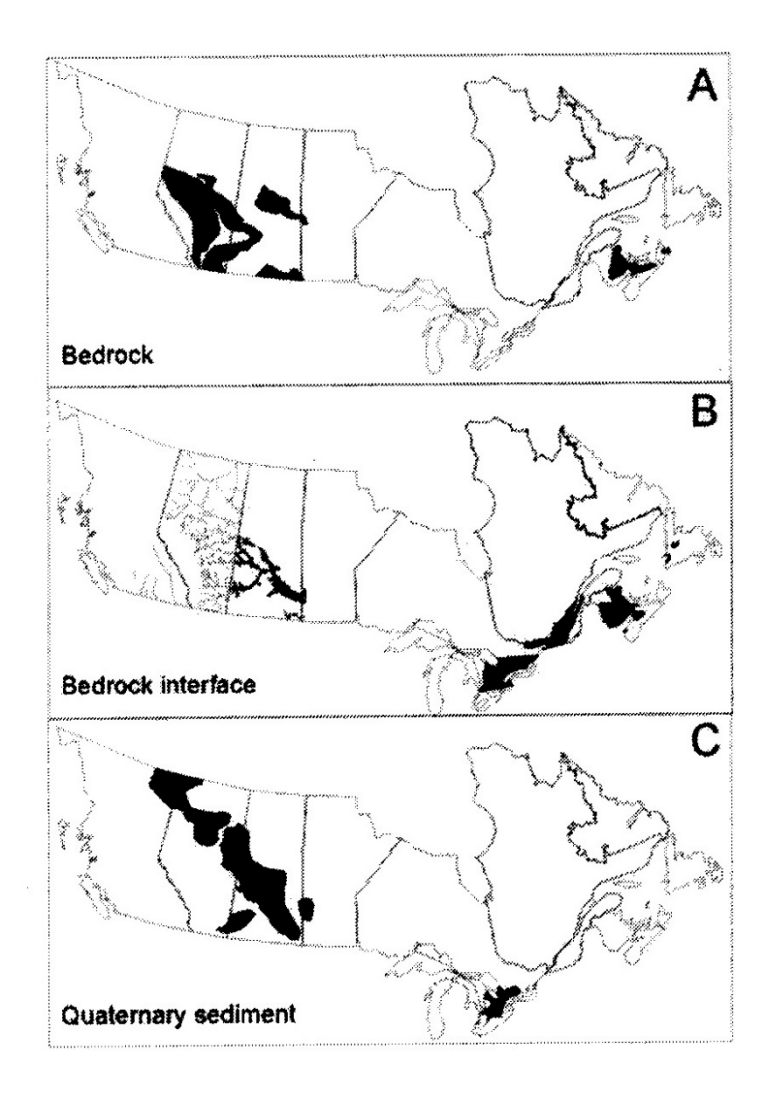


Figure 11. Delineated buried channel aquifers in Canada (from Russell, Hinton, van der Kamp, and Sharpe, 2004)

4.1 Conceptual model for a buried channel aquifer

An essential aspect of buried channel aquifers that controls their response to pumping is the proximity of boundaries. For relatively brief tests, it may be appropriate to ignore the presence of boundaries. This assumption may be too restrictive for channel aquifers. It may limit our analysis to a consideration of drawdowns from only the first few minutes or hours of pumping. The application of an infinite-aquifer analysis does not provide much insight into understanding the effects that boundaries have on the response to pumping, and may provide misleading impressions of the long-term yield of a well.

The idealized conceptual model for a buried channel aquifer is shown in Figure 12. In reality, these aquifers wind their way beneath the present landscape and may have highly heterogeneous distributions of material properties.

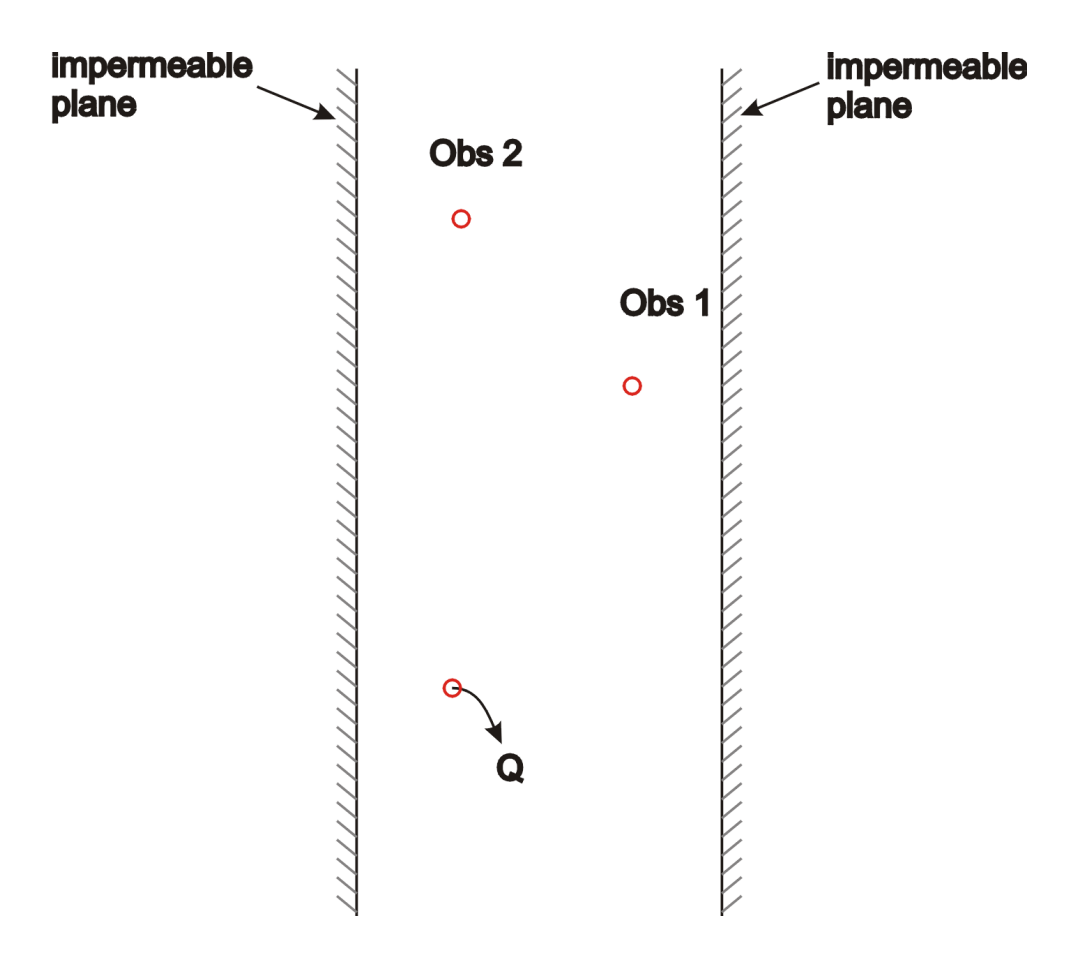


Figure 12. Conceptual model for a buried channel aquifer

An analytical model of a channel aquifer can be assembled using the Theis solution with superposition of image wells. Kruseman and de Ridder (1990; p. 114) present the following formula for pumping between two linear impermeable boundaries:

$$s(r,t) = \frac{Q}{4\pi T} \left[W(u) + \sum_{i=1}^{N} W(A_{ri}^{2}u) \right]$$

where i through N are the image wells. The quantity A_{ri} is defined as:

$$A_{ri} = \frac{r_i}{r}$$

Here r is the distance between the real well and the observation well, and r_i is the distance between the image well i and the observation well. The set-up of the image wells is shown in Figure 13. The black circle indicates the real well. The white circles indicate the image wells, all of which pump at the same rate as the real well.

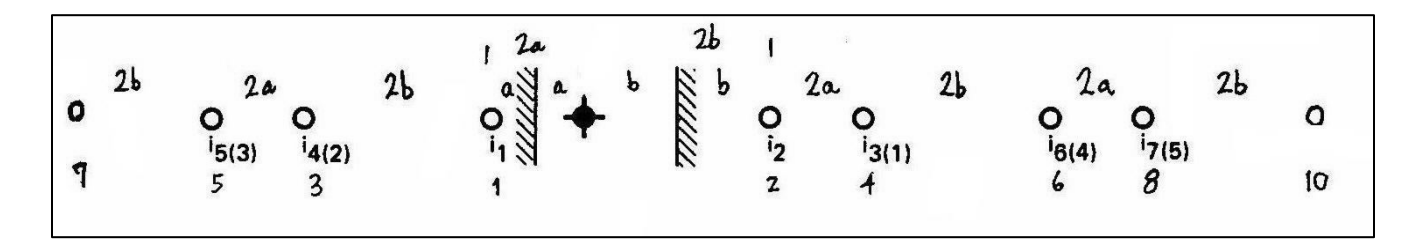


Figure 13. Image well set-up for a buried channel aquifer

Kruseman and De Ridder's formula is presented without a derivation. A good development of the theory of image wells is presented in Ferris and others (1962; p. 144).

In theory, an infinite number of image wells is required. In practice the calculations frequently converge for a relatively small number; however, there may be cases in which many image wells are required to evaluate the solution correctly. The number of image wells required depends on the location of the observation well and the elapsed time, and, in my experience, there is no easy way to anticipate how much computational effort is appropriate. A convergence analysis is generally required, in which the number of image wells is increased until the addition of another image well has negligible effect on the calculated drawdowns.

Vandenburg (1977) and Motz (1991) developed type curves for the interpretation of pumping tests in channel aquifers. van der Kamp and Maathuis (2002) demonstrated the application of these type curves in the context of a case study in Saskatchewan. The capability to interpret tests in channel aquifers is incorporated in AQTESOLV (versions Version 3.71.003 and later). The results of benchmark analyses are presented here to check the implementation of this capability and to develop our intuition regarding the responses to pumping in buried channel aquifers.

4.2 Benchmark analysis for pumping from a buried channel aquifer

Benchmark results are calculated using the finite-difference simulation code MODFLOW. We consider a perfectly confined aquifer with uniform thickness, and uniform, isotropic transmissivity. The aquifer is relatively long and thin, and is truncated along its left and right by impermeable boundaries. The conceptual model for the problem is shown in Figure 14.

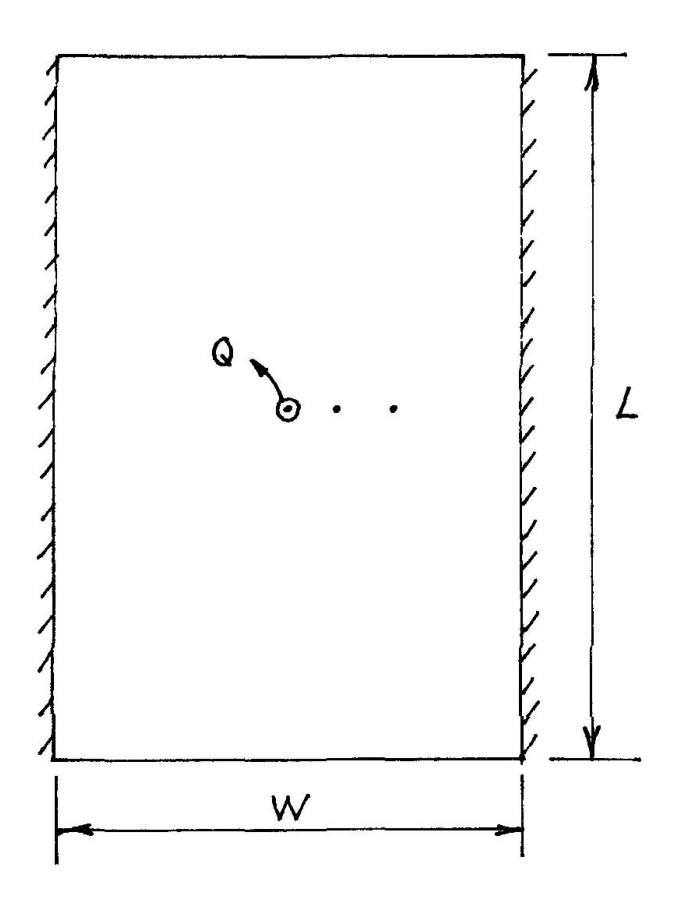


Figure 14. Schematic of MODFLOW model of a buried channel aquifer

Parameters

- Aquifer width, W = 510 m
- Transmissivity, $T = 8.64 \text{ m}^2/\text{day}$ (medium sand, $K_H = 10^{-3} \text{ cm/sec}$, B = 10 m)
- Storativity, $S = 10^{-4}$
- Pumping rate, $Q = 109.02 \text{ m}^3/\text{day} (20 \text{ US gpm})$

The coordinates of the wells are listed below.

Well	x-coordinate (m)	y-coordinate (m)
PW-1	0.0	0.0
OW-1	20.0	0.0
OW-2	50.0	0.0

MODFLOW model

- A single model layer is used to represent the aquifer with an arbitrary thickness of 1.0 m;
- The model is discretized with 51 columns across its width, with a uniform spacing of 10.0 m;
- By necessity, the model must also be truncated along its north and south boundaries. The aquifer is 2000 m long, and is discretized with 200 rows along its length, with a uniform spacing of 10.0 m; and
- The duration of the simulation is 10 days. A single stress period is divided into 200 time steps, with a time-step multiplier of 1.1.

The analytical solution that we will compare with the MODFLOW results is based on the assumption that the aquifer is infinitely long. In this example, the duration of pumping is sufficiently long that the effects of pumping extend to the north and south boundaries of the model, violating this assumption. To assess the boundary effects, two numerical simulations are conducted with different boundary conditions along the north and south boundaries of the model:

- Analysis #1: Constant-head conditions; and
- Analysis #2: No-flow conditions.

The results for constant-head conditions along the north and south model boundaries of the MODFLOW model are shown in Figure 15. The match between AQTESOLV and the MODFLOW results is excellent. A comparison of the two sets of results suggests that the north and south boundaries manifest themselves after about 3 days of pumping. As expected, the drawdowns calculated with the numerical model eventually decline below the analytical solution.

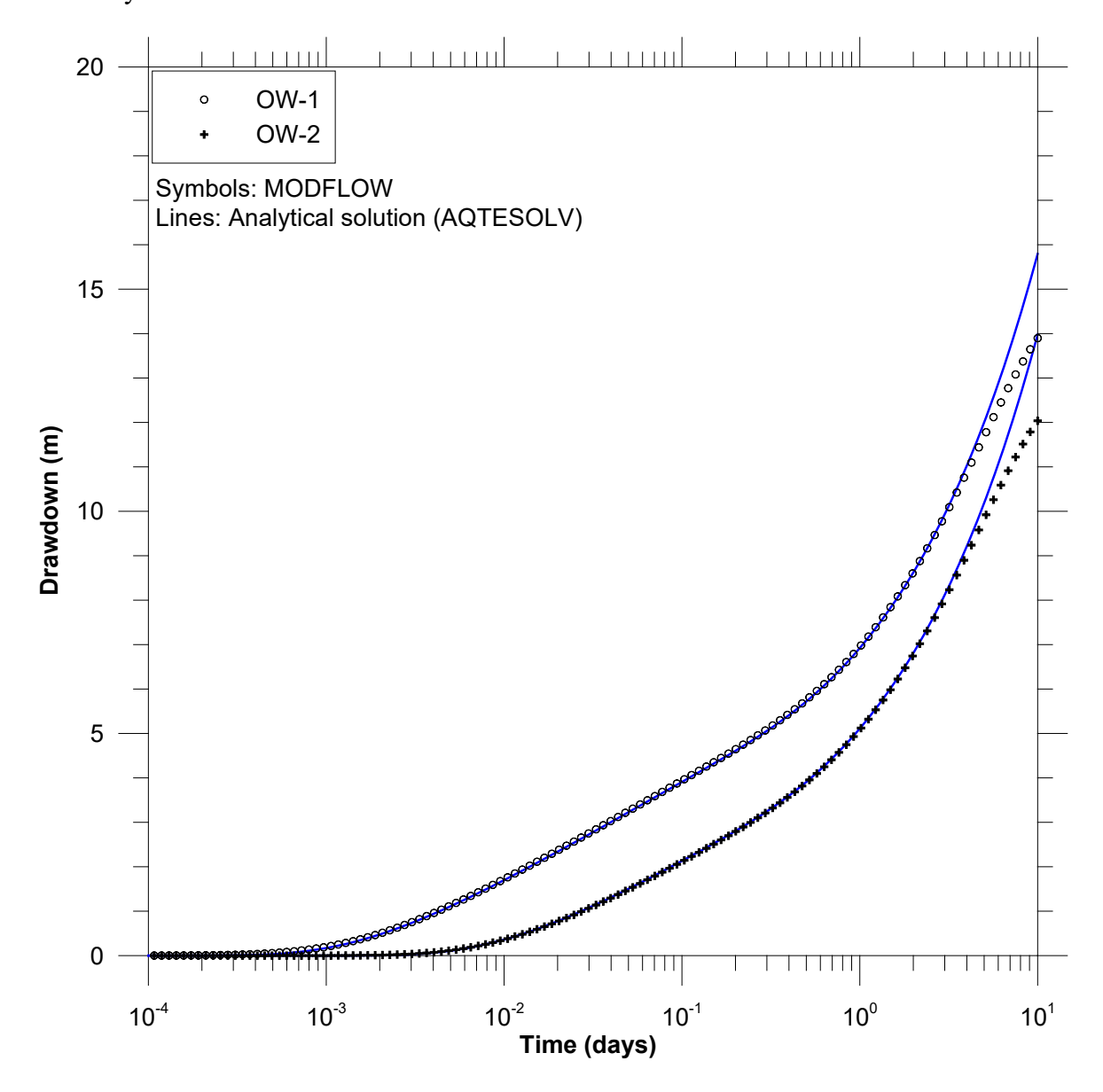


Figure 15. Comparison of drawdowns, constant-head conditions

The results for no-flow conditions along the north and south model boundaries of the MODFLOW model are shown in Figure 16. The match between AQTESOLV and the MODFLOW results is again excellent. A comparison of the two sets of results suggests that the influence of the north and south boundaries is detected about 3 days of pumping. Beyond that time, the drawdowns calculated with the numerical model exceed those predicted by the analytical solution.

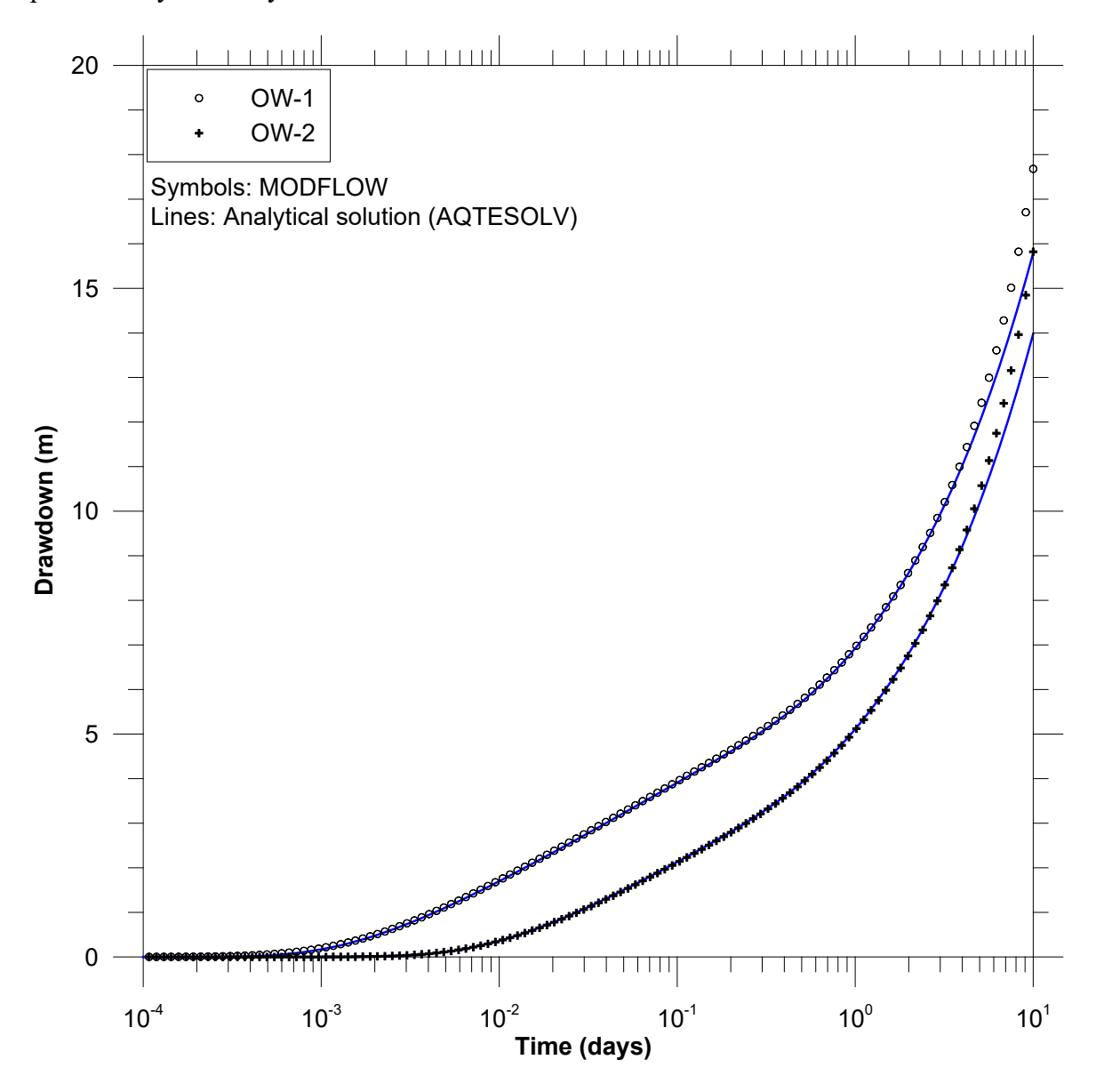


Figure 16. Comparison of drawdowns, no-flow conditions

4.3 Diagnostic plots for buried channel aquifers

The most appropriate way to diagnose the response to pumping in a channel aquifer is with separate plotting approaches for early and late time, including the derivative plots. A semi-log diagnostic plot for the early time response for OW-1 is shown in Figure 17. The semi-log straight line plot of the drawdown and the plateau of the derivative are characteristic of the infinite aquifer response that precedes the drawdown cone expanding to the boundaries. The derivative increases rapidly beyond the departure from the infinite-aquifer response and shows no sign of stabilizing. These results demonstrate that the presence of two linear no-flow boundaries causes more than a simple doubling of the slope on a semilog plot.

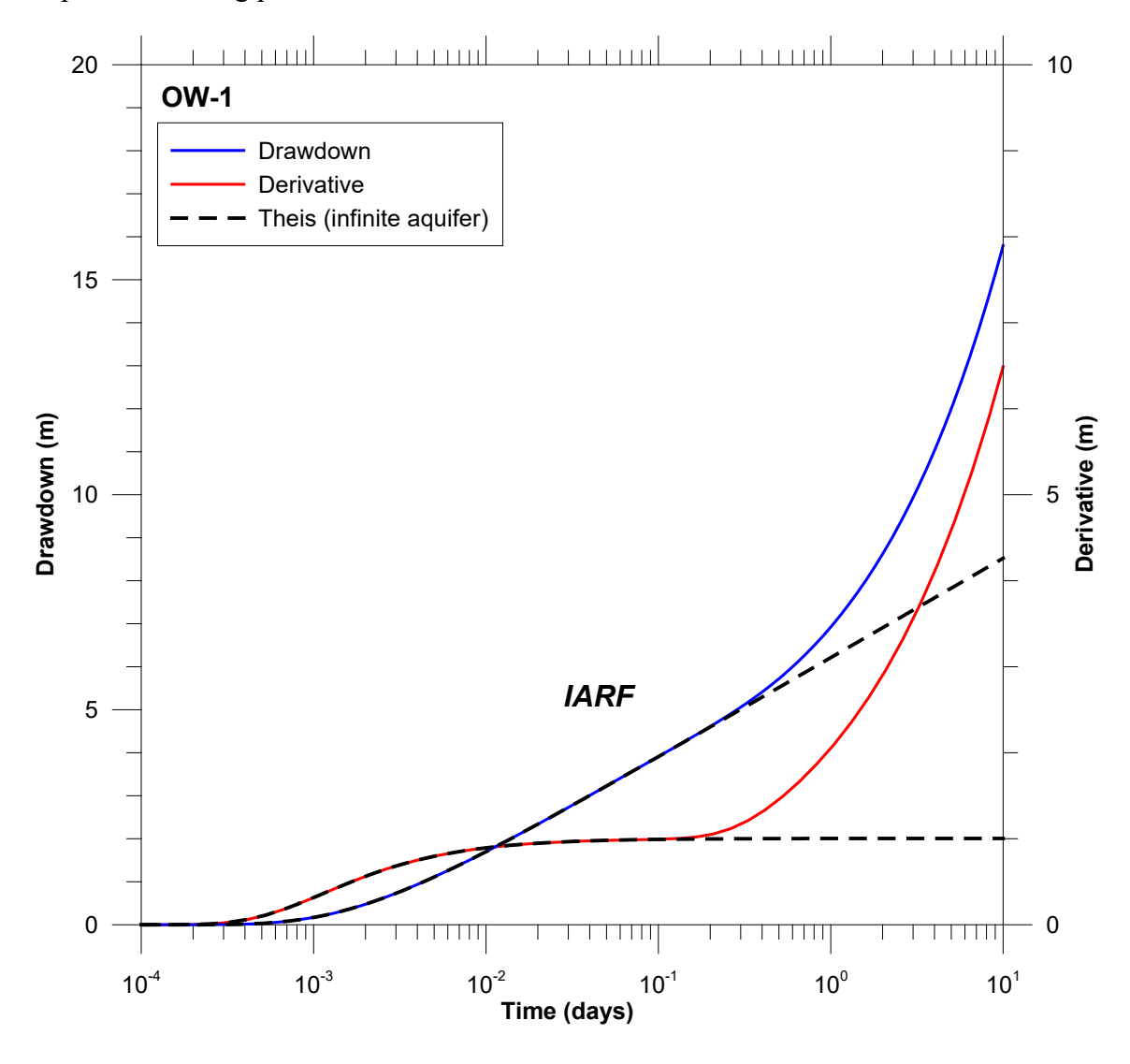


Figure 17. Drawdown and derivative plots for the analytical solution

Another way to look at the response for OW-1 is shown in Figure 18. In this figure, the drawdowns and derivatives for the analytical solution are plotted on log-log axes. This alternative form provides two more diagnostic suggestions of a channel aquifer. For later times, the drawdown and derivative plot as straight lines on log-log axes. The late-time slope of the drawdown is 1 log cycle of drawdown vs. 2 log cycles of time. This slope is characteristic of a linear flow regime.

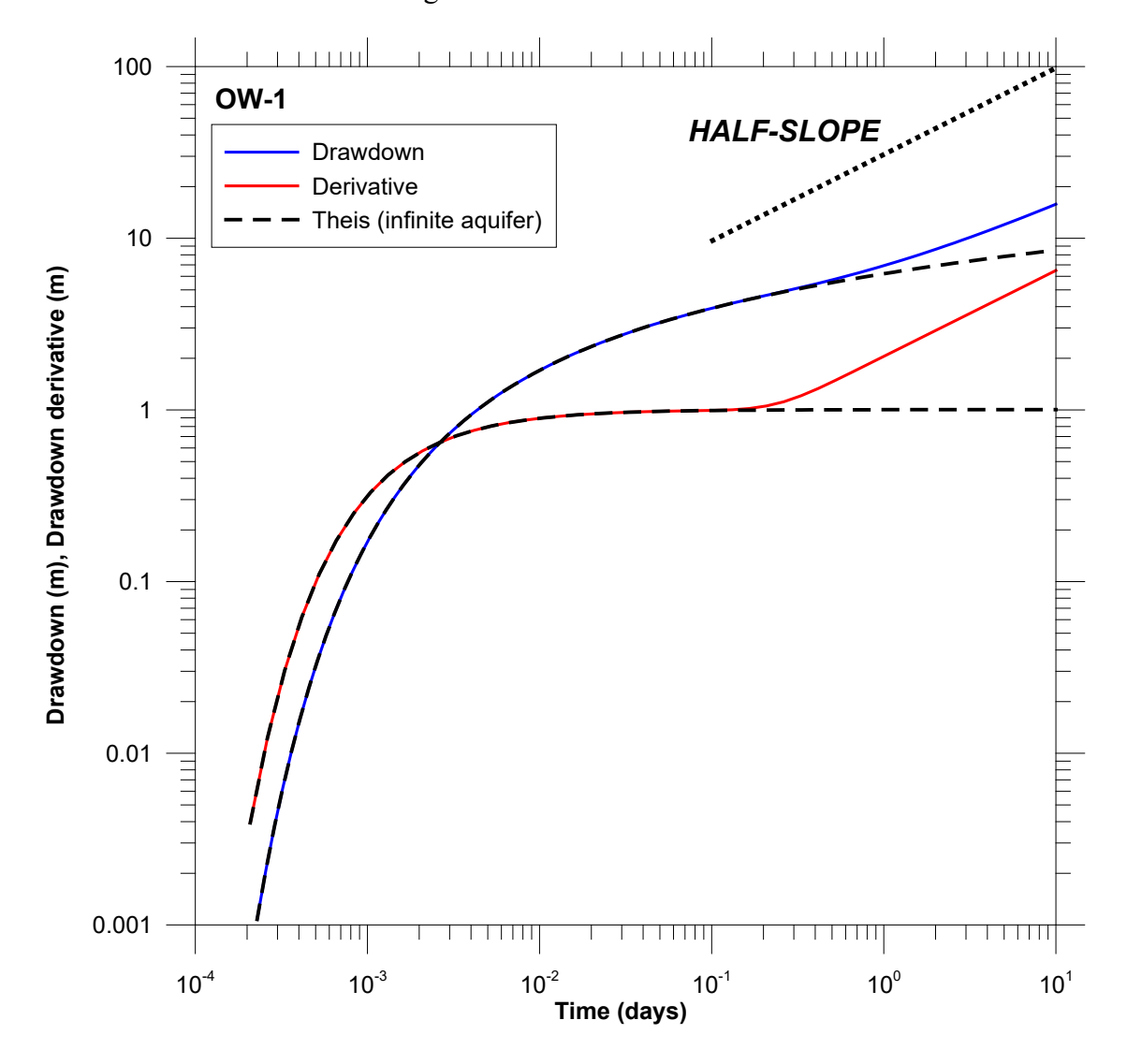


Figure 18. Drawdown and derivative plots for the analytical solution: log-log axes

5. Case study: Estevan, Saskatchewan

In March 1965, the Saskatchewan Research Council conducted a pumping test in an aquifer about 13 miles northwest of Estevan, Saskatchewan. In this case study, we revisit the original analysis of the pumping test presented in Walton (1970). The original analysis made use of data from the first few minutes of a long-term test. The data are reexamined using composite plots and derivative analysis. A re-analysis of the complete data set is conducted using an analytical approach for channel aquifers that incorporates the effects of the boundaries.

The aquifer is a long, sinuous paleochannel infilled with permeable sand and gravel and overlain by about 150 m of low-permeability glacial till. The geologic data available at the time of the pumping test suggested that the aquifer was a strip of sand and gravel approximately 1,700 feet wide, trending north-northwest through the production well. Descriptions of the hydrogeology of the Estevan area and the responses to pumping are presented in the excellent papers of van der Kamp and Maathuis (2002) and Maathuis and van der Kamp (2003).

The location of the pumping test site is shown in Figure 19. The generalized stratigraphic logs and construction features of the wells are shown in Figure 20. The wells were all screened in approximately the same depth intervals and are open to the coarse sand and gravel materials near the base of the glacial deposits. Johnson stainless steel continuous-slot screens were installed at selected depth intervals.

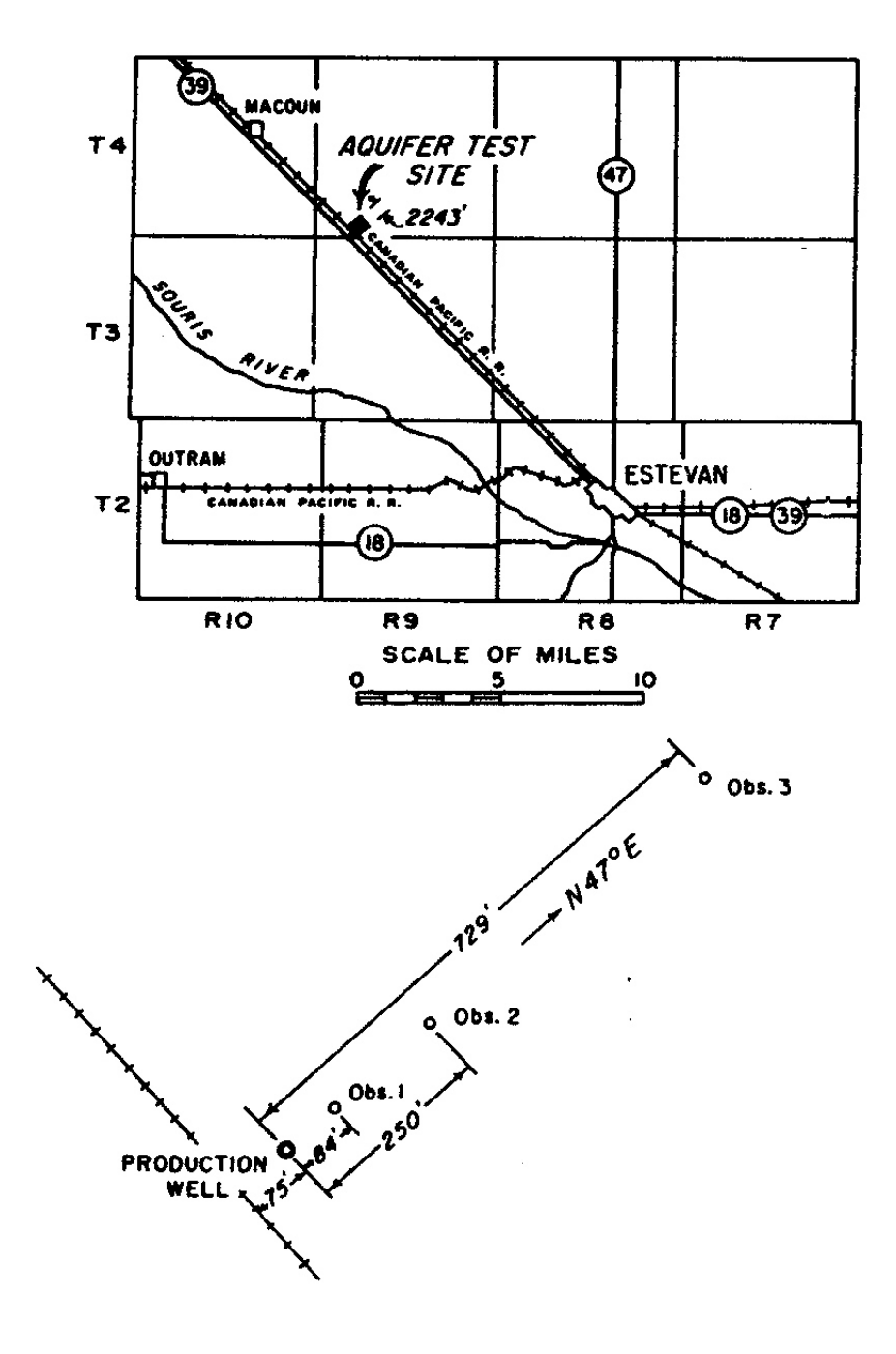


Figure 19. Locations of wells monitored during Estevan pumping test
Reproduced from Walton (1970)

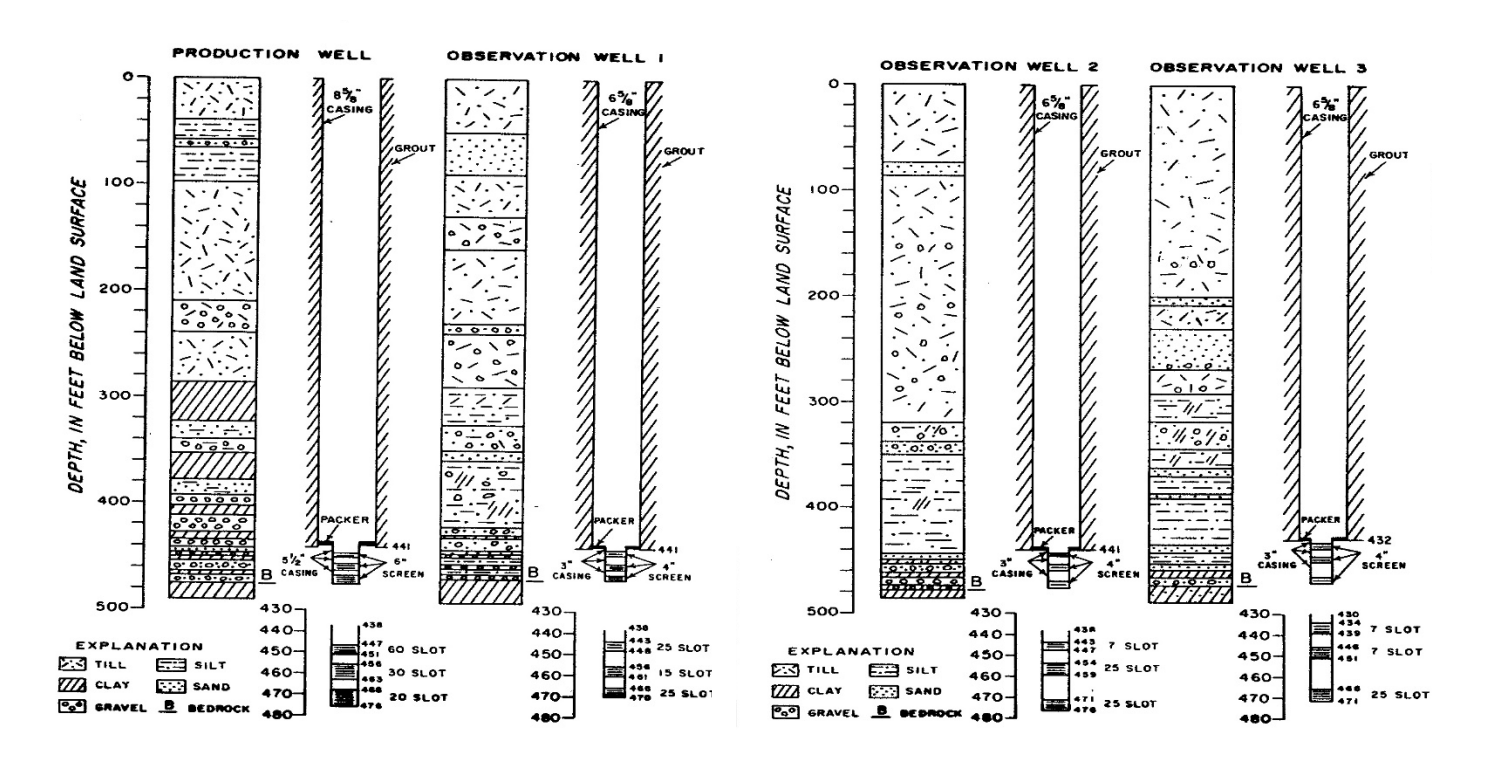


Figure 20. Geologic logs and completion details for wells
Reproduced from Walton (1970)

Pumping test data

Pumping started at 3:00 PM on March 4 and continued at a constant rate of 460 Igpm until 2:00 PM on March 12. The duration of pumping was 11,520 minutes. The pumping rate was held constant by means of a gate valve installed in the discharge pipe. A circular orifice and a manometer tube installed in the end of the discharge pipe were used to measure the rate of pumping. The rate of pumping varied between 457 Igpm and 464 Igpm.

Water levels were measured at the production well and at three observation wells. Water levels in the production well were frequently measured with a steel tape; water levels in the observation wells were continuously measured by means of recording gages. Atmospheric-pressure changes were measured with a recording Belfort microbarometer.

Drawdowns in the wells were determined by comparing water levels measured before pumping started with water levels measured during the pumping period. The drawdowns were corrected for changes in atmospheric pressure. The drawdowns in the wells at the end of the test are tabulated below.

Well	Drawdown at end of test (ft)
Production well	16.03
Observation well 1	10.97
Observation well 2	10.88
Observation well 3	9.54

A drawdown of 0.59 foot was observed in well GSC-3A which penetrated the lower aquifer about 9 miles northeast of the production well. This drawdown indicates that cones of depression under heavy pumping conditions may spread to great distances.

Original analysis (Walton, 1970)

Walton remarked that observation wells 1 and 2 were close to the pumped well and their time-drawdown curves were relatively flat. Analysis of the time-drawdown curves for these wells was most difficult and emphasis was placed on the time-drawdown graph for observation well 3 in determining *T* and *S*. The original analysis of Walton (1970) for observation well 3 is reproduced in Figure 21.

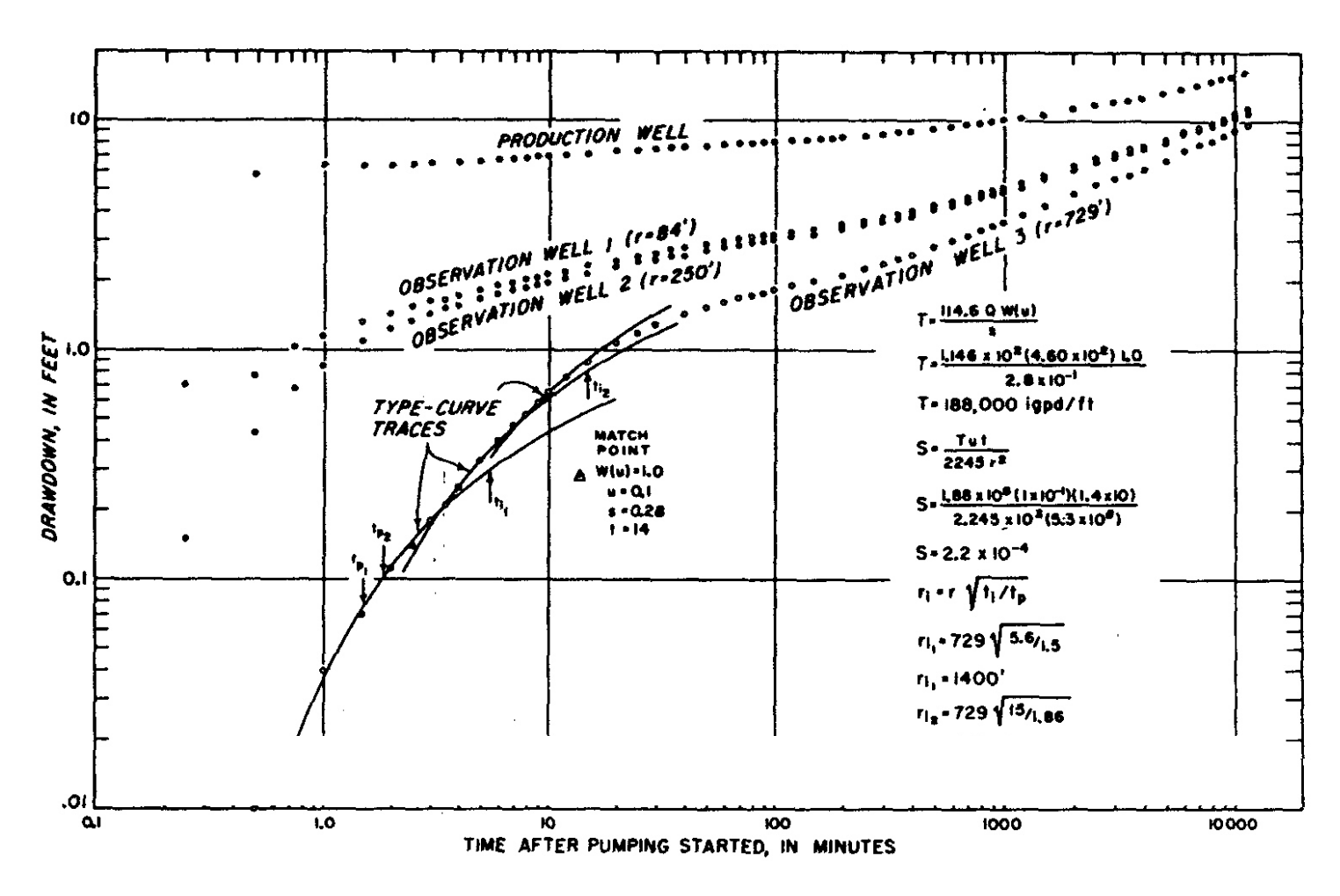


Figure 21. Original analysis Reproduced from Walton (1970)

Walton interpreted the test data using the Theis type-curve matching method. As shown in Figure 21, Walton matched the type curve to early time-drawdown data. The coordinates of the match point are:

- u = 0.1; • W(u) = 1.0;
- t = 14 min; and
- s = 0.28 ft.

The type curve matching yielded a transmissivity of 188,000 Igpd/ft (30,220 ft²/day) and storativity of 0.00022, respectively. According to Walton, the transmissivity is very high and the storage coefficient is in the normal range for a confined aquifer.

After about 3 minutes of pumping, the time-rate of drawdown in the observation wells increased and field data deviated upward from the type-curve trace, indicating the presence of a barrier boundary. The type curve was again matched to drawdown data for time values between 3.5 and 8.0 minutes. After about 8 minutes, the time-rate of drawdown again increased, indicating the presence of a second barrier boundary. The type curve was again matched to drawdown data for time vales between 8 and 15 minutes. The divergence of the three type-curve traces was determined and the distances from the observation wells to image wells associated with the two barrier boundaries were calculated.

We object to several aspects of Walton's original analysis. There are at least four reasons why we cannot place much reliability in the transmissivity estimated in the original analysis:

- The analysis ignored essential aspects of the site. Walton (1970) describes these aspects clearly but they are not incorporated in the analysis;
- The analysis was conducted on a well-by-well basis;
- The analysis focused on only the very earliest portion of the test. For observation well #3, the transmissivity was estimated based on data from only the first 3 minutes of a test that lasted more than 10,000 minutes; and
- No attempt is made to diagnose the response to pumping or to interpret the data with an analysis that incorporates the conceptual model for this site.

Alternative analyses

Diagnostic plots

A log-log plot of the drawdowns is presented in Figure 22. This is the key plot for identifying that we are pumping from a buried channel aquifer. As shown in the plot, towards the end of the test the drawdowns appear to approximate straight lines with a half slope (one log cycle of drawdown per two log cycles of time). The half-slope is characteristic of linear flow in a channel aquifer.

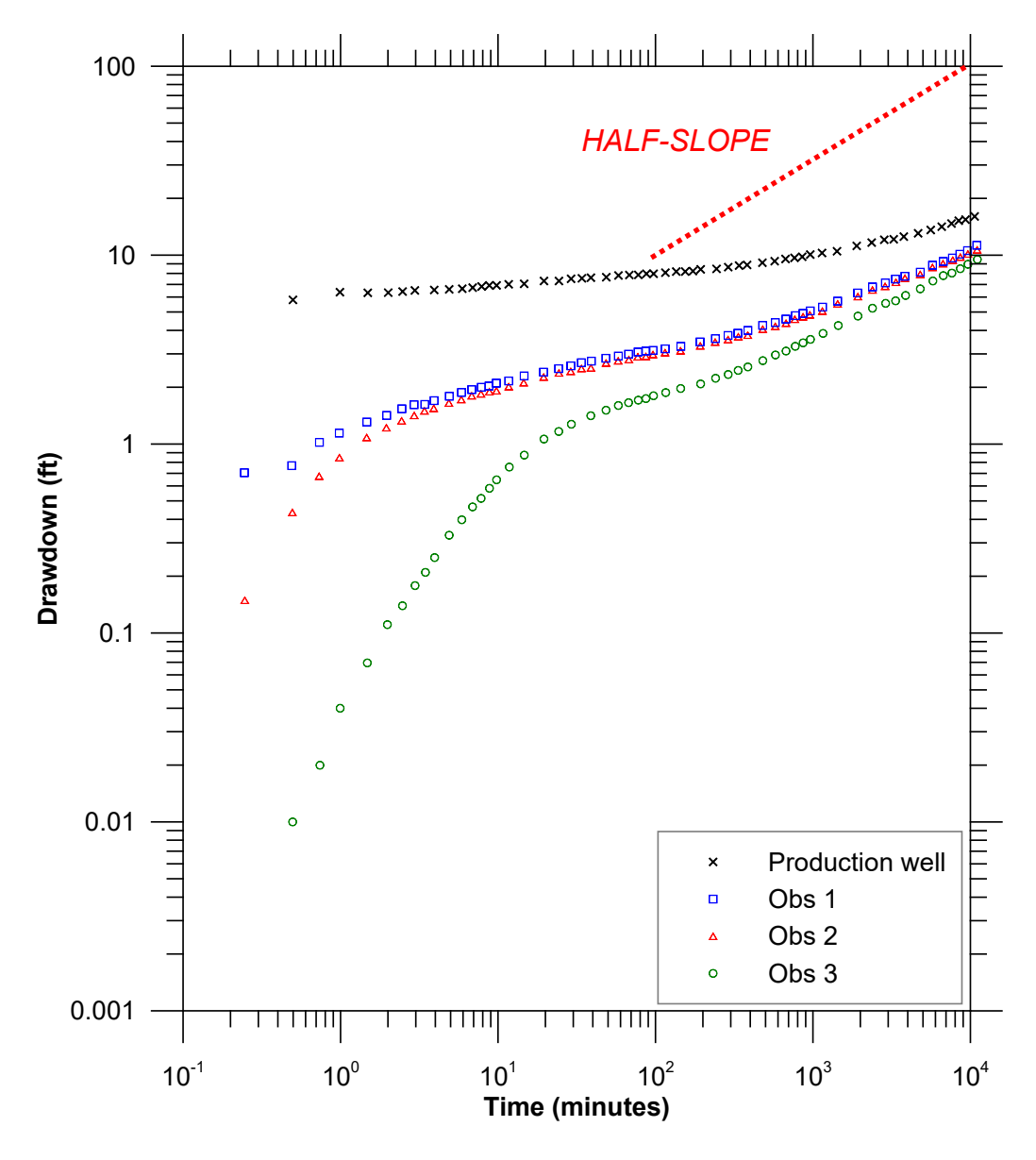


Figure 22. Time-drawdown records on a log-log plot

The derivatives are plotted on log-log axes in Figure 23. The theoretical late-time derivative for a channel aquifer also has a half-slope of a log-log plot, and this is clearly evident in the Estevan data.

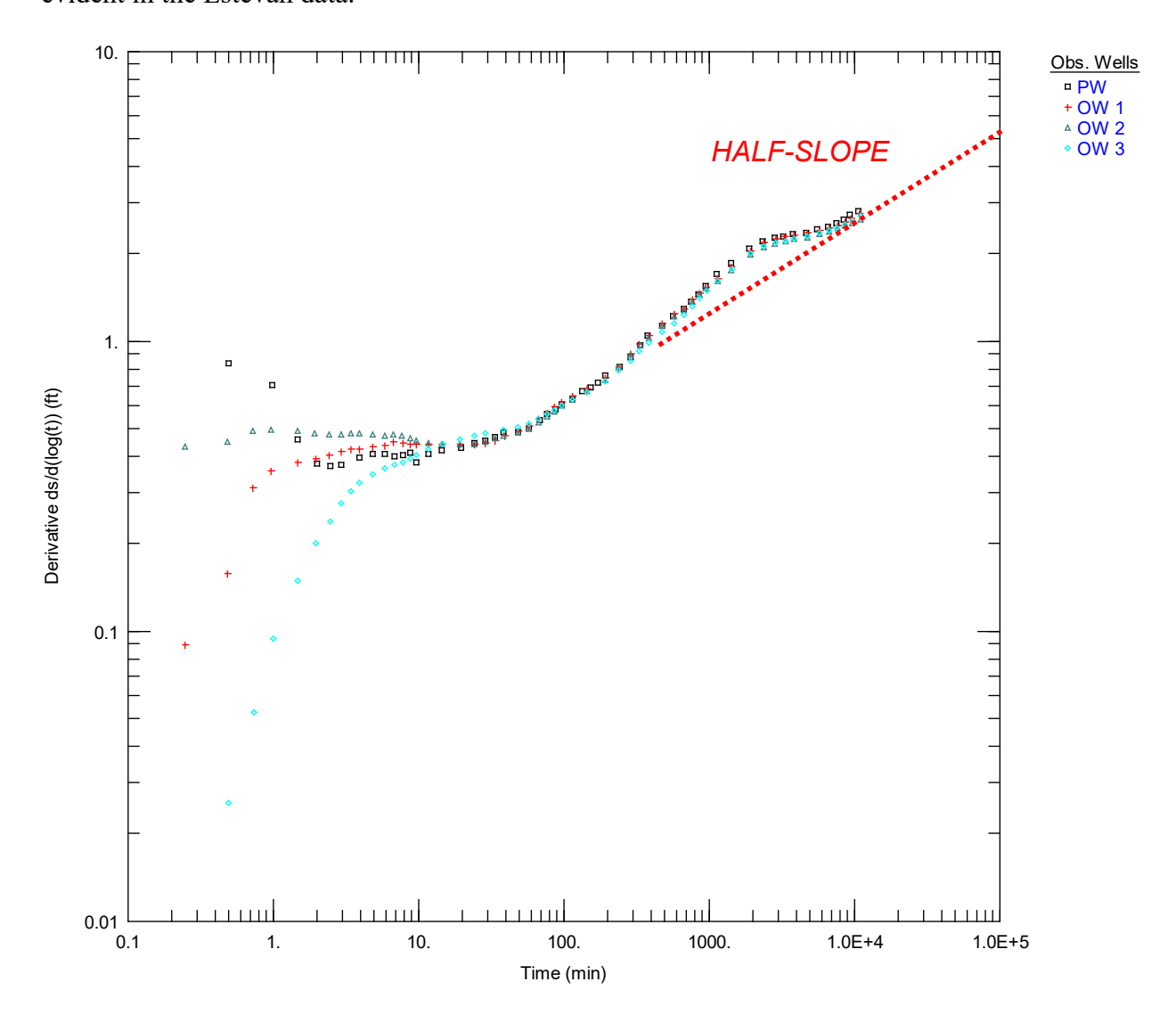


Figure 23. Derivative plot on log-log axes

To estimate the bulk-average transmissivity we assemble the drawdowns on a semilog composite plot. The original drawdown data from all of the wells are re-plotted in Figure 24, with the abscissa being elapsed time divided by the square of the distance from the production well (t/r^2) . This plot is in effect a diagnostic plot for the early-time, infinite-aquifer response.

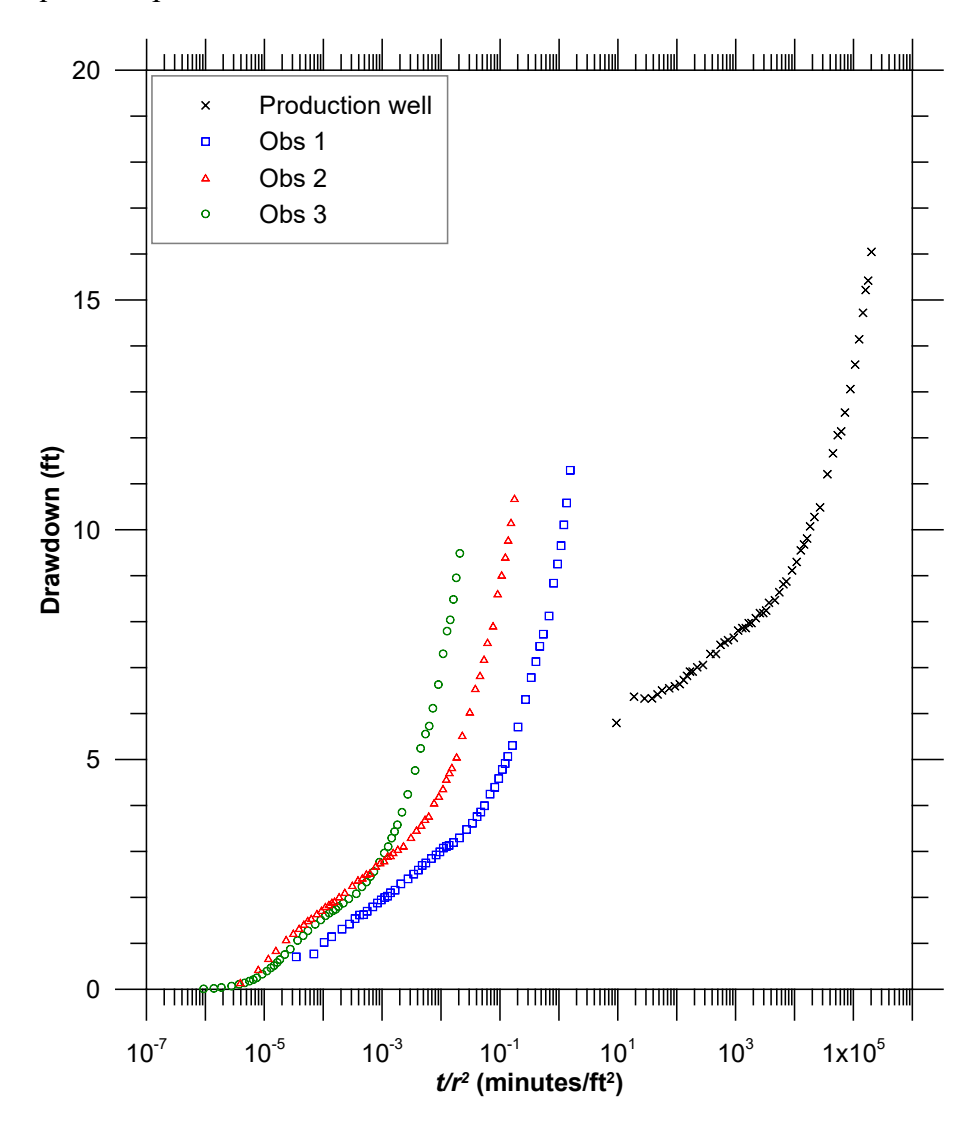


Figure 24. Semilog composite plot

The early portions of the responses from all wells, including the production well, appear to converge on parallel straight lines on the semi-log composite plot shown in Figure 24. The parallel straight lines superimposed on the data in Figure 25 represent the combination of values of t/r^2 over which the aquifer responds as a perfectly confined aquifer of infinite extent.

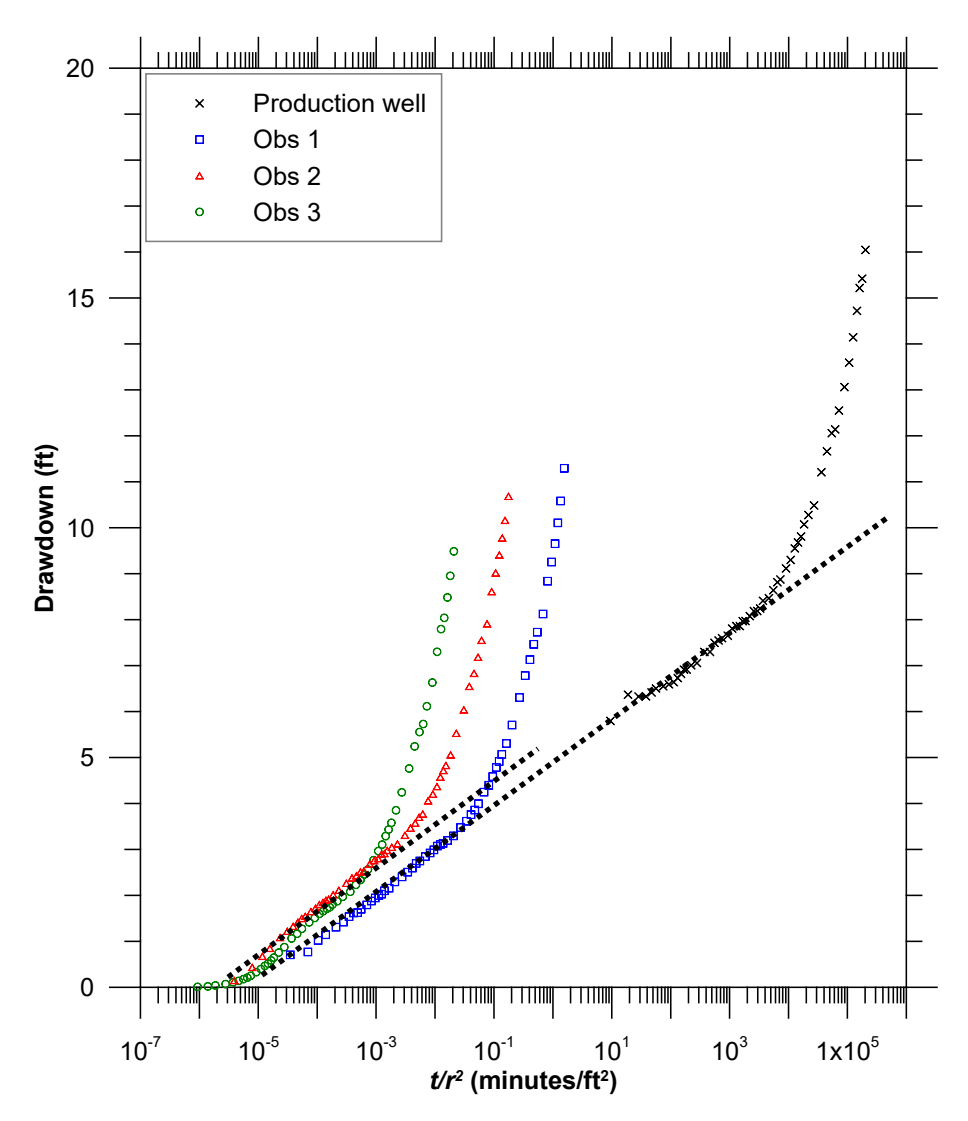


Figure 25. Composite plot with infinite aquifer response

The derivative can also be used to confirm the diagnosis of the early portions of the aquifer response. The "raw" drawdown derivatives for all of the wells are shown in Figure 26. The derivative is calculated using the nearest-neighbor approach.

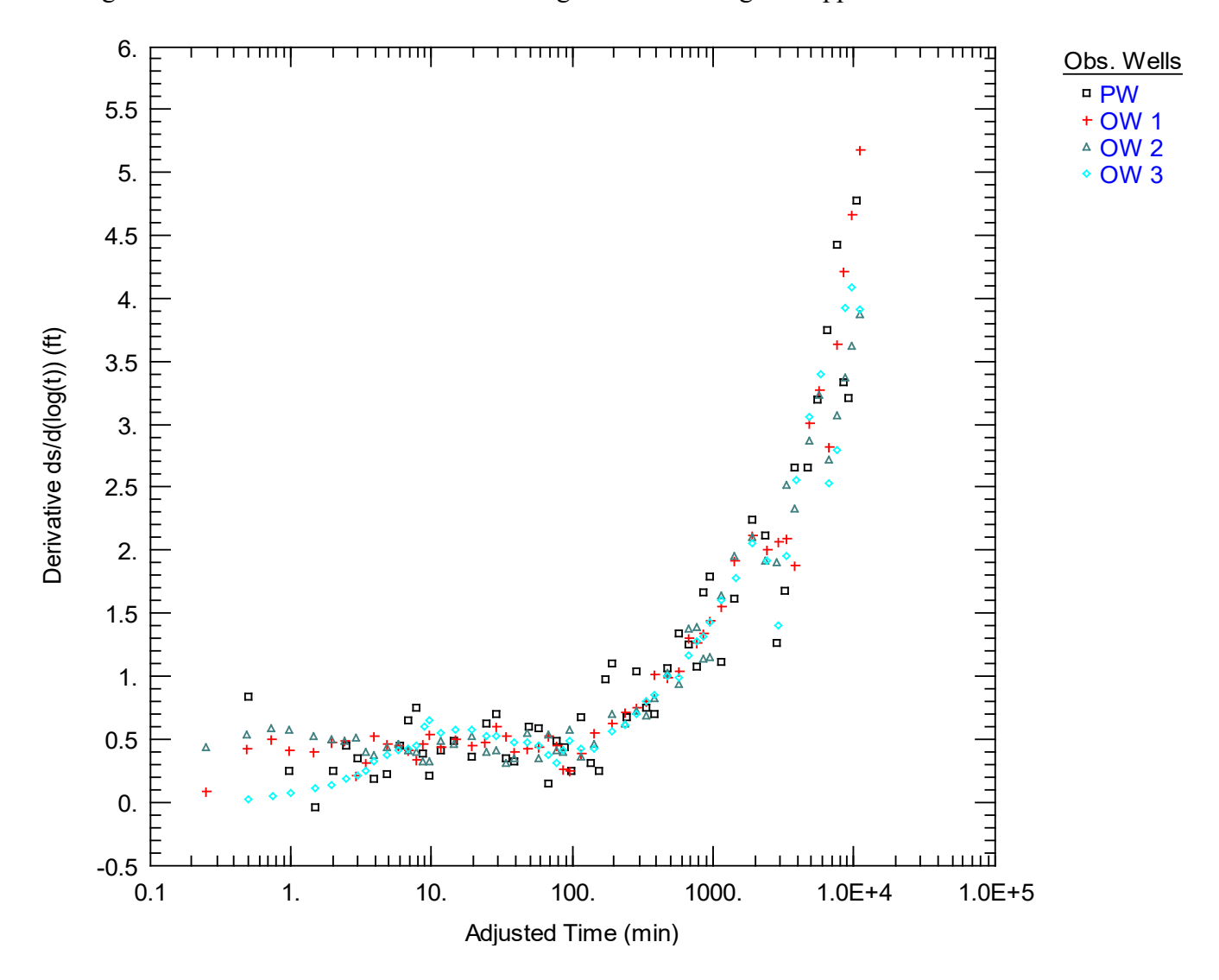


Figure 26. Drawdown derivatives calculated with the nearest neighbour approach

The "raw" drawdown derivatives are not that rough. It is possible to identify gross trends. To improve the visualization, we apply a relatively small amount of smoothing. The "smoothed" drawdown derivatives for all of the wells are shown in Figure 27. We see that the drawdowns reach a plateau between 10 and 100 minutes, followed by a rapid increase. The presence of a plateau suggests that there is a period during which the aquifer responds as if it were unbounded, the period of Infinite Acting Radial Flow (IARF). The increasing rate of change beyond the IARF period is characteristic of a groundwater system with that is enclosed by more than one impermeable boundary.

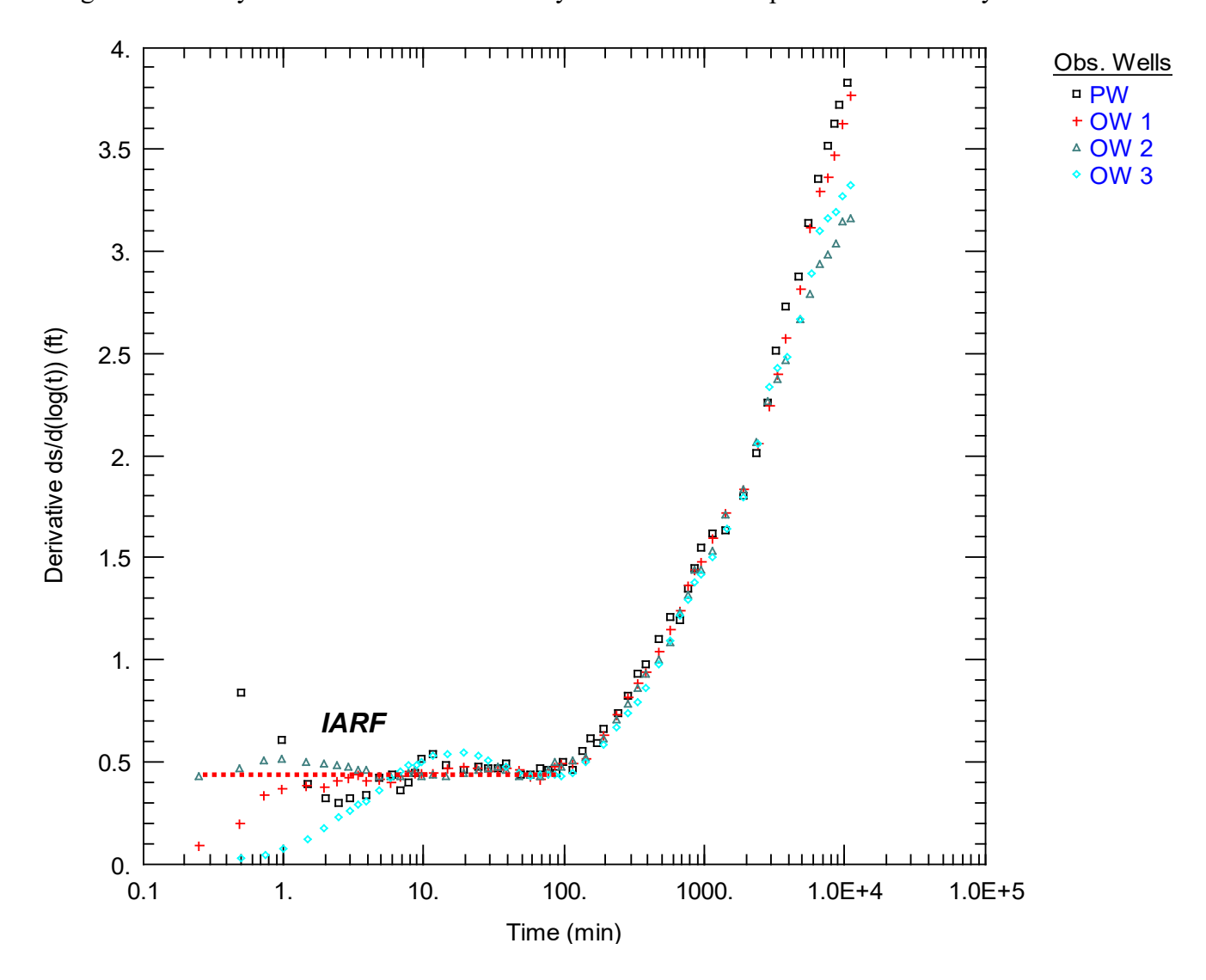


Figure 27. Smoothed drawdown derivatives

Estimation of transmissivity

The Cooper and Jacob straight-line (CJSL) analysis on the composite plot provides a reliable basis for estimating the transmissivity. The slope and intercept of the linear portion of the data are 3.65 ft per \log_{10} cycle of (t/r^2) , and $(t/r^2)_0 = 3.0 \times 10^{-6}$, respectively. When these values are substituted into the Cooper and Jacob formulae, a transmissivity of 21,000 ft²/d is estimated, along with a storativity of 1.0×10^{-4} .

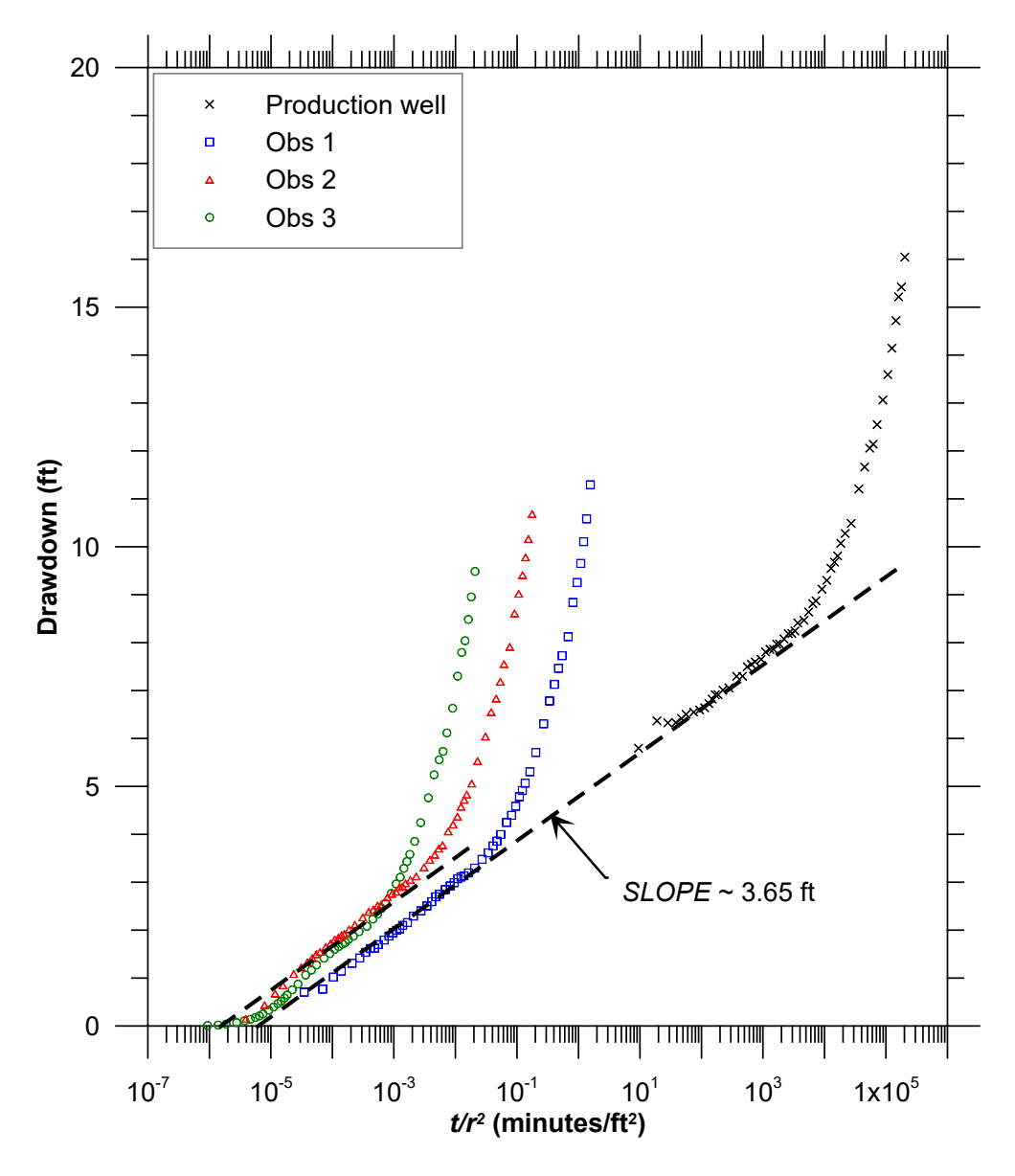


Figure 28. Cooper-Jacob straight-line analysis

As a check on the estimation of the transmissivity and storativity, the estimated parameters are used to calculate the drawdown with the Theis solution. As shown in the log-log composite plot in Figure 29, the match between the theoretical solution and the common portions of the data from each observation well is excellent. The deviations from the Theis curve become very clear when the data are plotted in this format.

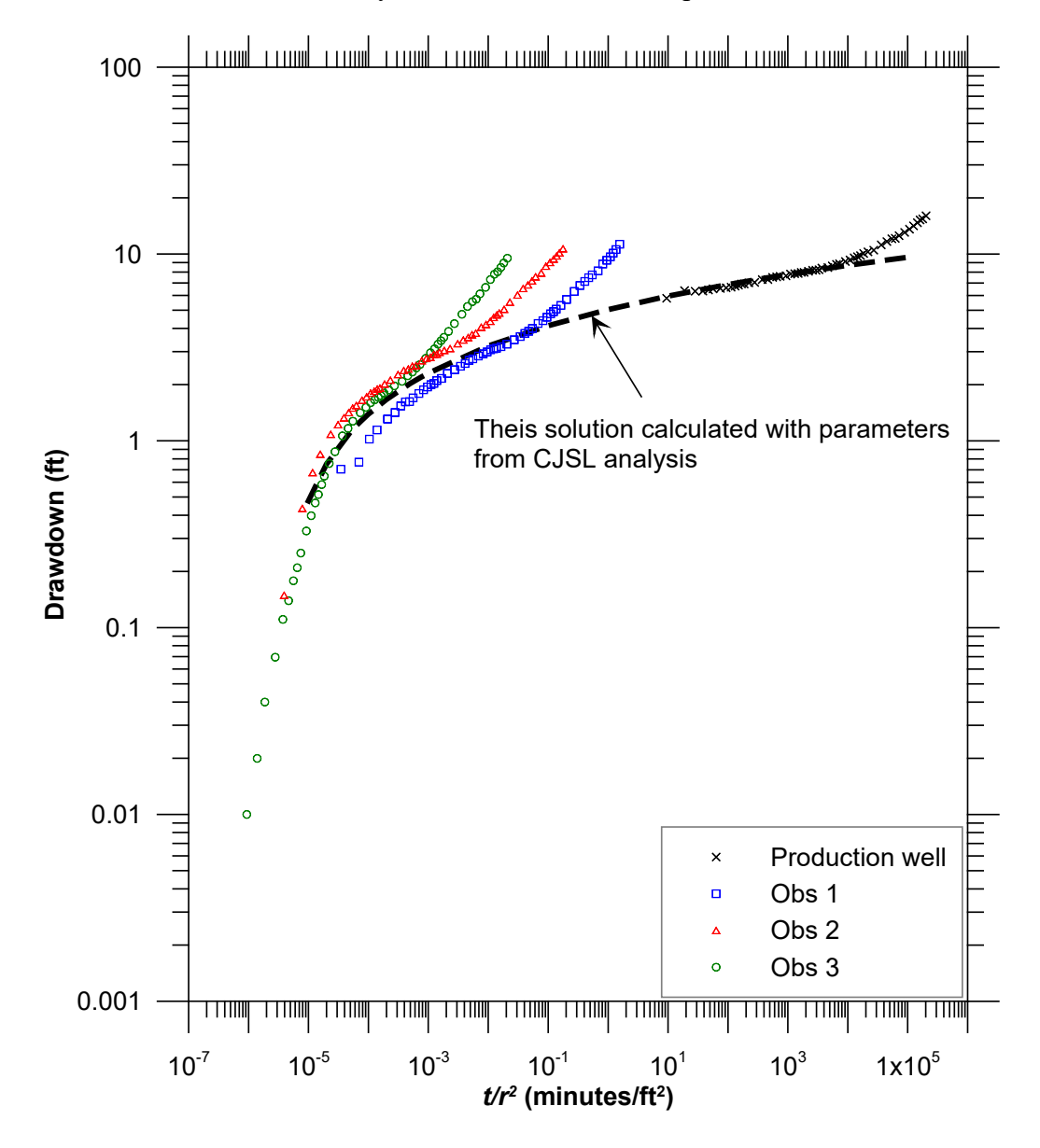
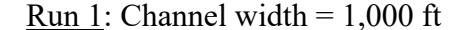


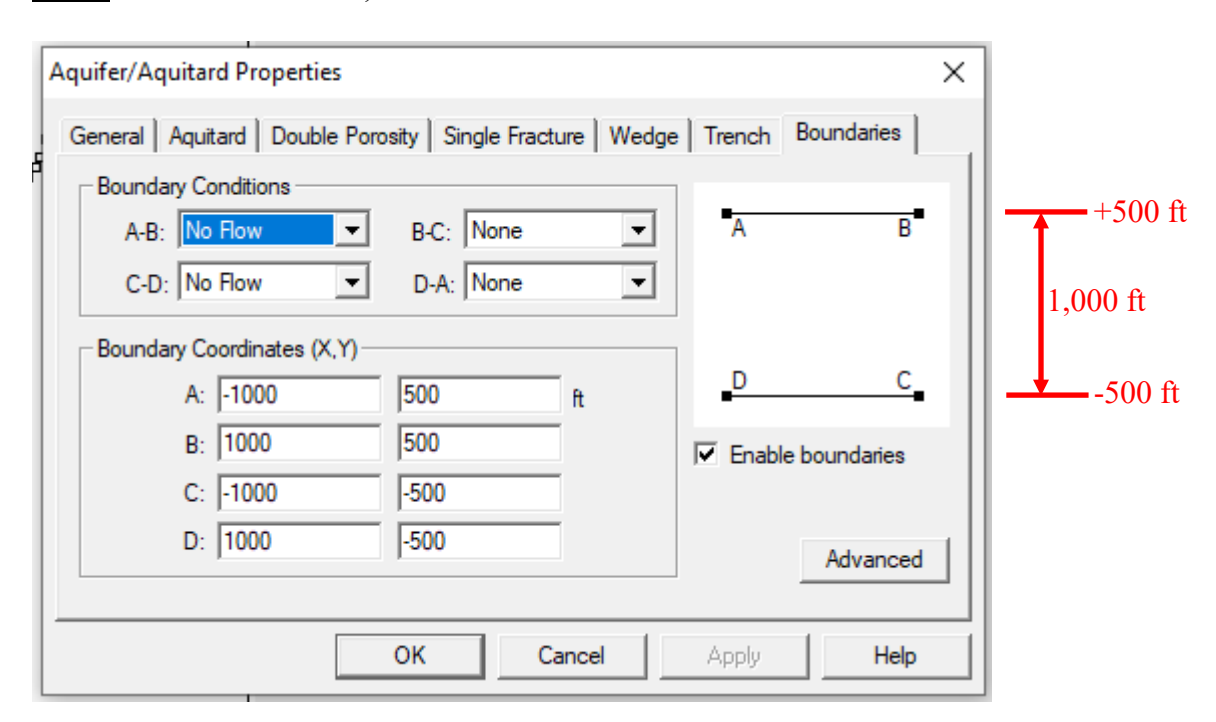
Figure 29. Check on Cooper-Jacob straight-line analysis with Theis solution

Re-analysis of the Estevan test using a channel aquifer model

As a final analysis, we retain the parameter estimates from the Cooper-Jacob analysis in Figure 28, but we invoke the model for a channel aquifer. The only change we make is that we assume the pumping well and observation wells are located in a long channel aquifer with impermeable walls. We don't know how wide the channel is, or where the wells are located with respect to the valley walls. For simplicity, we will assume that the pumping well and the observation wells are located along the axis of the channel (*x*-axis). We will try to estimate the width of the channel through trial-and-error.

For the following trials we retain the transmissivity estimated from the Cooper-Jacob composite analysis.





The results of the first guess of the channel width are shown in Figure 29. As shown in the figure, the Theis solution supplemented with image well analysis doesn't match the observations particularly well, but the general trends appear to be correct. We are on to something.

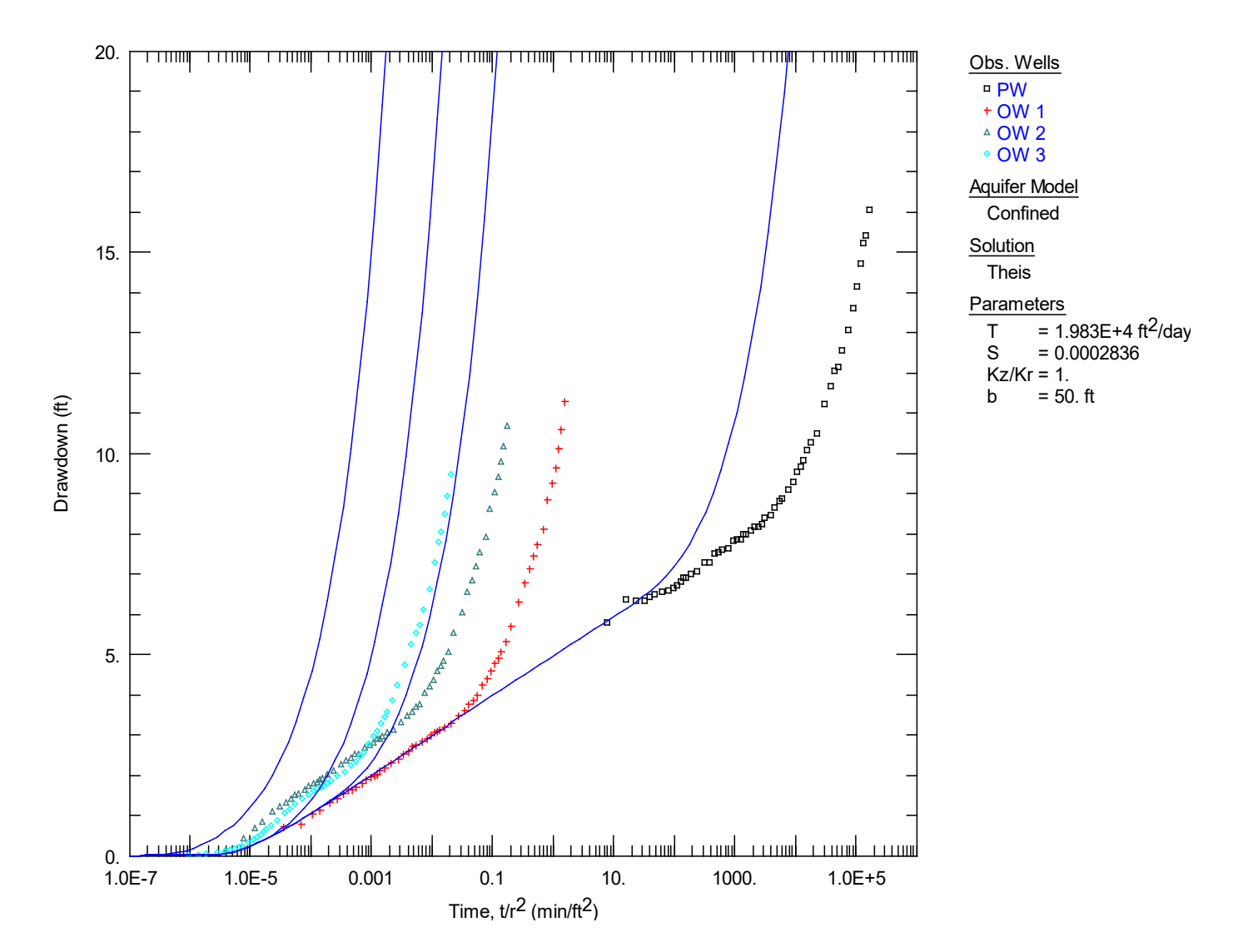
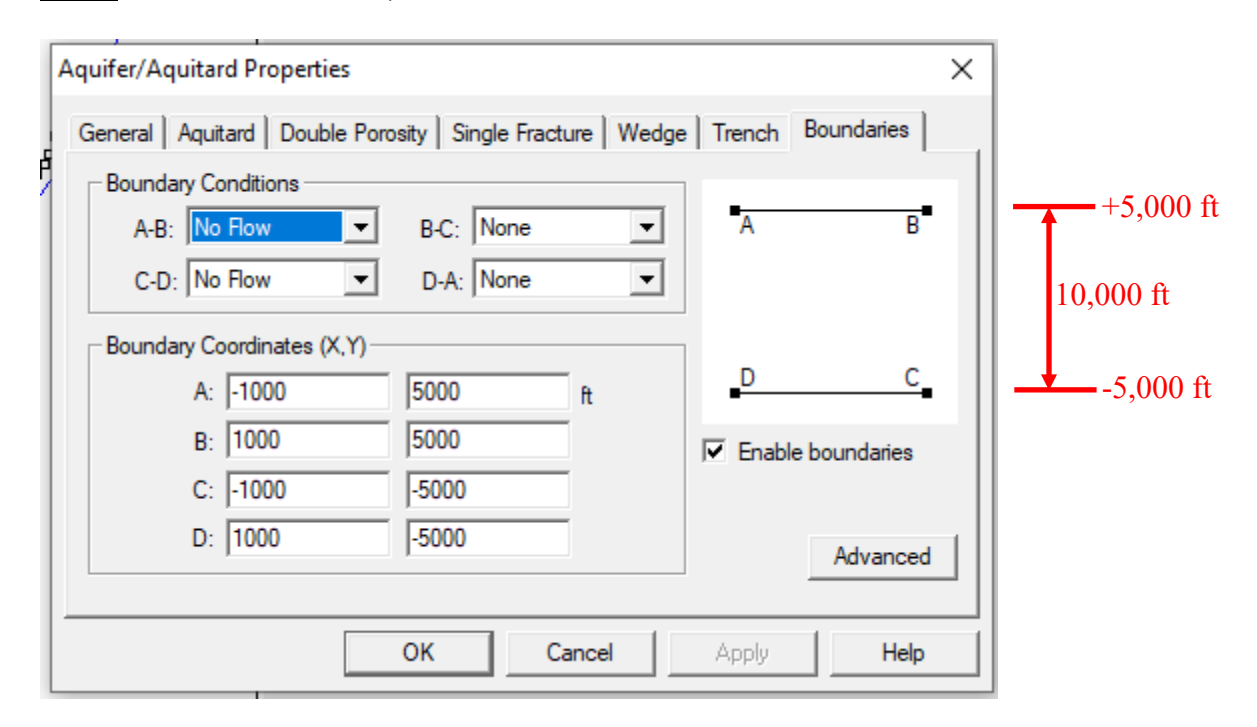


Figure 29. Buried channel analysis for a valley 1,000 ft wide

Run 2: Channel width = 10,000 ft



The results of the second guess of the channel width are shown in Figure 30. As shown in the figure, the Theis solution supplemented with image well analysis is much closer to reproducing both the magnitudes and trends of the observed drawdowns. One more trial ought to do it.

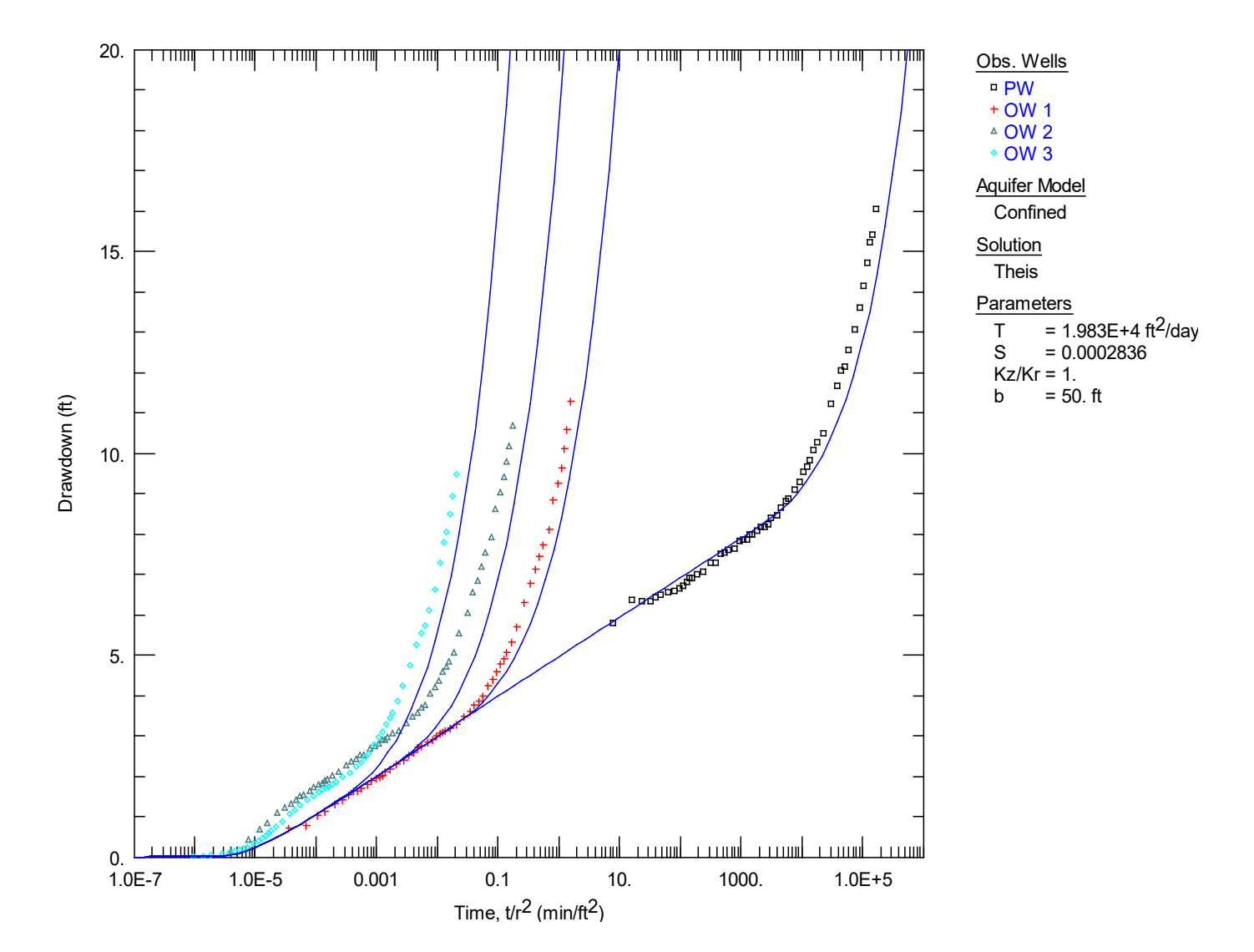
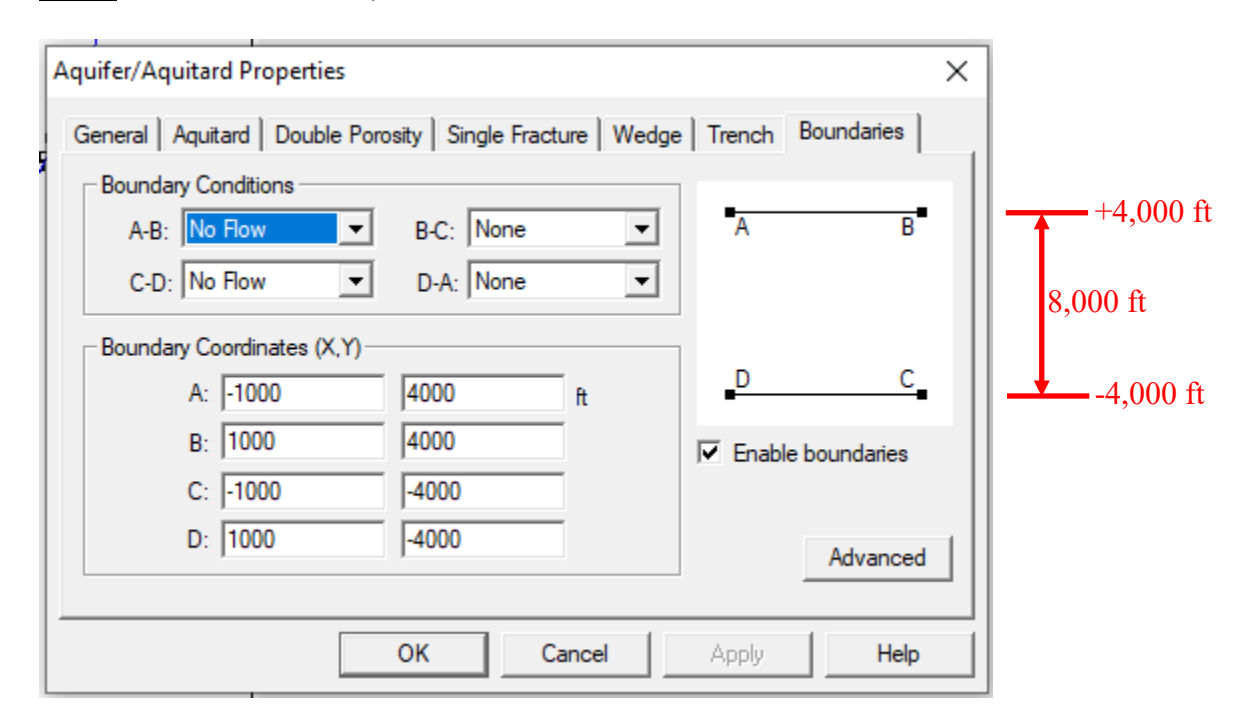


Figure 30. Buried channel analysis for a valley 10,000 ft wide

Run 3: Channel width = 8,000 ft



The results of the third guess of the channel width are shown in Figure 31. As shown in the figure, the Theis solution supplemented with image well analysis matches closely the observed drawdowns with the transmissivity estimated from the Cooper-Jacob composite analysis. The corresponding derivative plot is shown in Figure 32. The match to the drawdowns reproduces the key trend in the derivative: a steeply increasing semilog rate of drawdown, with no suggestion of a late-time plateau.

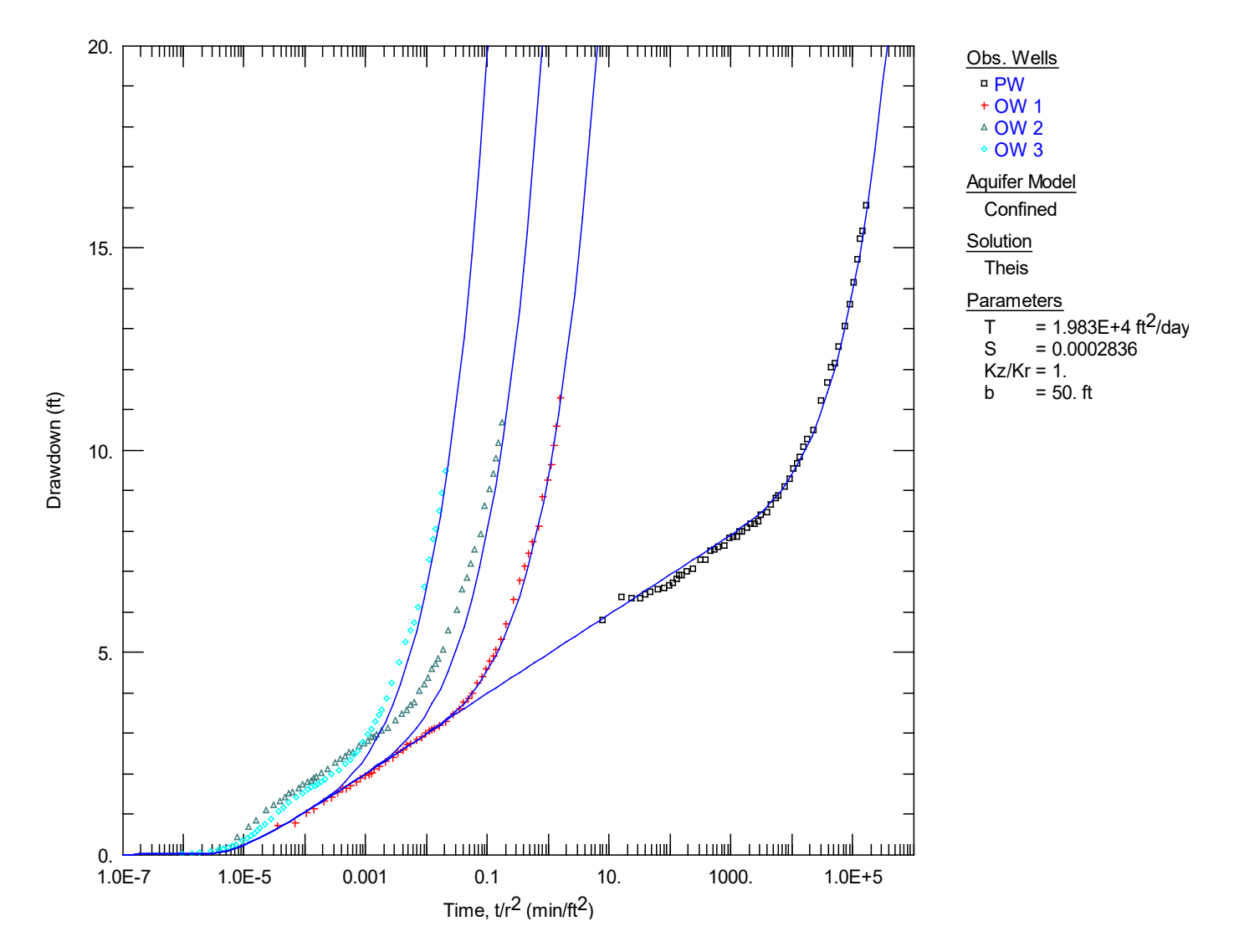


Figure 31. Buried channel analysis for a valley 8,000 ft wide

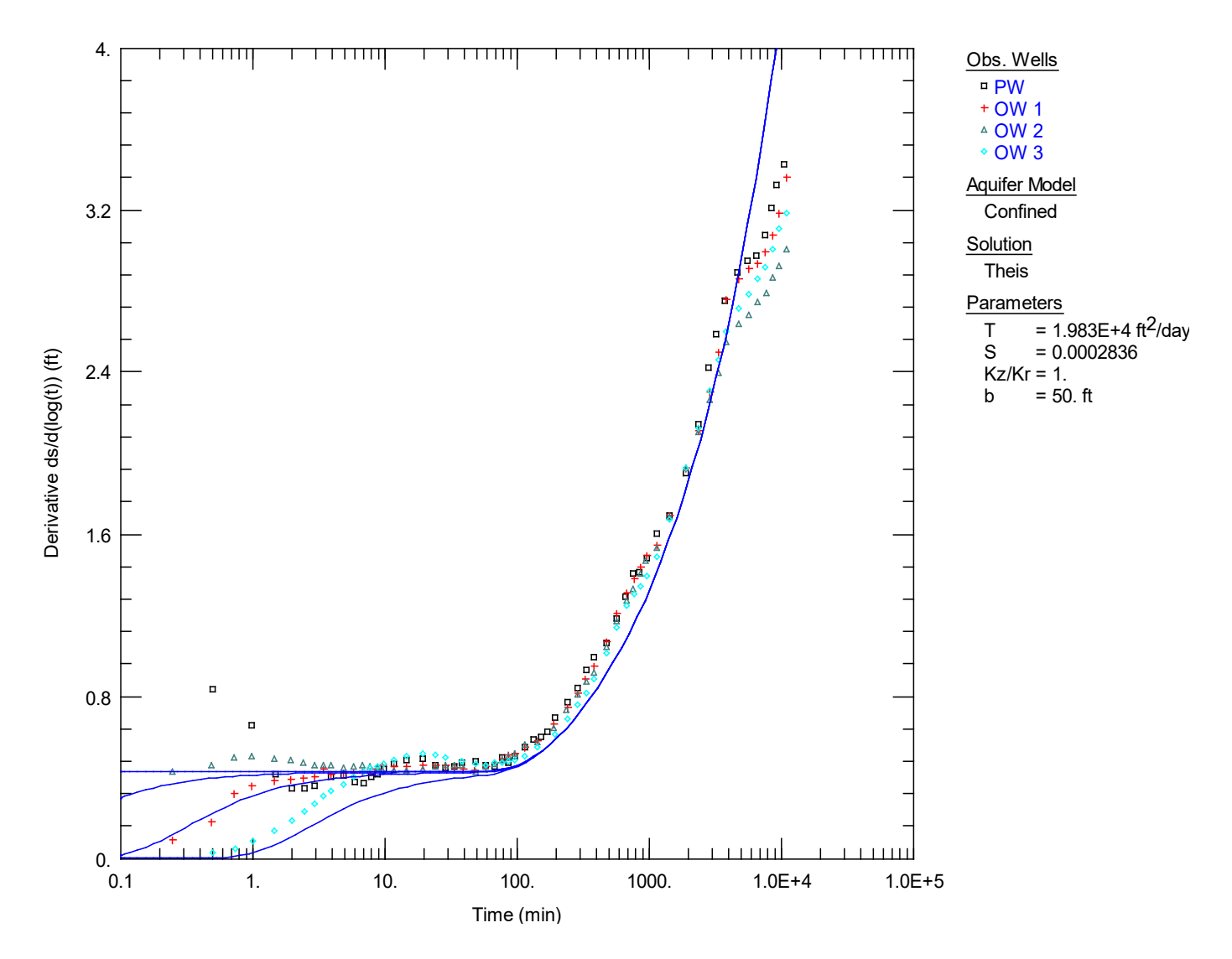


Figure 32. Calculated drawdown derivative for a channel aquifer 8,000 ft wide

Additional analyses considering aquitard leakage

In our previous analysis of the pumping test conducted in the Estevan Aquifer in 1965, we assumed that the aquifer is a perfectly confined strip. In reality, no aquifer is perfectly confined and if pumping continues sufficiently long we can expect to observe the effects of leakage across confining units. Here we demonstrate that the analysis for a confined strip aquifer can be generalized for an aquifer model that considers leakage. We will consider the simplest implementation of this conceptual model, the solution of Hantush and Jacob (1955). A conceptual model for the analysis is shown in Figure 33.

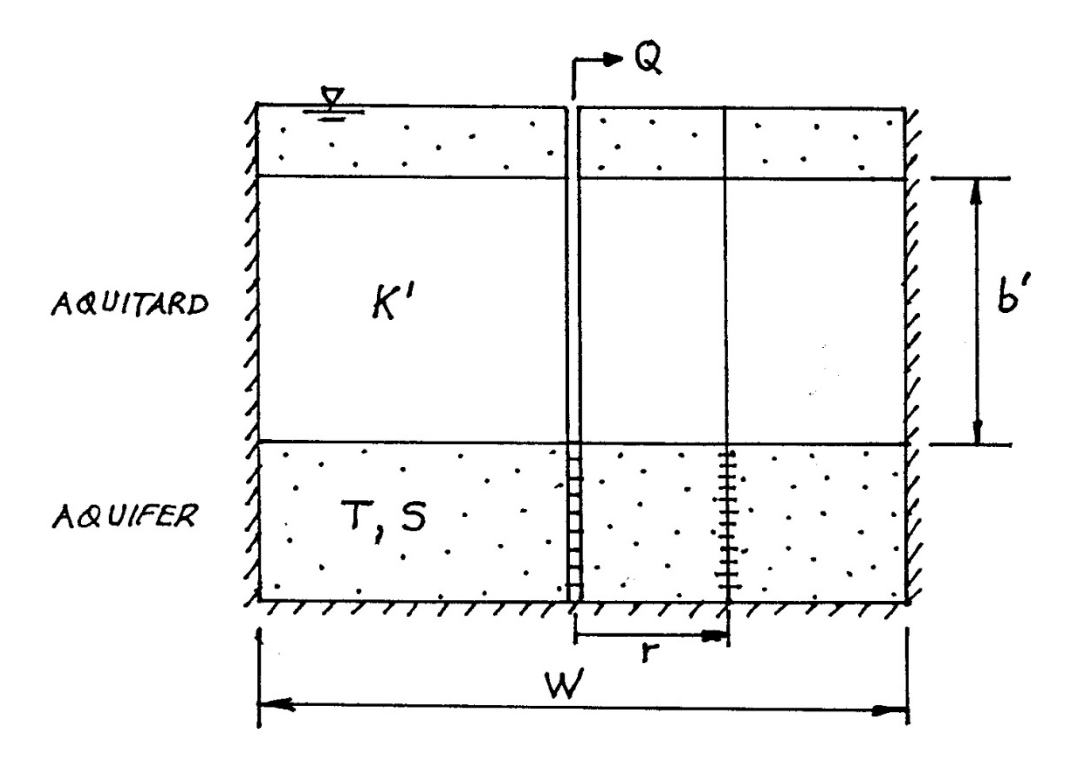


Figure 33. Conceptual model for a strip aquifer with leakage [Cross-section transverse to the axis of the buried channel aquifer]

Analysis #1: Negligible leakage

For a first analysis, we check that the AQTESOLV calculations with the Hantush-Jacob solution, with image wells representing the impermeable valley walls, are the same as those obtained with the Theis solution, when leakage is negligible. The results shown in Figure 34, for a leakage parameter $1/B = 10^{-6}$ ft⁻¹, are identical to those obtained with the Theis solution.

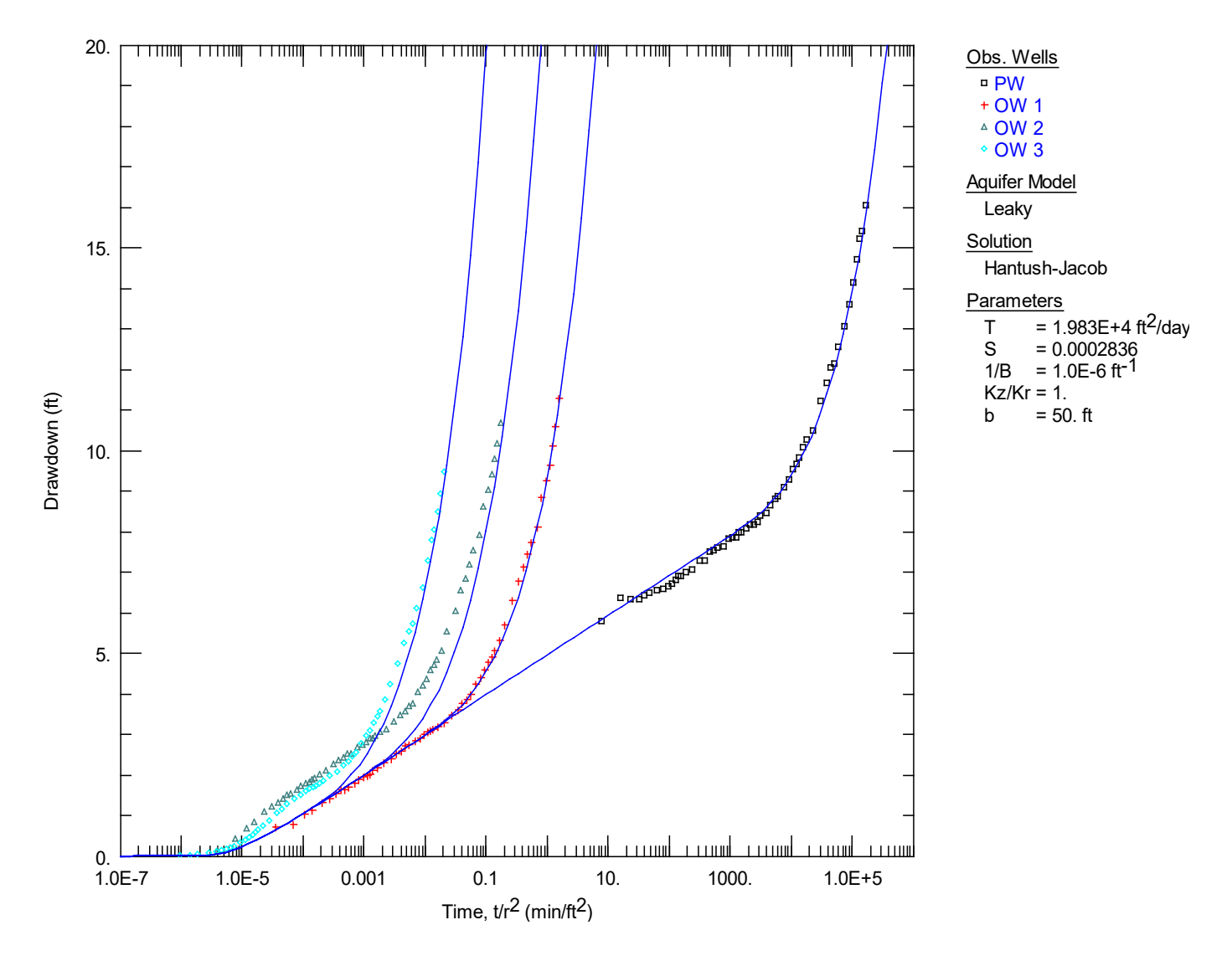


Figure 34. Hantush-Jacob analysis for a strip aquifer, $1/B = 10^{-6}$ ft⁻¹

Analysis #2: More significant leakage

Results with the Hantush-Jacob solution for a strip aquifer for a higher leakage parameter $1/B = 4 \times 10^{-5}$ ft⁻¹ are shown in Figure 35. The results suggest that for this value of 1/B, it should have been possible to detect the stabilization caused by leakage by the end of the test. Since this is not the case, the results suggest that $1/B = 4 \times 10^{-5}$ ft⁻¹ is too high.

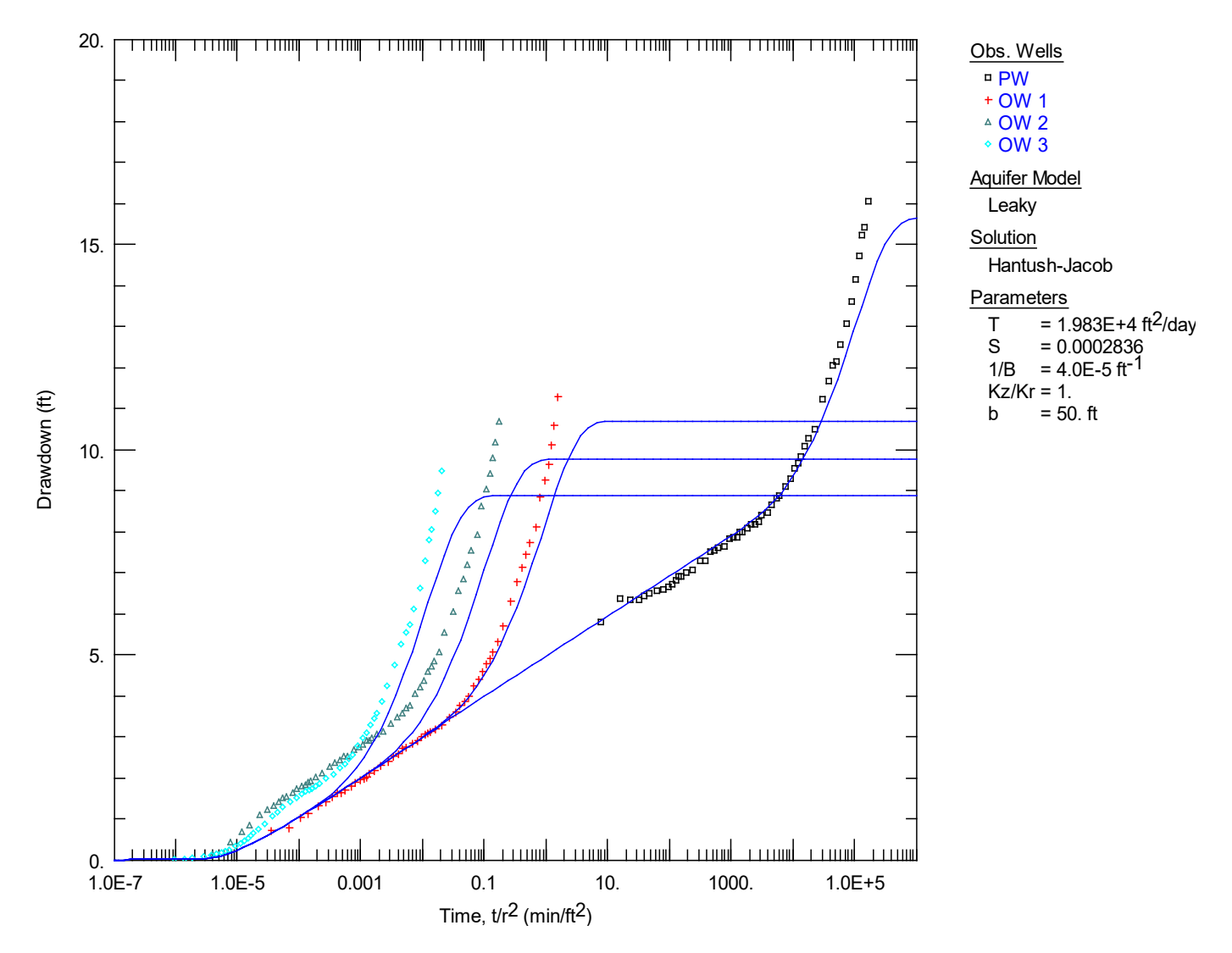


Figure 35. Hantush-Jacob analysis for a strip aquifer, $1/B = 4 \times 10^{-5}$ ft⁻¹

Analysis #3: Reduced leakage

Results with the Hantush-Jacob solution are shown in Figure 36 for a smaller value of the leakage parameter $1/B = 3 \times 10^{-5}$ ft⁻¹. The results of the analytical calculations are not inconsistent with the observations.

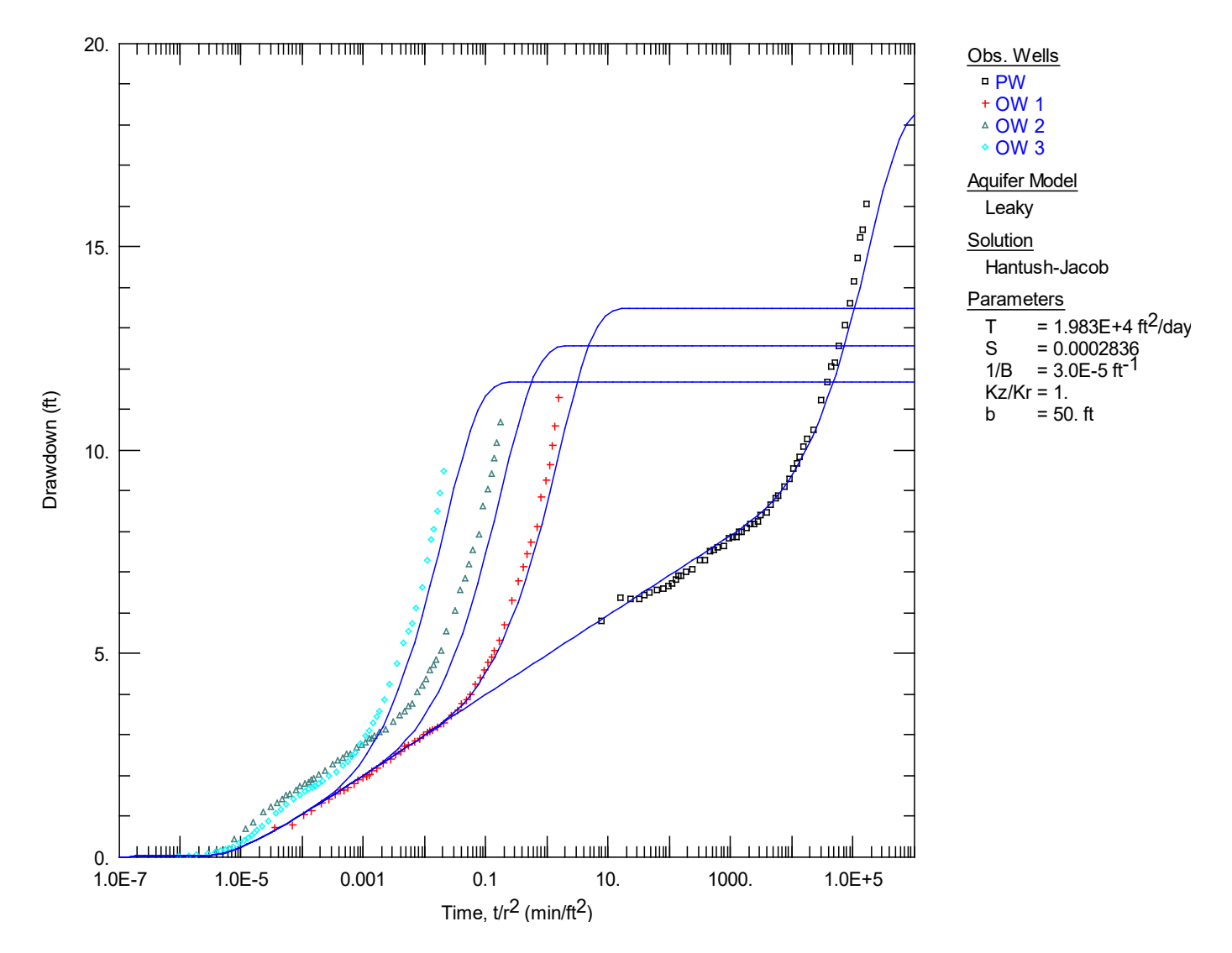


Figure 36. Hantush-Jacob analysis for a strip aquifer, $1/B = 3 \times 10^{-5}$ ft⁻¹

The results shown in Figure 36 place an *upper* bound on the likely value of 1/B that can be inferred from the observations. What does a value of 1/B of 3×10^{-5} ft⁻¹ tell us about the vertical hydraulic conductivity of the aquitard that overlies the Estevan Aquifer?

The parameter 1/B is defined as:

$$\frac{1}{B} = \sqrt{\frac{K'}{Tb'}}$$

Here *K*' and *b*' are the vertical hydraulic conductivity and thickness of the aquitard, respectively, and *T* is the transmissivity of the aquifer.

Solving for *K* 'yields:

$$K' = \left(\frac{1}{B}\right)^2 Tb'$$

- The transmissivity of the aquifer is estimated as 19,800 ft²/day.
- The thickness of the aquitard is about 75 m (this is the "effective thickness" of the aquitard reported in van der Kamp and Maathuis, 2012).

The upper bound estimate for the vertical hydraulic conductivity of the aquitard is:

$$K' = (3 \times 10^{-5} \text{ ft}^{-1})^2 (19,380 \text{ ft}^2/\text{d}) \left(75 m \left| \frac{3.281 \text{ ft}}{m} \right| \right)$$

= $4.3 \times 10^{-3} \text{ ft/d} = 5 \times 10^{-8} \text{ m/s}$

van der Kamp and Maathuis (2012) suggested that a representative vertical hydraulic conductivity for the glacial till overlying the Estevan Aquifer is 1.8×10^{-10} m/s. This corresponds to a value of $1/B=3.2\times 10^{-6}$ ft⁻¹. It is important to note that the vertical hydraulic conductivity estimated here represents an *upper* bound. It is certainly possible that the aquitard conductivity is less than 1.5×10^{-8} m/s. As suggested in Figure 37, it would have been necessary to continue pumping for much longer to infer the effects of aquitard leakage with a vertical hydraulic conductivity of 1.8×10^{-10} m/s.

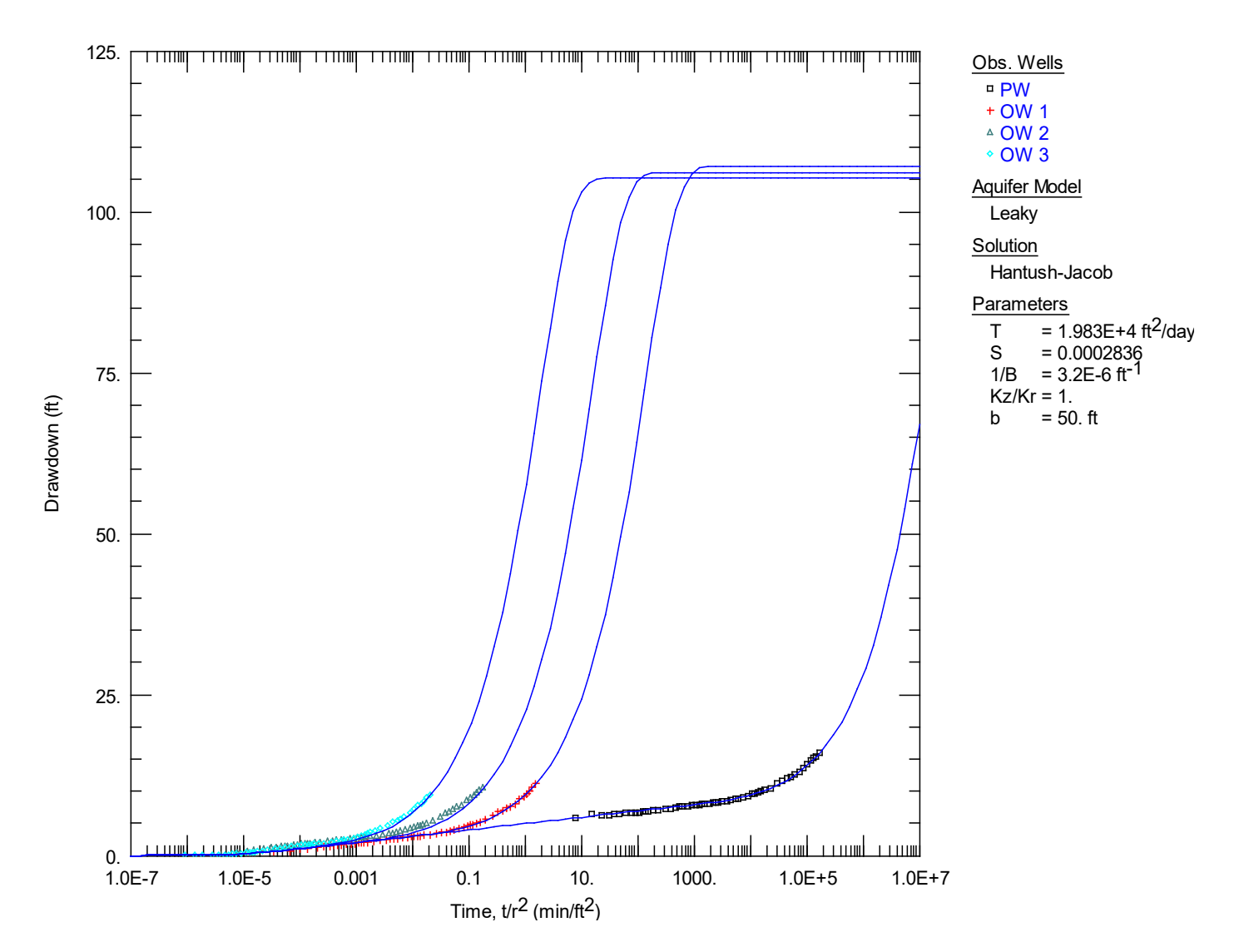


Figure 37. Hantush-Jacob analysis for a strip aquifer, $1/B = 3.2 \times 10^{-6} \text{ ft}^{-1}$

6. Key points

- 1. All aquifers are bounded. In many cases of practical significance, neglecting the boundaries may be highly restrictive.
- 2. Pumping tests conducted near a linear boundary (for example, a stream or a fault) can be interpreted by superposing Theis solutions in space, using what are referred to as *image wells*.
- 3. A linear constant-head boundary is simulated with an imaginary well placed an equal distance from the boundary, pumping at a rate equal in magnitude, but opposite in sign, to the actual well.
- 4. A linear no-flow boundary is simulated with an imaginary well placed an equal distance from the boundary, pumping at a rate equal in magnitude, with the same sign, as the actual well.
- 5. For a strip aquifer that is bounded on both sides by no-flow boundaries, an infinite number of image wells are required. In practice, the calculations frequently converge to the same result with a relatively small number of image wells.
- 6. The application of the Derivative Analysis enhances our ability to diagnose the effects of boundaries.
- 7. The composite plot is an effective method for synthesizing drawdown data and identifying the appropriate portion of the response for the estimation of aquifer properties.

7. References

- Betcher, R.N., G. Matile, and G. Keller, 2005: Yes Virginia, there are buried valley aquifers in Manitoba, in *Proceedings of the 58th Canadian Geotechnical and 6th Joint IAH-CNC and CGS Conference*, Saskatoon, Saskatchewan, 6 p.
- Cooper, H.H., Jr., and C.E. Jacob, 1946: A generalized graphical method for evaluating formation constants and summarizing well-field history, *Trans. American Geophysical Union*, vol. 27, no. 4), pp. 526-534.
- Farvolden, R.N., 1963: Bedrock channels of southern Alberta, in *Early Contributions to Groundwater Hydrology of Alberta*, Research Council of Alberta Bulletin 12, pp. 63-75.
- Kruseman, G.P., and N.A. de Ridder, 1990: **Analysis and Evaluation of Pumping Test Data**, 2nd ed., International Institute for Land Reclamation and Improvement, Wageningen, The Netherlands.
- Maathuis, H., and G. van der Kamp, 2003: Groundwater resource evaluations of the Estevan Valley aquifer in southeastern Saskatchewan: A 40-year historical perspective, in *Proceedings of the 56th Canadian Geotechnical and 3rd Joint IAH-CNC and CGS Conference*, Winnipeg, Manitoba, 4 p.
- Motz, L.H., 1991: Aquifer parameters from constant discharge Nonsteady-leaky type curves, *Ground Water*, vol. 29, no. 2, pp. 181-185.
- Russell, H.A.J., M.J. Hinton, G. van der Kamp, and D.R. Sharpe, 2004: An overview of the architecture, sedimentology and hydrogeology of buried-valley aquifers in Canada, in *Proceedings of the 57th Canadian Geotechnical and 4th Joint IAH-CNC and CGS Conference*, Québec, Québec, 8 p.
- Vandenberg, A., 1977: Type curves for analysis of pump tests in leaky strip aquifers, *Journal of Hydrology*, vol. 33, pp. 15-26.
- van der Kamp, G., and H. Maathuis, 2002: The peculiar groundwater hydraulics of buried-channel aquifers, in *Proceedings of the 55th Canadian Geotechnical and 3rd Joint IAH-CNC and CGS Groundwater Specialty Conference*, Niagara Falls, Ontario, pp. 695-698.

van der Kamp, G., and H. Maathuis, 2012: The unusual and large drawdown response of buried-valley aquifers to pumping, *Ground Water*, vol. 50, no. 2, pp. 207-215.

Walton, W.C., 1970: **Groundwater Resource Evaluation**, McGraw-Hill Book Company, New York, New York.

Critical Thinking in Aquifer Test Interpretation

Pumping tests in aquifers with linear boundaries: Additional readings

Christopher J. Neville S.S. Papadopulos & Associates, Inc. Last update: April 28, 2025

- 1. Ferris, J.G., D.B. Knowles, R.H. Brown, and R.W. Stallman, 1962: excerpt from *Theory of Aquifer Tests*: Theory of Images and Hydrologic Boundary Analysis, United States Geological Survey, Water-Supply Paper 1536-E, pp. 144-166.
- 2. van der Kamp, G., and H. Maathuis, 2012: The unusual and large drawdown response of buried-valley aquifers to pumping, *Ground Water*, vol. 50, no. 2, pp. 2207-215.
- 3. Rafini, S., R. Chesnaux, A. Ferroud, 2017: A numerical investigation of pumping-test responses from continuous aquifers, *Hydrogeology Journal*, vol. 25, no. 3, pp. 877-894.

Theory of Aquifer Tests

By J. G. FERRIS, D. B. KNOWLES, R. H. BROWN, and R. W. STALLMAN

GROUND-WATER HYDRAULICS

GEOLOGICAL SURVEY WATER-SUPPLY PAPER 1536-E



THEORY OF IMAGES AND HYDROLOGIC BOUNDARY ANALYSIS

The development of the equilibrium and nonequilibrium formulas discussed in the preceding sections was predicated in part on the as-

sumption of infinite areal extent of the aquifer, although it is recognized that few if any aguifers completely satisfy this assumption. many instances the existence of boundaries serves to limit the continuity of the aquifer, in one or more directions, to distances ranging from a few hundred feet to as much as tens of miles. Thus when an aquifer is recognized as having finite dimensions, direct analysis of the test data by the equations previously given is often precluded. It is often possible, however, to circumvent the analytical difficulties posed by the aquifer boundary. The method of images, widely used in the theory of heat conduction in solids, provides a convenient tool for the solution of boundary problems in ground-water flow. Imaginary wells or streams, usually referred to as images, can sometimes be used at strategic locations to duplicate hydraulically the effects on the flow regime caused by the known physical boundary. Use of the image thus is equivalent to removing a physical entity and substituting a hydraulic entity. The finite flow system is thereby transformed by substitution into one involving an aquifer of infinite areal extent, in which several real and imaginary wells or streams can be studied by means of the formulas already given. Such substitution often results in simplifying the problem of analysis to one of adding effects of imaginary and real hydraulic systems in an infinite aquifer.

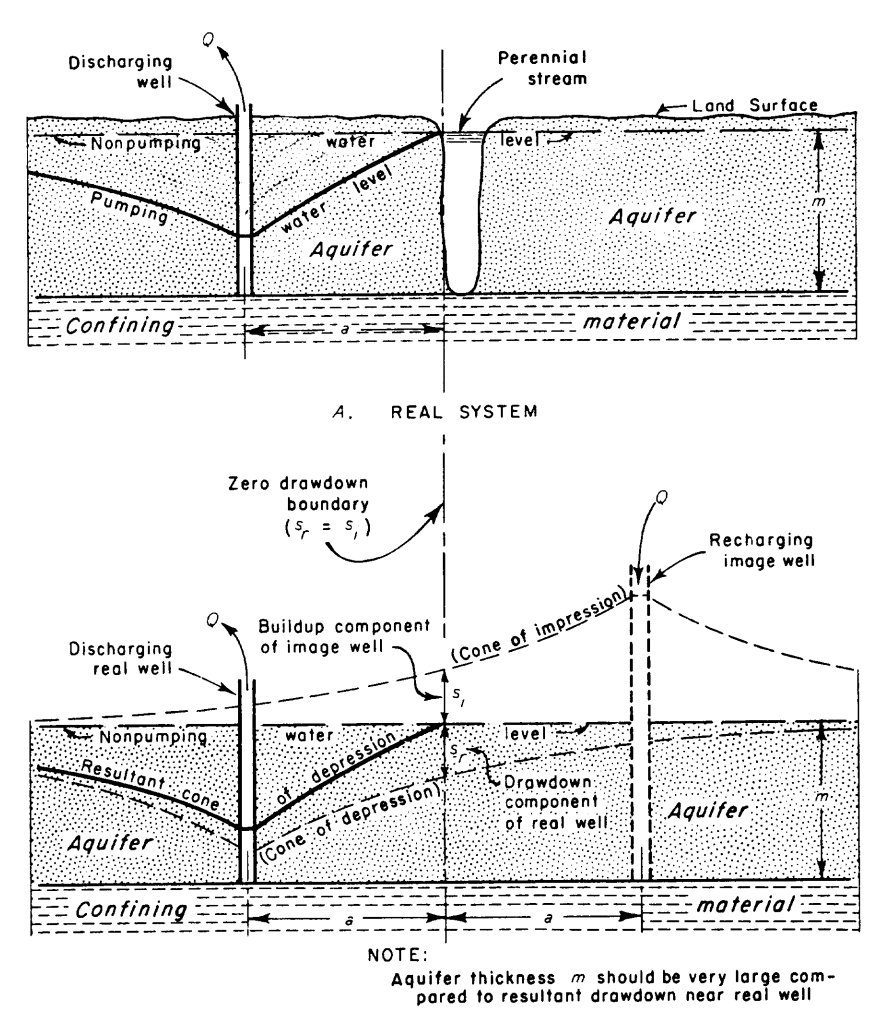
An aquifer boundary formed by an impermeable barrier, such as a tight fault or the impermeable wall of a buried stream valley that cuts off or prevents ground-water flow, is sometimes termed a "negative boundary." Use of this term is discouraged, however, in favor of the more meaningful and descriptive term "impermeable barrier." A line at or along which the water levels in the aquifer are controlled by a surface body of water such as a stream, or by an adjacent segment of aquifer having a comparatively large transmissibility or water-storage capacity, is sometimes termed a "positive boundary." Again, however, use of the term is discouraged in favor of the more precise terms line source or line sink, as may be appropriate.

Although most geologic boundaries do not occur as abrupt discontinuities, it is often possible to treat them as such. When conditions permit this practical idealization, it is convenient for the purpose of analysis to substitute a hypothetical image system for the boundary conditions of the real system.

In this section, where the analysis of pumping-test data is considered, several examples are given of image systems required to duplicate, hydraulically, the boundaries of certain types of areally restricted aquifers. It should be apparent that similar methods can be used to analyze flow to streams or drains through areally limited aquifers.

PERENNIAL STREAM-LINE SOURCE AT CONSTANT HEAD

An idealized section through a discharging well in an aquifer hydraulically controlled by a perennial stream is shown in figure 35A. For thin aquifers the effects of vertical-flow components are small at relatively short distances from the stream, and if the stream stage is not lowered by the flow to the real well there is established the boundary condition that there shall be no drawdown along the stream position. Therefore, for most field situations it can be assumed for practical purposes that the stream is fully penetrating and equivalent



parea to resultant arawaown lieur real well

B. HYDRAULIC COUNTERPART OF REAL SYSTEM

FIGURE 35.—Idealized section views of a discharging well in a semi-infinite aquifer bounded by a perennial stream, and of the equivalent hydraulic system in an infinite aquifer.

to a line source at constant head. An image system that satisfies the foregoing boundary condition, as shown in figure 35B, allows a solution of the real problem through use, in this example, of the Theis nonequilibrium formula. Note in figure 35B that an imaginary recharging well has been placed at the same distance as the real well from the line source but on the opposite side. Both wells are situated on a common line perpendicular to the line source. The imaginary recharge well operates simultaneously with the real well and returns water to the aguifer at the same rate that it is withdrawn by the real well. It can be seen that this image well produces a buildup of head everywhere along the position of the line source that is equal to and cancels the drawdown caused by the real well which satisfies the boundary condition of the problem. The resultant drawdown at any point on the cone of depression in the real region is the algebraic sum of the drawdown caused by the real well and the buildup produced by its The resultant profile of the cone of depression, shown in figure 19B, is flatter on the landward side of the well and steeper on the riverward side, as compared with the shape it would have if no boundary were present. Figure 36 is a generalized plan view of a flow net for the situation given in figure 35A. The distribution of stream lines and potential lines about the real discharging well and its recharging image, in an infinite aquifer, is shown. If the image region is omitted, the figure represents the stream lines and potential lines as they might be observed in the vicinity of a discharging well obtaining water from a river by induced infiltration.

IMPERMEABLE BARRIER

An idealized section through a discharging well in an aquifer bounded on one side by an impermeable barrier is shown in figure 37A. It is assumed that the irregularly sloping boundary can, for practical purposes, be replaced by a vertical boundary, occupying the position shown by the vertical dashed line, without sensibly changing the nature of the problem. The hydraulic condition imposed by the veritcal boundary is that there can be no ground-water flow across it, for the impermeable material cannot contribute water to the pumped well. The image system that satisfies this condition and permits a solution of the real problem by the Theis equation is shown in figure 37B. An imaginary discharging well has been placed at the same distance as the real well from the boundary but on the opposite side, and both wells are on a common line perpendicular to the boundary. At the boundary the drawdown produced by the image well is equal to the drawdown caused by the real well. dently, therefore, the drawdown cones for the real and the image wells will be symmetrical and will produce a ground-water divide at every point along the boundary line. Because there can be no flow

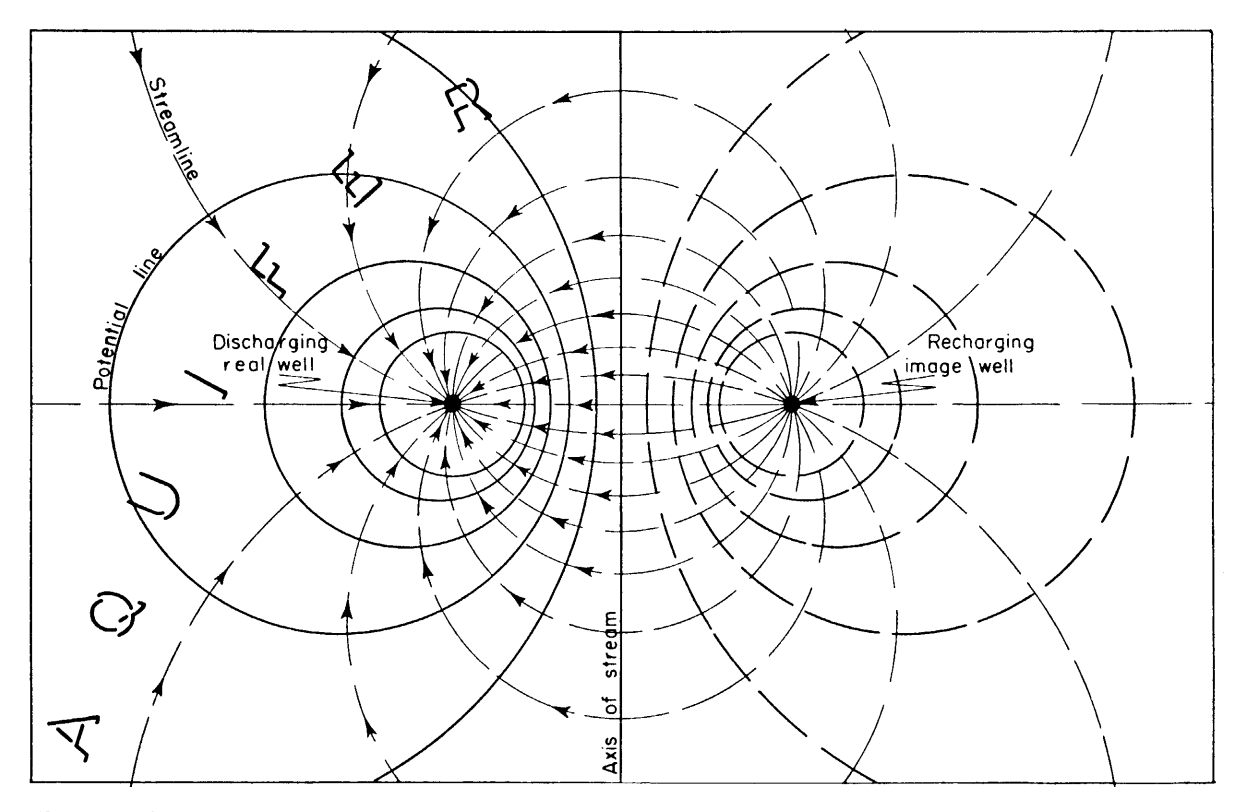
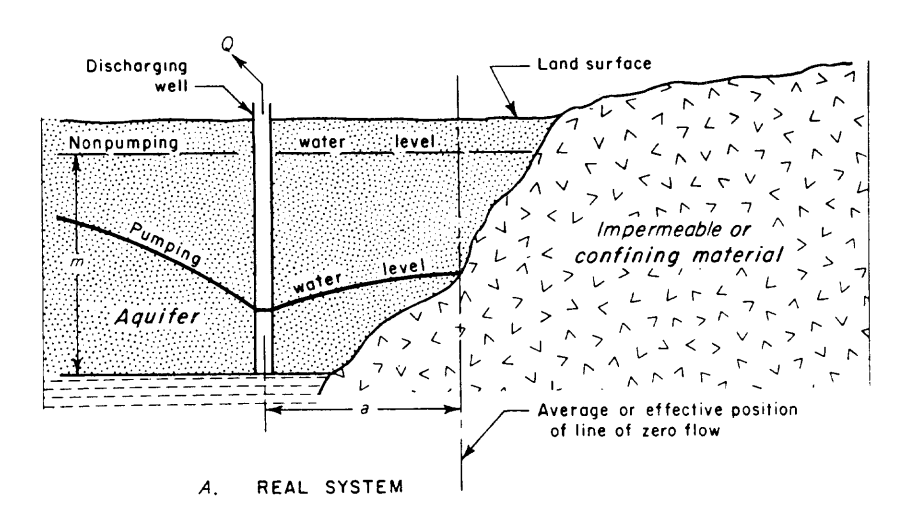
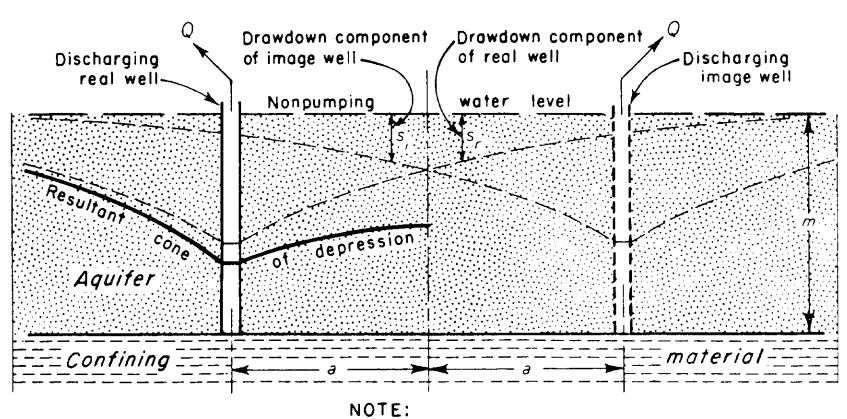


FIGURE 36.—Generalized flow net showing stream lines and potential lines in the vicinity of a discharging well dependent upon induced infiltration from a nearby stream.





Aquifer thickness $\,m\,$ should be very large compared to resultant drawdown near real well

B. HYDRAULIC COUNTERPART OF REAL SYSTEM

Figure 37.—Idealized section views of a discharging well in a semi-infinite aquifer bounded by an impermeable formation, and of the equivalent hydraulic system in an infinite aquifer.

across a divide, the image system satisfies the boundary condition of the real problem and analysis is simplified to consideration of two discharging wells in an infinite aquifer. The resultant drawdown at any point on the cone of depression in the real region is the algebraic sum of the drawdowns produced at that point by the real well and its image. The resultant profile of the cone of depression, shown in figure 37B, is flatter on the side of the well toward the boundary and steeper on the opposite side away from the boundary than it would be if no boundary were present. Figure 38 is a general-

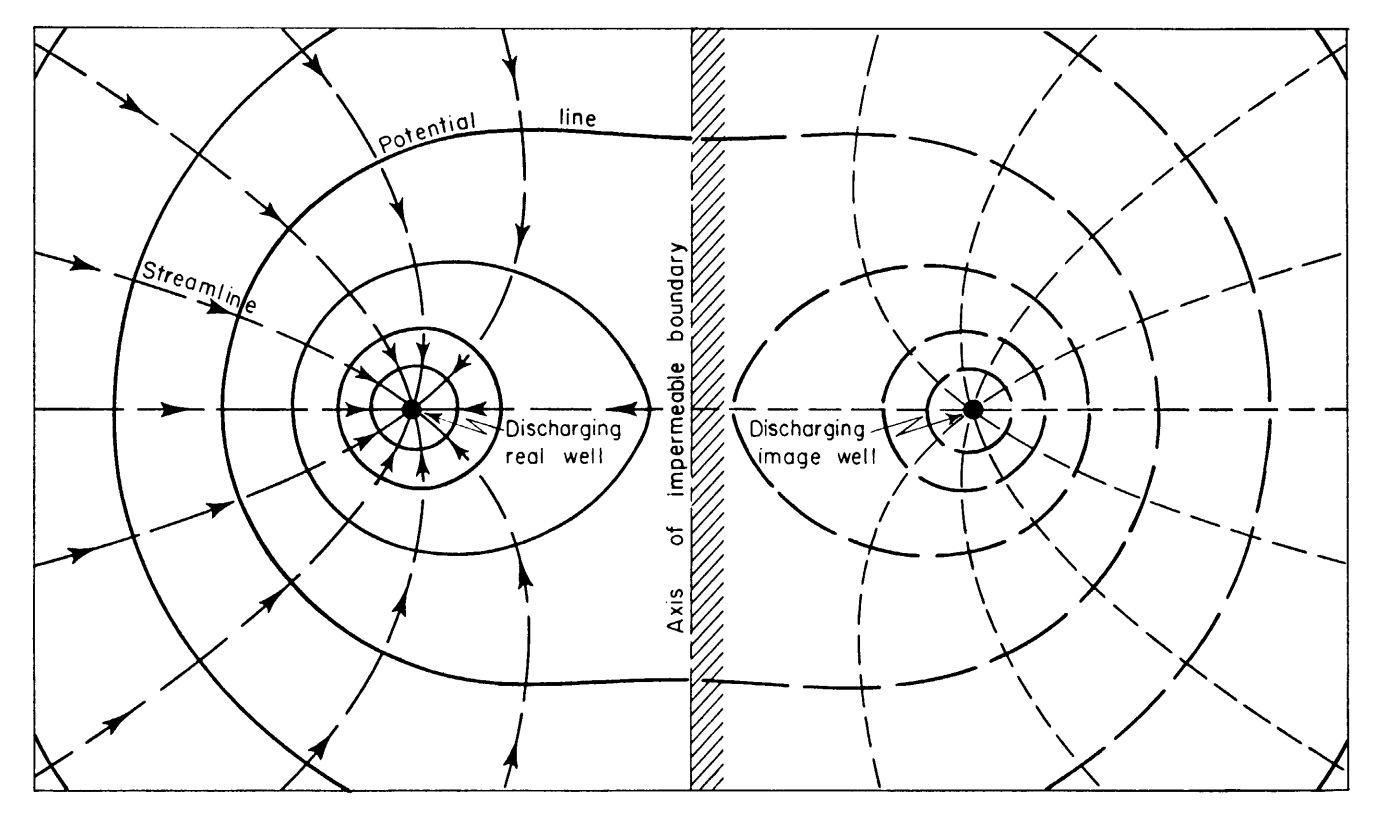
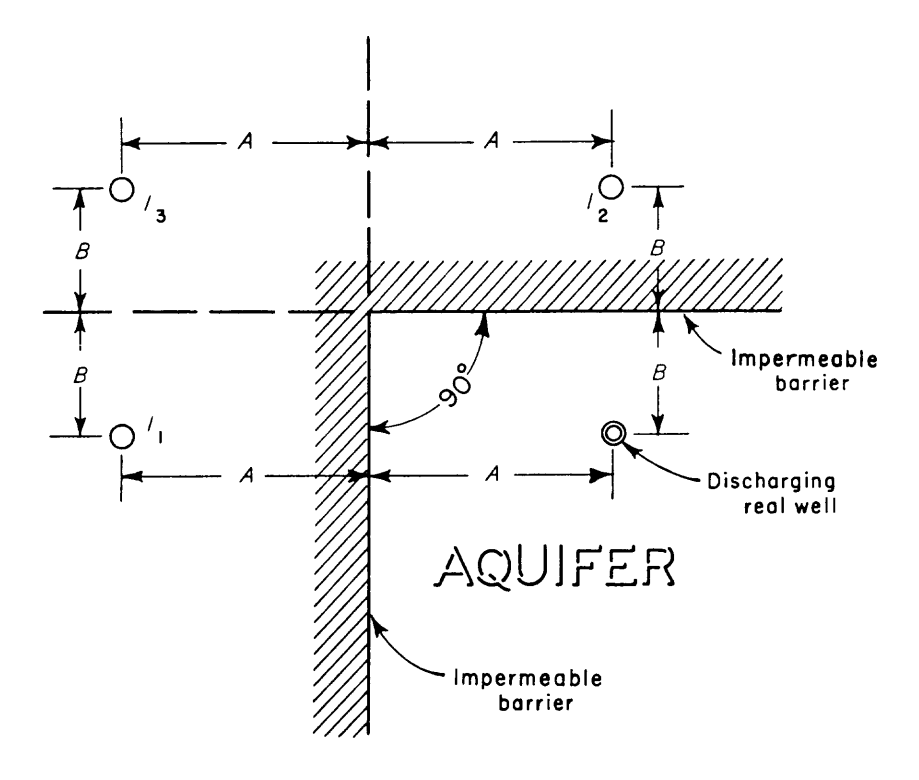


FIGURE 38.—Generalized flow net showing stream lines and potential lines in the vicinity of a discharging well near an impermeable boundary.

ized plan view of a flow net for the situation given in figure 37A. The distribution of stream lines and potential lines about the real discharging well and its discharging image, in an infinite aquifer, is shown. If the image region is omitted, the diagram represents the flow net as it might be observed in the vicinity of a discharging well located near an impermeable boundary.

TWO IMPERMEABLE BARRIERS INTERSECTING AT RIGHT ANGLES

The image-well system for a discharging well in an aquifer bounded on two sides by impermeable barriers that intersect at right angles is shown in figure 39. Although the drawdown effects of the primary image wells, I_1 and I_2 , combine in the desired manner with the effect



NOTES:

Image wells, /, are numbered in the sequence in which they were considered and located

Open circles signify discharging wells

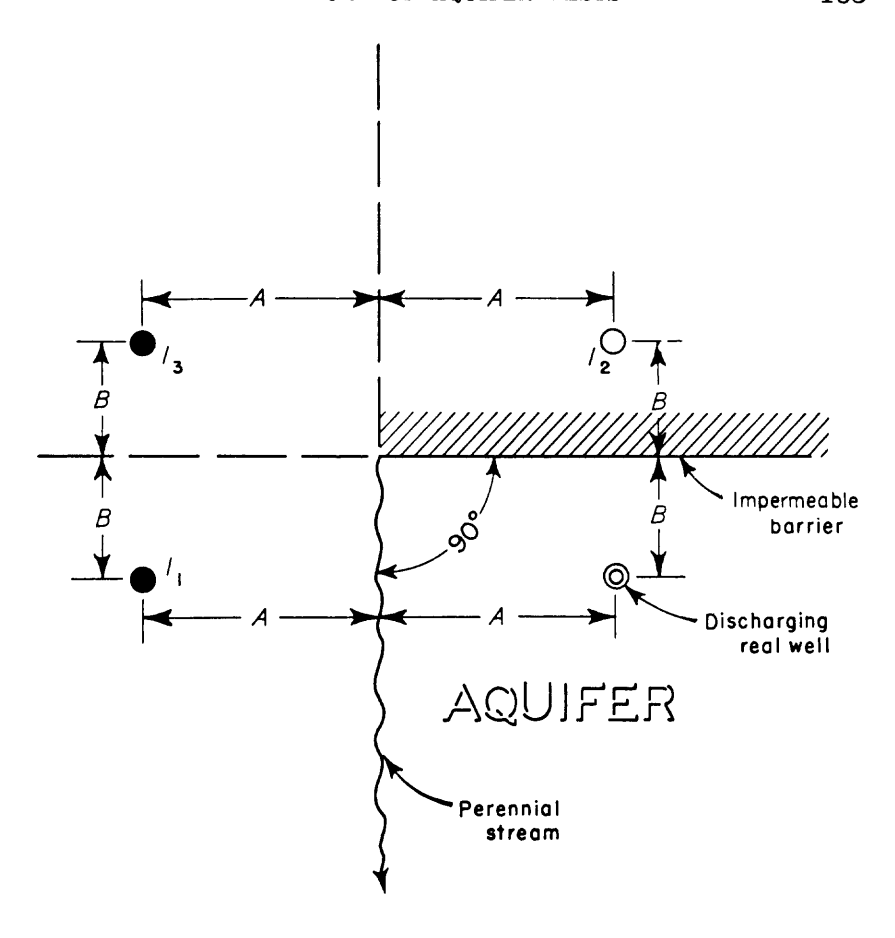
FIGURE 39.—Plan of image-well system for a discharging well in an aquifer bounded by two impermeable barriers intersecting at right angles.

of the real well at their respective boundaries, each image well produces an unbalanced drawdown at the extension (reflection) of the other boundary. These unbalanced drawdowns at the boundaries produce a hydraulic gradient, with consequent flow across the extension of each boundary, and therefore do not completely satisfy the requirement of no flow across the boundaries of the real system. It is necessary, therefore, to use a secondary image well, I_3 , which balances the residual effects of the two primary image wells at the two extensions of the boundaries. The image system is then hydraulically in complete accord with the physical boundary conditions. The problem thereby has been simplified to consideration of four discharging wells in an infinite aquifer.

IMPERMEABLE BARRIER AND PERENNIAL STREAM INTERSECTING AT RIGHT ANGLES

The image-well system for a discharging well in an aquifer bounded on two sides by an impermeable barrier and a perennial stream which intersect at right angles is shown in figure 40. The perennial stream of figure 40 might also represent a canal, drain, lake, sea, or any other line source of recharge sufficient to maintain a constant head at this As before, the drawdown effects of the primary images, I_1 and I_2 , combine in the desired manner with the effects of the real well at their respective boundaries. However, discharging image well I_1 produces a drawdown at the extension of the line source, which is a no-drawdown boundary, and recharging image well I_2 causes flow across the extension of the impermeable barrier, which is a no-flow boundary. By placing a secondary recharging image well, I_3 , at the appropriate distance from the extension of each boundary, the system is balanced so that no flow occurs across the impermeable barrier and no drawdown occurs at the perennial stream. Thus again the problem has been simplified to consideration of an infinite aquifer in which there operate simultaneously two discharging and two recharging wells.

The simplest way to analyze any multiple-boundary problem is to consider each boundary separately and determine how best to meet the condition of no flow or no drawdown, as the case may be, at that boundary. After the positions of the primary image wells have been established, the boundary positions should be reexamined to see if the net drawdown effects of the primary image wells satisfy all stipulated conditions of no flow or no drawdown. For each primary image causing an unbalance at a boundary position, or extension thereof, it is necessary to place a secondary image well at the same distance from the boundary but on the opposite side, both wells occupying a common line perpendicular to the boundary. When the combined drawdown (or buildup) effects of all image wells are found to produce the desired effect at this boundary the same procedure is executed with



NOTES:

Image wells, /, are numbered in the sequence in which they were considered and located

Open circles signify discharging wells

Filled circles signify recharging wells

FIGURE 40.—Plan of image-well system for a discharging well in an aquifer bounded by an impermeable barrier intersected at right angles by a perennial stream.

respect to the second boundary. Thus, the inspection and balancing process is repeated around the system until everything is in balance and all boundary conditions are satisfied, or until the effects of additional image wells are negligible compared to the total effect.

TWO IMPERMEABLE BARRIERS INTERSECTING AT AN ANGLE OF 45°

Although it is intended here to consider the particular image-well system required for analyzing flow to a well in a 45-degree wedgeshaped aguifer, it is appropriate first to comment briefly on some general aspects of image-well systems in wedge-shaped aquifers. By analogy with similar heat-flow situations it is possible to analyze the flow to a well in a wedge-shaped aquifer, and equivalent image systems can be constructed regardless of the wedge angle involved. However, closed image systems that are the simplest to construct and analyze occur when the wedge angle, θ , of the aquifer equals (or can be approximated as equal to) one of certain aliquot parts of 360°. These particular values of θ may be specified as follows (after Walton, 1953, p. 17), keeping in mind that it is required to analyze flow to a single pumped well situated anywhere in the aquifer wedge: If the aguifer wedge boundaries are of like character, θ must be an aliquot part of 180°. If the boundaries are not of like character, θ must be an aliquot part of 90°.

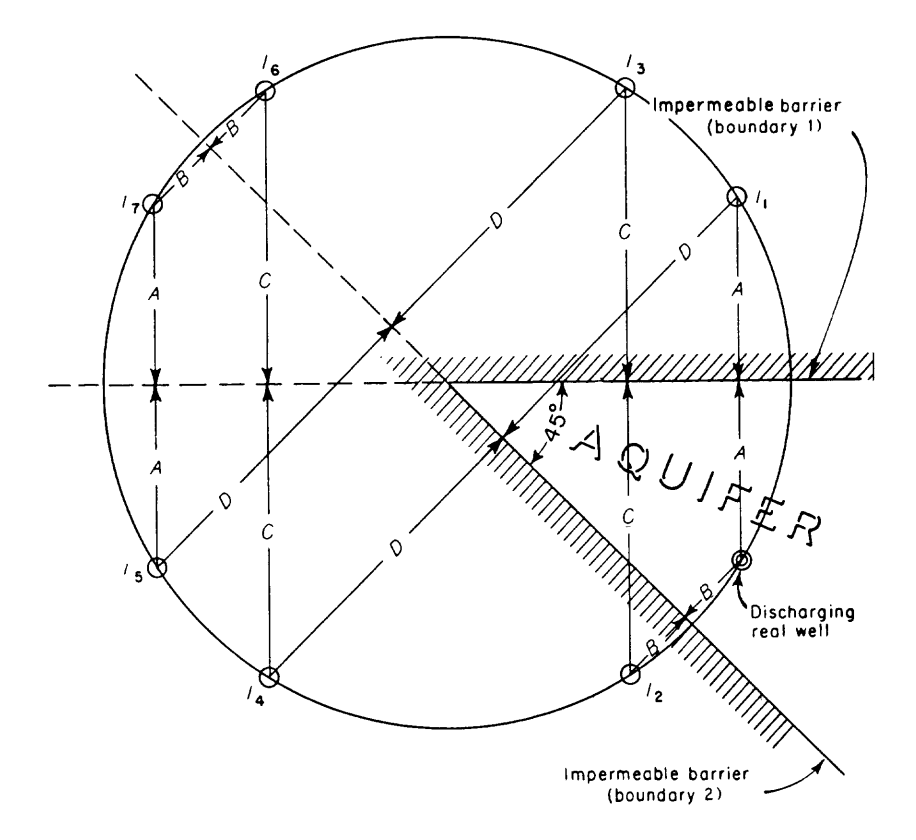
Other simple solutions not covered by the above rule appear possible when θ is an odd aliquot part of 360°, the pumped well is on the bisector of the wedge angle, and the boundaries are similar and impermeable. For any of the foregoing special situations it can be shown, with the aid of geometry, that the number of image wells, n, required in analyzing the flow toward the single real pumping well is given by the relation

$$n = \frac{360^{\circ}}{\theta} - 1. \tag{79}$$

It can also be shown that the locus of all image-well locations, for a given aquifer-wedge problem, is a circle whose center is at the wedge apex and whose radius equals the distance from the apex to the real discharging well (see figure 45).

The image-well system for a discharging well in a wedge-shaped aquifer bounded by two impermeable barriers intersecting at an angle of 45° is shown in figure 41. The real discharging well is reflected across each of the two boundaries which results in location of the two primary image wells I_1 and I_2 as shown. Considering boundary 1 only, the effects of the real well and image well I_1 , are seen to combine so that, as desired, no flow occurs across that boundary. However, image well I_2 will produce flow across boundary 1 unless image well I_3 is added at the location shown. The system now satisfies the condition of no flow across boundary 1. Repeating this examination process for boundary 2 only, it is seen that the effects of the real well and image well I_2 combine, as desired, to produce no flow across boundary 2. However, image wells I_1 and I_3 will produce flow

across this boundary unless image wells I_4 and I_5 are added as shown. The image system now satisfies the condition of no flow across boundary 2. Reexamining, it is seen that image wells I_4 and I_5 will produce flow across boundary 1 unless image wells I_6 and I_7 are added as shown. A final appraisal of the effects at boundary 2, shows that the entire system of image wells, plus the real well, satisfies the requirement of no flow across the boundary. Thus the flow field caused by a discharging well in this wedge-shaped aquifer can be simulated by a total of eight discharging wells in an infinite aquifer. The seven image wells have replaced the two barriers. The drawdown at any point between the two barriers can then be computed by adding the



NOTES:

Image wells, I, are numbered in the sequence in which they were considered and located

Open circles signify discharging wells

FIGURE 41.—Plan of image-well system for a discharging well in an aquifer bounded by two impermeable barriers intersecting at an angle of 45°.

effects produced at that point by the real well and the seven image wells. Each image well begins discharging at the same rate and at the same time as the real well.

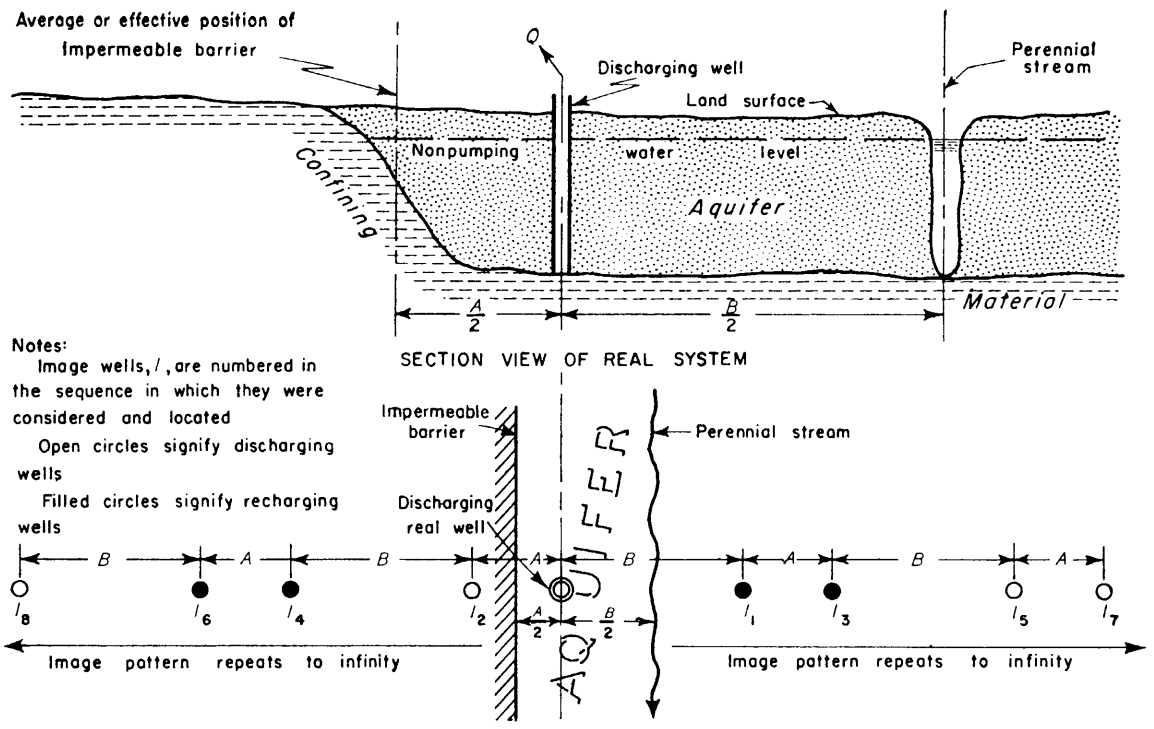
IMPERMEABLE BARRIER PARALLEL TO A PERENNIAL STREAM

Shown in figure 42 is the image-well system for a discharging well in an aquifer bounded by an impermeable barrier and cut by a fully penetrating perennial stream parallel to the barrier. A recharging image well, I_1 , and a discharging image well, I_2 , are placed as shown to satisfy respectively the conditions that no drawdown can occur along the line source, and no flow can occur across the impermeable Although these two primary image wells produce, in conjunction with the real well, the desired effects at their respective boundaries, each image well produces a residual effect at the opposite boundary which conflicts with the stipulated boundary conditions. is therefore necessary to add a secondary set of image wells, I_3 and I_4 , as shown, to produce effects that will combine properly with the residual effects of the primary images. Each image well in the secondary set will again produce residual effects at the opposite boundary, and similarly with each successively added image pair there will be residual effects at the boundaries. It should be evident, however, that as more pairs of image wells are added the effects of adding a new pair have lesser influence on the cumulative effect at each boundary. In other words it is only necessary to add pairs of image wells until the residual effects associated with addition of the next pair can be considered to have negligible influence on the cumulative effect at each boundary. It is seen in figure 42 that there is a repeating pattern in the locations of the image wells. Therefore, after the positions of the first images have been determined, it is possible to locate by inspection as many more as are needed for the practical solution of the problem. Once the required number of image pairs has been determined, the aquifer boundaries can be ignored and the problem analyzed like any other multiple-well problem in an infinite aquifer.

If the two parallel boundaries are of like character—that is, if the perennial stream in figure 42 were replaced by an impermeable barrier or if the impermeable barrier were replaced by a perennial stream—the positions of the image wells would not be changed. In the first case, however, all the images would be discharging wells, and in the second case the image system would be an alternating series of recharging and discharging wells.

TWO PARALLEL IMPERMEABLE BARRIERS INTERSECTED AT RIGHT ANGLES BY A THIRD IMPERMEABLE BARRIER

The image-well system for a discharging well in this type of areally restricted aquifer is shown in figure 43. The positions of the images are determined as before by adding imaginary discharging wells so



REDUCED PLAN VIEW OF HYDRAULIC COUNTERPART OF REAL SYSTEM

FIGURE 42.—Image-well system for a discharging well in an aquifer bounded by an impermeable barrier parallel to a perennial stream.

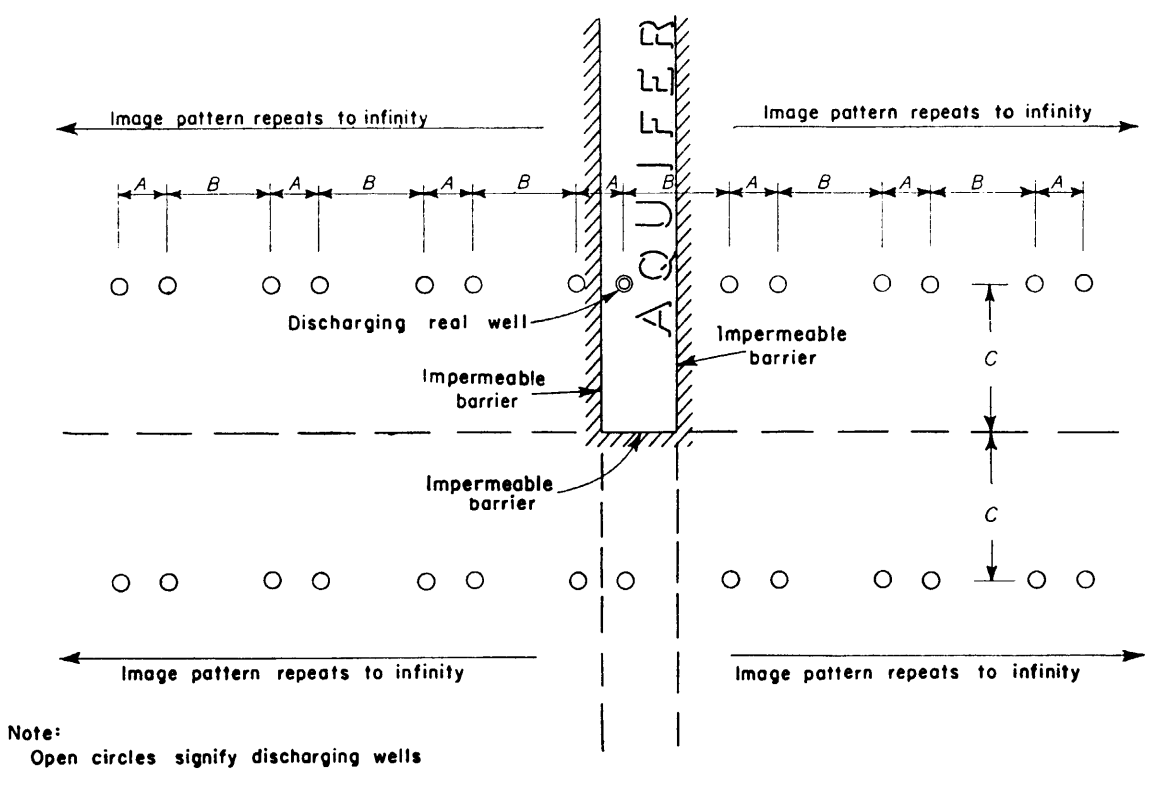


FIGURE 43.—Plan of image-well system for a discharging well in an aquifer bounded by two parallel impermeable barriers intersected at right angles by a third impermeable barrier.

that, in combination with the real discharging well, the condition of no ground-water flow across any of the three boundaries is established. As shown in the figure, two parallel lines of discharging image wells are required, separated by twice the distance between the real well and the barrier that intersects the two parallel barriers. Theoretically the two lines of image wells extend to infinity in both directions from the real well. The practical analysis of a problem of this kind, however, requires the addition of only enough images so that the effect of adding the next image, in any of the directions involved, has a negligible influence on the cumulative effect at each of the boundaries. It is seen from figure 43 that there is a repeating pattern in the positions of the image wells, so that the locations of only the first few images are required to determine the locations of as many succeeding image wells as are needed. For the case of two parallel impermeable barriers intersected at right angles by a perennial stream, the image system would be the same as shown by figure 43 except that all images on the line reflected across the stream would be recharging wells.

RECTANGULAR AQUIFER BOUNDED DY TWO INTERSECTING IMPERMEABLE BARRIERS PARALLELING PERENNIAL STREAMS

The image-well system for a discharging well in such an aquifer is shown by figure 44. The positions of the images are determined in the manner previously described. It is seen from figure 44 that there is again a repeating pattern that extends to infinity in all directions from the real well. Thus only the first few images need be located to determine the positions of as many succeeding images as are required in the practical solution of the problem. If the four boundaries in figure 44 were all impermeable barriers, all images would be discharging wells; and if the four boundaries were all perennial streams, the image system would be alternating series of recharging and discharging wells.

APPLICABILITY OF IMAGE THEORY INVOLVING INFINITE SYSTEMS OF IMAGE WELLS

Referring to the three problems discussed in the three preceding sections, it will be observed that in each situation the aquifer involved is limited in areal extent by two or more boundaries. Furthermore, the arrangement of the boundaries is such that at least two are parallel to each other, which means that analysis by the image theory requires use of an image-well system extending to infinity.

It has been stated, in discussing the practical aspects of using an infinite image-well system, that the individual effects of image wells need be added only out to the point where the effect associated with the addition of the next more distant well (or wells, depending on the symmetry of the array) can be considered to have negligible influence on the cumulative effect. Although this criterion ostensibly provides

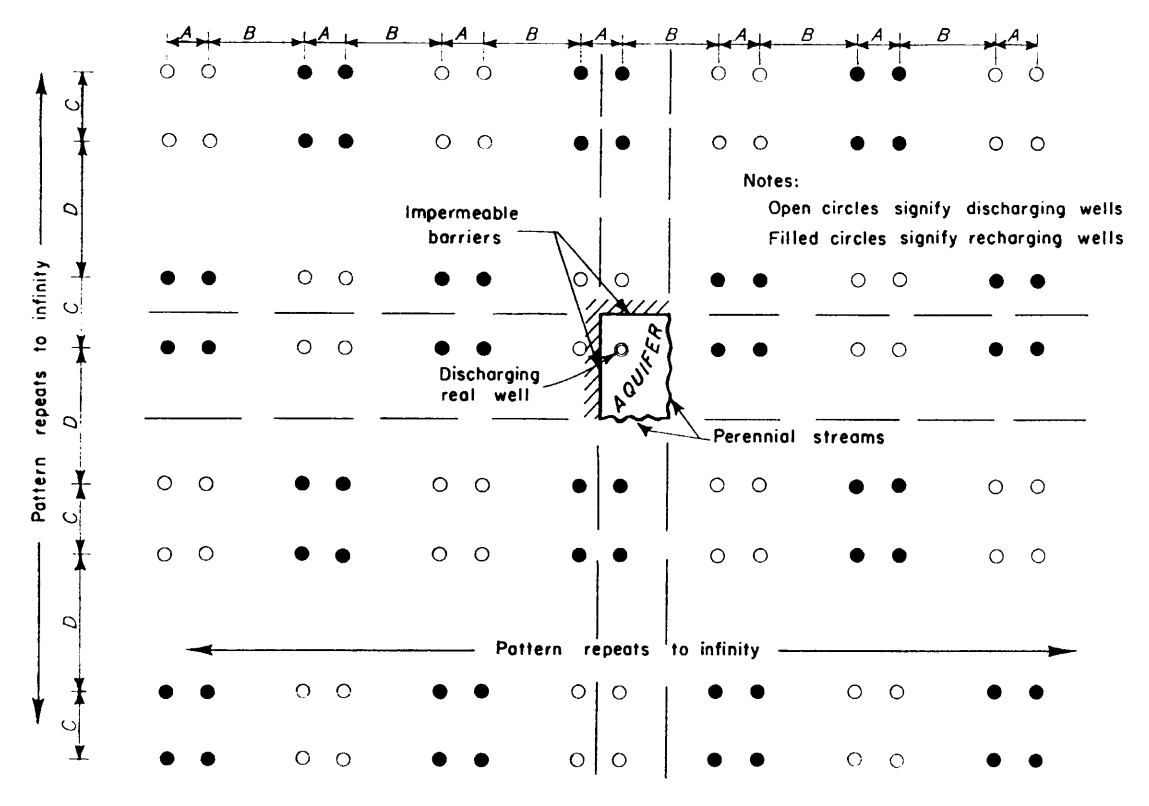


FIGURE 44.—Plan of image-well system for a discharging well in a rectangular aquifer enclosed by 2 intersecting impermeable barriers and 2 intersecting perennial streams.

a reliable and practical means of terminating what would otherwise be an endless analytical process, closer scrutiny appears warranted. There is no reason to state categorically that this practical approach to a solution should never be tried. Undoubtedly there will occur situations wherein sensible results can be obtained. On the other hand it seems prudent to observe that if the process of algebraically summing the individual effects of an infinite system of image wells is terminated anywhere short of infinity, there is no simple way of determining what proportion of the infinite summation is represented by the partial summation. Although addition of the next image well (or wells) might have a negligible influence on the sum of all imagewell effects considered out to that point, there is no simple way of deciding whether the same may be said of the total influence represented by adding the effects of say the next 10 or 20 or 100 more distant image wells. Thus it would appear wise to keep in mind the possible limitations of any solution involving the use of an infinite system of image wells.

COROLLARY EQUATIONS FOR APPLICATION OF IMAGE THEORY

The nature and location of hydrologic boundaries of water-bearing formations in some cases can be determined from the analysis of pumping-test data. Considering the discussion in the preceding sections, it should be evident that in an aquifer whose extent is limited by one or more boundaries, a plot of drawdown or recovery data will depart from the form that would be expected if the aquifer were of infinite extent. Thus, in a problem involving a discharging well in a semi-infinite aquifer bounded by an impermeable barrier, some part of a time-drawdown plot may be steepened by the boundary effects. Conversely, if the boundary involved in the same type of problem were a perennial stream, a part of the time-drawdown plot may be flattened because of the boundary effects.

Imagine a pumping test made in an aquifer whose extent is limited by one or more boundaries. During the early part of the test, the drawdown data for observation wells close to the pumped well will reflect principally the pumping effects. As the test continues, however, there will very likely come a time for each observation well when the measured drawdowns reflect the net effect of the pumped well and any boundaries that are present. At distant observation wells boundary effects may arrive almost simultaneously with the effect of the real discharging well. Thus determination of the aquifer coefficients of transmissibility and storage should be based on the early drawdown data, as observed in a well near the pumped well, before the boundary effects complicate the analysis. Superposition and matching of a plot of these early data (s versus r^2/t) on the Theis type curve permits

drawing in the type-curve trace. Extension or extrapolation of this trace beyond the early data indicates the trend the drawdowns would have taken if the pumping had occurred in an infinite aquifer. departure, s_i, of the later observed data from this type-curve trace represents effects of the boundaries on the drawdown. The subscript irefers to the image-well system substituted as the hydraulic equivalent of the boundaries. Usually it is convenient to note values of s, at a number of points along the data curve and to replot these departures versus values of r_r^2/t on the same graph sheet that was used in determining the coefficient of storage and transmissibility from the early The subscript r refers to the real discharging well. The latter part of the replotted departure data may again deviate from the type-curve trace if the cone of depression has intercepted a second boundary. As before, the departures can be replotted against corresponding values of r_r^2/t to form a second departure curve. process should be repeated until the last departure curve shows no deviation from the type curve. The observed data array will then have been separated into its component parts which can be used to compute the distances between the observation wells and the image wells.

Inasmuch as the aquifer is assumed to be homogeneous (that is, the coefficients of transmissibility and storage are constant throughout the aquifer) it follows from equation 8 that

$$\frac{1.87S}{T} = \frac{u_r}{r_r^2/t} = \frac{u_t}{r_r^2/t},\tag{80}$$

where the subscripts r and i have the significance previously given. If on the plots of early drawdown data and first-departure curve a pair of points is selected so that the drawdown component caused by the real well, s_t , and the drawdown component caused by the image well, s_t , are equal, it follows that $u_r = u_t$. On the plots of observed early drawdowns and first departures just described, s_t and s_t obviously occur at different elapsed times, which can be labelled t_r and t_t respectively. Equation 80 can therefore be rewritten as follows:

$$\frac{r_i^2}{t_t} = \frac{r_r^2}{t_r},\tag{81}$$

or

$$r_i = r_r \sqrt{\frac{t_i}{t_r}}. (82)$$

Equation 81, known as the "law of times" in the physics of heat conduction, shows that at a given observation well location the times of occurrence of equal drawdown components vary directly and only

as the squares of the distances from the observation well to the pumped well and to its image.

Referring to the data plots mentioned earlier in this section, note, for the pair of points selected, that values of s_r and r_r^2/t_r will be read from the early drawdown data while values of s_t and r_r^2/t_t will be read from the first departure curve. Equation 82 can be made more useful, therefore, if it is rewritten in the form

$$r_i = r_r \sqrt{\frac{r_r^2/t_r}{r_r^2/t_i}}. (83)$$

Equation 83 now affords a ready means of computing the distance from an observation well to an image well. Similar analysis may be made of each departure curve constructed from the original drawdown data.

Stallman (1952) has described a convenient method for computing r_i when the observed drawdown in the aquifer represents the algebraic sum of the drawdown effects from one real well and one image well. If equation 6 is used to provide expressions for s_i and s_i , and w(u) is substituted as a symbolic form of the exponential integral, it is seen that the drawdown at the observation well is

$$s = s_t \pm s_t = \frac{114.6Q}{T} [W(u), \pm W(u)_t].$$
 (84)

From equation 80,

 $\frac{r_i}{r_r} = \sqrt{\frac{u_i}{u_r}},$ $r_i = r_r \sqrt{\frac{u_i}{u_r}}.$ (85)

or

From equations 84 and 85, it can be seen that r_i and the sum of the W(u) terms in equation 84 can be expressed in terms of r_r and the ratio u_i/u_r . Thus for any given values of $\sqrt{u_i/u_r} = K$, a type curve can be constructed by plotting assumed values of u_r against corresponding computed values of the bracketed portion of equation 84 [which may be written in abbreviated form as $\sum_{r,i} W(u)$]. The data plot, s versus t, will match this constructed type of curve if the observation well is located so that the ratio r_i/r_r equals the given value of K. However, if a family of type curves is drawn for a number of given values of K, the observed data plot, s versus t, for any observation well, can be compared with the set of type curves. Once

the best matching curve is found, any convenient matchpoint is selected and the coordinate values, s, t, u_{τ} , $\sum_{r,i} W(u)$, and K are noted. These values, substituted in equations 80, 84, and 85 provide the means for computing T, S, and r_t .

Stallman's set of curves is the familiar type-curve u versus W(u), used in conjunction with the Theis formula, with a series of appendage curves (two for each value of K) asymptotic to it. The trend of the appendage curve for a recharging image well is below, and for a discharging image above, the Theis curve. Appendage curves could have been constructed by assuming values of u_t instead of u_τ . In this event, however, the matching process would not be as direct inasmuch as the parent type curve, instead of occupying a single position, would shift along the u axis with each pair of appendage (K) curves.

The appendage curves, computed by Stallman, are for ideal image wells—those which are pumped or recharged at the same rate as the real well. The hydrogeologic structure which gives rise to the hypothetical image is not always ideal; therefore the hypothetical images are not always ideal. For this case the method of plotting departures may yield an erroneous and misleading analysis. On the other hand, the deviations from ideality can be seen immediately if the observed data plot s versus t is matched to Stallman's set of type curves. Furthermore, for nonideal images, the most accurate selection of K is made by utilizing the portion of the appendage curve that is nearest the parent or Theis type curve.

If little is known of the possible location of a local hydraulic boundary a minimum of three observation wells is required to fix the position of an image well, which in turn permits location of the boundary. After the distances from the individual observation wells to the image well have been computed, arcs are scribed with their centers at the observation wells and their radii equal to the respective computed distances to the image well. The intersection of the arcs at a common point fixes the location of the image well, and the strike of the boundary is represented by the perpendicular bisector of a line connecting the pumped well and the image well.

Another graphical method for locating a hydraulic boundary in the vicinity of a discharging well was devised by E. A. Moulder (1951, written communication, p. 61). The geometry is shown in figure 45. A circle is scribed whose center is at a nearby observation well, O, and whose radius, r_i , is equal to the computed distance from the observation well to the image well. The image well lies somewhere on this circle, say, at point I. Lines are drawn from the selected point I to the observation well and to the real discharging well, P. If point I is the image-well location and if I is the midpoint of the

line IP, then point A lies on the boundary. It can be proved by geometry, that the locus of all points A determined in this manner is a circle, of radius BA or $r_i/2$, with its center, B, located midway between the discharing well and the observation well. Moulder's method is particularly useful in aquifer-test situations where data from only one or two observation wells are available for locating a boundary position. If the approximate position of a suspected boundary is known before a pumping test begins, it is desirable to locate most of the observation wells along a line parallel with the boundary and passing through the pumped well. If feasible the range of distances from the observation wells to the pumped well should be distributed logarithmically to assure well-defined arc intersections in the graphics of locating a point on that boundary. At least one observation well

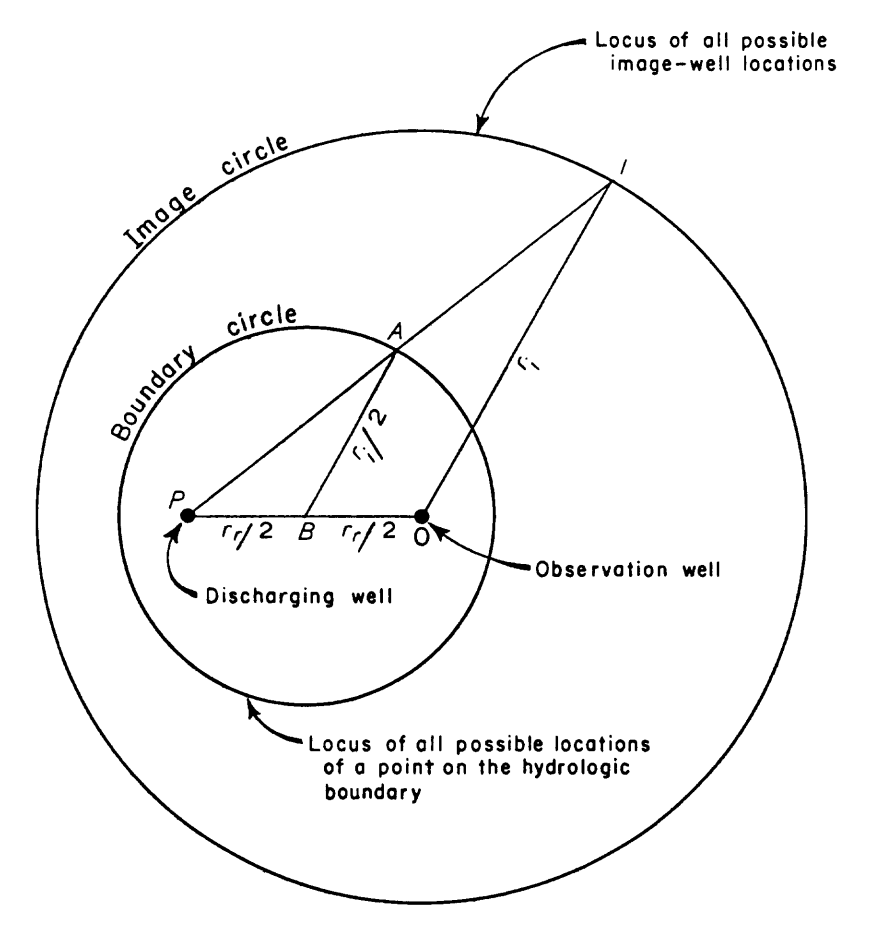


FIGURE 45.—Geometry for locating a point on a hydrologic boundary, with reference to the locations of a discharging well and a nearby observation well.

should be located close enough to the pumped well so that the early drawdown data, unaffected by the boundary, can be used in computing the aquifer coefficients of storage and transmissibility.

REFERENCES

- Andreasen, G. E., and Brookhart, J. W., Reverse water-level fluctuations: U.S. Geol. Survey open-file rept.
- Barksdale, H. C., Sundstrom, R. W., and Brunstein, M. S., 1936, Supplementary report on the ground-water supplies of the Atlantic City region: New Jersey State Water Policy Comm. Spec. Rept. 6, p. 87-91.
- Bennett, R. R., and Meyer, R. R., 1952, Geology and ground-water resources of the Baltimore area: Maryland Dept. Geology, Mines and Water Resources Bull. 4, p. 54-58.
- Brown, R. H., and Ayer, G. R., 1948, Upstate New York, in Paulsen, C. G., and others, Water levels and artesian pressure in observation wells in the United States in 1945: U.S. Geol. Survey Water-Supply Paper 1023, Part 1, Northeastern States, p. 193-195.
- Byerly, Perry, 1933, Analysis of seismograms of near earthquakes, chap. 16 in Seismology: Natl. Research Council Bull. 90, Physics of the Earth, v. 6.
- Casagrande, Arthur, 1937, Seepage through dams: Harvard Graduate School Eng. Pub. 209.
- Darcy, Henry, 1856, Les Fontaines publiques de la ville de Dijon (The water supply of Dijon): Paris, Victor Dalmont, 647 p.
- Dupuit, Jumes [Jules], 1848, Études théoriques et pratiques sur le mouvement des eaux courantes [Theoretical and practical studies on the movement of running water]: Paris, Carilian-Goeury et V. Dalmont, 275 p.
- Ferris, J. G., 1950, Quantitative method for determining ground-water characteristics for drainage design: Agr. Engineering, v. 31, no. 6, p. 285-291.
- Ferris, J. G., and Knowles, D. B., 1954, Slug test for estimating transmissibility: U.S. Geol. Survey Ground Water Note 26.
- Forchheimer, Philipp, 1901, Wasserbewegung durch Boden (Ground-water motion): Ver. Deutscher Ing. Zeitschr., [Berlin], v. 45, p. 1736-1741, 1781-1788.
- ----- 1930, Hydraulik: 3d ed., Leipzig and Berlin, Teubner.
- Gray, Andrew, Mathews, C. B., and MacRobert, T. M., 1931, Treatise on Bessel functions and their applications to physics: London, Macmillan Co., Ltd.
- Glee, G. J. de, 1930, Over grondwaterstroomingen bij wateronttrekking door middel van putten [On ground-water currents through draining by means of wells]: Delft [Netherlands] Tech. Hogeschool Thesis.
- Hagen, G. H. L., 1839, Ueber die Bewegung des Wassers in engen cylindrischen Rohren [Movement of water in a narrow cylindrical tube]: Annalen Physik u. Chemie [Leipzig], v. 46, p. 423-442.
- Ha: tush, M. S., 1955, Preliminary quantitative study of the Roswell ground-water reservoir, New Mexico: Socorro, New Mexico Inst. Mining and Technology, 113 p.
- Hantush, M. S., and Jacob, C. E., 1955, Non-steady radial flow in an infinite leaky aquifer: Am. Geophys. Union Trans., v. 36, no. 1, p. 95-100.
- Ingersoll, L. R., Zobel, O. J., and Ingersoll, A. C., 1948, Heat conduction: New York, McGraw-Hill Book Co.
- Israelsen, O. W., 1950, Irrigation principles and practices: 2d ed., New York, John Wiley & Sons.

- Jacob, C. E., 1939, Fluctuations in artesian pressure produced by passing railroad trains as shown in a well on Long Island, New York: Am. Geophys. Union Trans., Pt. 4, p. 666-674, August; dupl. as U.S. Geol. Survey Ground Water Note 16, 1953.

- Jacob, C. E., and Lohman, S. W., 1952, Nonsteady flow to a well of constant drawdown in an extensive aquifer: Am. Geophys. Union Trans., v. 33, no. 4, p. 559-569.
- Klonne, F. W., 1880, Die periodischen Schwankungen in den inundirten Kohlenschächten von Dux [The periodical fluctuations in the flooded coal shafts of Dux]: Akad. Wiss. Wien Sitzungsber., v. 81, p. 101, Wien.
- Krul, W. F. J. M., and Liefrinck, F. A., 1946, Present ground-water investigations in the Netherlands: New York and Amsterdam, Elsevier Pub. Co.
- LaRocque, G. A., Jr., 1941, Fluctuations of water level in wells in the Los Angeles basin, California, during five strong earthquakes, 1933–1940: Am. Geophys. Union Trans., pt. 2, p. 374–386.
- Leggette, R. M., and Taylor, G. H., 1935, Earthquakes instrumentally recorded in artesian wells: Seismol. Soc. America Bull., v. 25, p. 169-175.
- Lohman, S. W., 1957, Method of determining the coefficient of storage from straight-line plots without extrapolation: U.S. Geol. Survey Ground Water Note 33.
- Meinzer, O. E., and Fishel, V. C., 1934, Tests of permeability with low hydraulic gradients: Am. Geophys. Union Trans., v. 15, pt. 2, p. 405-409, June.
- Meinzer, O. E., and Hard, H. A., 1925, Artesian-water supply of the Dakota sandstone in North Dakota, with special reference to the Edgeley quadrangle: U.S. Geol. Survey Water-Supply Paper 520-E, p. 73-95, pls. 6-7.
- Milne, W. E., 1953, Numerical solution of differential equations: New York, John Wiley & Sons.
- Parker, G. G., and Stringfield, V. T., 1950, Effects of earthquakes, trains, tides, winds, and atmospheric pressure changes on water in the geologic formations of southern Florida: Econ. Geology, v. 45, no. 5, p. 441-460.
- Piper, A. M., 1933, Fluctuations of water surface in observation wells and at stream-gaging stations in the Mokelumne area, California, during the earthquake of December 20, 1932: Am. Geophys. Union Trans., v. 14, p. 471-475.

- Poiseuille, J. L. M., 1846, Experimental investigations on the flow of liquids in tubes of very small diameter: Acad. Royal sci. et Inst. France, Math. Phys. Sci. Mem., v. 9, p. 433-543. (Translated by W. H. Herschel in Rheolog. Mem., v. 1, no. 1, 101 p., Easton, Pa., Jan. 1940.)
- Robinson, T. W., 1939, Earth tides shown by fluctuations of water levels in wells in New Mexico and Iowa: Am. Geophys. Union Trans., pt. 4, p. 656-666.
- Rouse, Hunter, ed., 1950, Engineering hydraulics: New York, John Wiley & Sons.
- Scarborough, J. B., 1950, Numerical mathematical analysis: 2d ed., Baltimore, Johns Hopkins Press.
- Shaw, F. S., 1953, Introduction to relaxation methods: New York, Dover Pub., Inc.
- Skibitzke, H. E., 1958, An equation for potential distribution about a well being bailed: U.S. Geol. Survey Ground Water Note 35.
- Slichter, C. S., 1899, Theoretical investigation of the motion of ground waters: U.S. Geol. Survey 19th Ann. Rept.; U.S. Geol. Survey Ground Water Note 22, 1954.
- Southwell, R. V., 1940, Relaxation methods in engineering science: London, Oxford Univ. Press.
- Stallman, R. W., 1952, Nonequilibrium type curves modified for two-well systems: U.S. Geol. Survey Ground Water Note 3.
- Stearns, H. T., 1928, Record of earthquake made by automatic recorders on wells in California: Seismol. Soc. America Bull., v. 18, p. 9-15.
- Stearns, N. D., 1928, Laboratory tests on physical properties of water-bearing materials: U.S. Geol. Survey Water-Supply Paper 596-F, p. 121-176, pls 11-13.
- Steggewentz, J. H., and Van Nes, B. A., 1939, Calculating the yield of a well, taking account of replenishment of the ground water from above: Water and Water Eng. [London], v. 41, no. 517, p. 561-563.
- Taylor, D. W., 1948, Fundamentals of soil mechanics: New York, John Wiley & Sons, p. 156-198.
- Theis, C. V., 1935, Relation between the lowering of the piezometric surface and the rate and duration of discharge of a well using ground-water storage: Am. Geophys. Union Trans., pt. 2, p. 519-524; dupl. as U.S. Geol. Survey Ground Water Note 5, 1952.
- Theis, C. V., and Brown, R. H., 1954, Drawdown in wells responding to cyclic pumping: U.S. Geol. Survey Ground Water Note 23.
- Thiem, Gunther, 1906, Hydrologische methoden (Hydrologic methods): Leipzig, J. M. Gebhardt, 56 p.
- Turneaure, F. E., and Russell, H. L., 1901, Public water supplies: New York, John Wiley & Sons.
- U.S. National Bureau of Standards, 1952, Tables of the Bessel functions $Y_0(x)$, $Y_1(x)$, $K_0(x)$, $K_1(x)$, $0 \le x \le 1$: U.S. Natl. Bur. Standards Appl. Math Ser. 25, Sept. 11.

Veatch, A. C., 1906, Fluctuations of the water level in wells, with special reference to Long Island, New York: U.S. Geol. Survey Water-Supply Paper 155, 83 p.
Vorhis, R. C., 1953, Milwaukee "hydroseismograms" and their interpretation:

U.S. Geol. Survey open-file rept.

- Walton, W. C., 1953, Hydraulic properties of a dolomite aquifer underlying the village of Ada, Ohio: Ohio Dept. Nat. Resources, Div. Water Tech. Rept. 1.
- Warren, M. A., 1952, Graphical short cuts in applying the nonequilibrium formula to ground-water problems: U.S. Geol. Survey open-file rept.
- Wenzel, L. K., 1942, Methods for determining permeability of water-bearing materials, with special reference to discharging-well methods, with a section on Direct laboratory methods and bibliography on permeability and laminar flow, by V. C. Fishel: U.S. Geol. Survey Water-Supply Paper 887, 192 p.
- Wenzel, L. K., and Sand, H. H., 1942, Water supply of the Dakota sandstone in the Ellendale-Jamestown area, North Dakota, with reference to changes between 1923 and 1938: U.S. Geol. Survey Water-Supply Paper 889-A.
- Werner, P. W., and Noren, Daniel, 1951, Progressive waves in non-artesian aquifers: Am. Geophys. Union Trans., v. 32, no. 2, p. 238-244.
- Wyckoff, R. D., Botset, H. G., and Muskat, M., 1932, Flow of liquids through porous media under the action of gravity: Physics, v. 3, no. 2, p. 90-113.
- Young, Andrew, 1913, Tidal phenomena at inland boreholes near Cradock: Royal Soc. South Africa Trans., v. 3, pt. 1, p. 61-105.



The Unusual and Large Drawdown Response of Buried-Valley Aquifers to Pumping

by Garth van der Kamp¹ and Harm Maathuis²

Abstract

The buried-valley aquifers that are common in the glacial deposits of the northern hemisphere are a typical case of the strip aguifers that occur in many parts of the world. Pumping from a narrow strip aguifer leads to much greater drawdown and much more distant drawdown effects then would occur in a sheet aquifer with a similar transmissivity and storage coefficient. Widely used theories for radial flow to wells, such as the Theis equation, are not appropriate for narrow strip aquifers. Previously published theory for flow to wells in semiconfined strip aquifers is reviewed and a practical format of the type curves for pumping-test analysis is described. The drawdown response of strip aguifers to pumping tests is distinctive, especially for observation wells near the pumped well. A case study is presented, based on extensive pumping test experience for the Estevan Valley Aquifer in southern Saskatchewan, Canada. Evaluation of groundwater resources in such buried-valley aquifers needs to take into account the unusually large drawdowns in response to pumping.

Introduction

Long and narrow strip aquifers in the form of buriedvalley deposits confined by low-permeability aquitards are common in the glaciated terrain of northern North America and north-western Europe (Andersen and Haman 1970; Kehew and Boettger 1986; Shaver and Pusc 1992; Parks and Bentley 1996; Maathuis and Thorleifson 2000; Desbarats et al. 2001; Sandersen and Jorgensen 2003; Russell et al. 2004; BurVal Working Group 2006; Seifert et al. 2008; Ahmad et al. 2009). These aguifers occur as long and narrow, highly transmissive, sand and gravel units that are incised into much less permeable clayrich formations or into the less permeable bedrock. The aquifers may be highly productive sources of groundwater, but their distinctive hydraulics can also lead to unexpectedly large drawdown of the groundwater levels over large distances. Hence it is important to have appropriate conceptual and theoretical models that provide understanding of how such strip aquifers function, and that can be used in analyzing pumping test data and predicting the impacts of pumping.

Most theoretical models for groundwater flow to a well are based on the assumption that the aquifers occur as sheets, extensive in every direction, and that the flow is radially symmetric (Kruseman and de Ridder 1990). The models can be extended to simple types of aquifer boundaries by means of the image well method. However, the radial flow models are not useful for long narrow aquifers, such as occur within valley deposits, in which the flow is strongly influenced by boundaries on either side and where the flow is not radially symmetric except very near the pumping well.

The purpose of this paper is to describe the large drawdowns caused by pumping that are encountered for narrow buried-valley aquifers and to present a simple conceptual and quantitative model for anticipating, predicting and analyzing such drawdown behavior, based on previously published theoretical analyses. Practical strip-aquifer type curves are described, an example of a

Received January 2011, accepted April 2011.

© 2011, Crown in the right of Canada

Ground Water © 2011, National Ground Water Association.

doi: 10.1111/j.1745-6584.2011.00833.x

¹Corresponding author: National Water Research Institute, 11 Innovation Boulevard, Saskatoon, Saskatchewan, Canada S7N 3H5; garth.vanderkamp@ec.gc.ca

²Cameco Corporation, 1131 Avenue W South, Saskatoon, Saskatchewan, Canada S7M 4E8; harm_maathuis@cameco.com

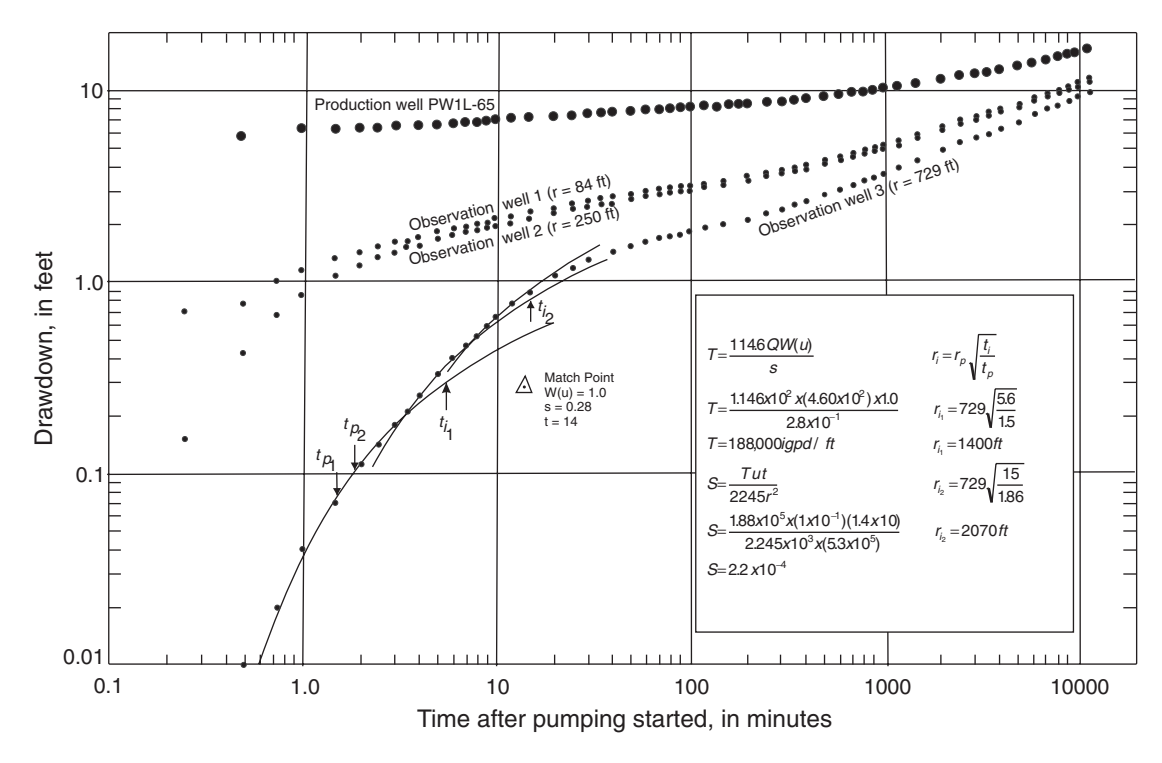


Figure 1. Data and type curve analysis for an 8-day pumping test of the Estevan Valley Aquifer (adapted from Walton 1965).

field application is given, and attention is drawn to the distinctive drawdown behavior of observation wells near the pumped well in strip aquifers.

Type-Curves for a Strip Aquifer

The shortcomings of using radial flow models to analyze drawdown data for strip aquifers is illustrated in Figure 1, which is a reproduction of the data and analysis for an 8-day pumping test carried out for a buried-valley aquifer near Estevan in Southern Saskatchewan, Canada (Walton 1965, 1970). An analysis with two image wells to take boundaries into account could use only the first 20 min of the data, and analysis of the full 11,500 min of data would have required many more image wells. Thus the desirability of a more general mathematical approach is indicated. The response to pumping of this aquifer will be further described in this paper.

Vandenberg (1976, 1977) developed type curves for the drawdown caused by pumping in semiconfined strip aquifers. Motz (1991) and Zhang (1992) carried out theoretical analyses of one-dimensional transient flow in a leaky aquifer in response to water level changes in rivers or canals. These analyses are mathematically equivalent to Vandenberg's results (Gill 1992). Related results were presented by Butler and Liu (1991) for the special case of a confined linear aquifer embedded in a matrix with different permeability.

Except for the assumption of one-dimensional flow rather than radial flow, the analyses by Vandenberg (1977), Motz (1991), and Zhang (1992) are based on assumptions about the aquifer-aquitard system and its properties that are identical to the assumptions for the

well-known theory of radial flow in a semiconfined aquifer as first developed by Hantush and Jacob (1955). These assumptions include:

- 1. The aquifer is uniform and infinitely long in both directions from the pumped well and the underlying and adjoining formations are impermeable.
- 2. The overlying aquitard has a zero elastic storage coefficient, so that all the storage is in the aquifer itself. Drawdown at the top of the aquitard is assumed to be zero, implying that the storage (or specific yield) at the top of the aquitard is very large.

Details of the mathematical derivations are not presented here since they are available in the aforementioned papers by Vandenberg, Motz, Zhang, and Gill.

The original equations derived by Vandenberg (1977) are:

$$s = \left(\frac{Qx}{2TW'}\right)F\left(u, \frac{x}{L}\right) \tag{1}$$

where:

$$u = \left(\frac{x^2 S}{4Tt}\right) \text{ and } F\left(u, \frac{x}{L}\right)$$
$$= \left(1/2\pi^{\frac{1}{2}}\right) \int_u^\infty y^{\frac{-3}{2}} \exp\left(-y - \frac{x^2}{4L^2y}\right) dy \qquad (2)$$

in which s = drawdown, Q = pumping rate (constant), $x = \text{distance between the pumped well and the observation well measured along the aquifer, <math>T = \text{transmissivity}$, W' = strip aquifer width, $L = \text{leakage length} = (Tb'/K'_{1})^{\frac{1}{2}}$,

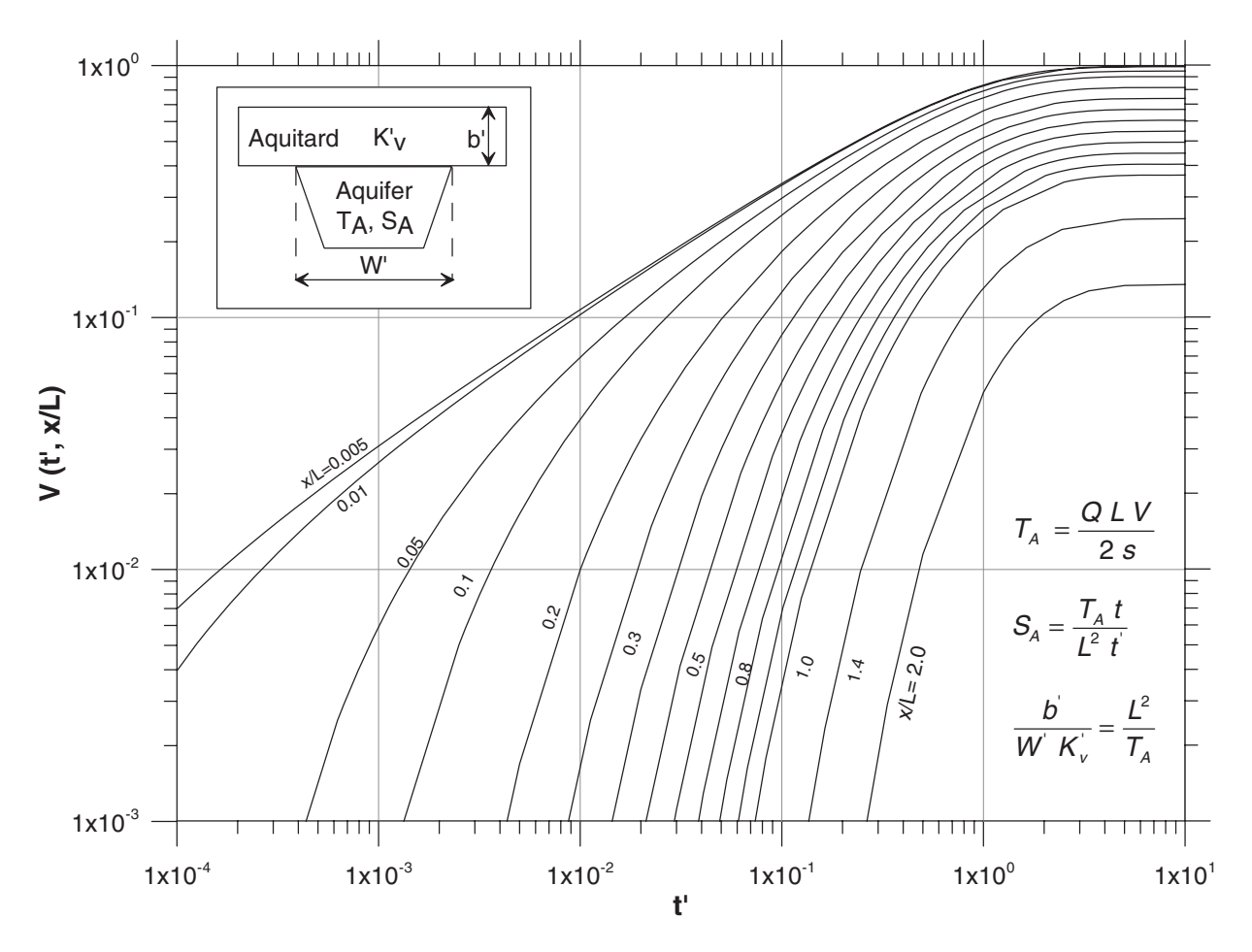


Figure 2. Type curves for semiconfined strip aquifers (adapted from Zhang 1992).

S= storage coefficient, t= time since pumping started, b'= thickness of the confining aquitard and $K'_v=$ vertical hydraulic conductivity of the aquitard. The leakage length L is the same as the leakage length for sheet aquifers, commonly denoted as L (Kruseman and de Ridder 1990) or as B (Hantush and Jacob 1955). Values for F(u, x/L) have been provided by Vandenberg (1977) and Kruseman and de Ridder (1990).

These equations are based on the assumption that the flow in the aquifer is one-dimensional, in other words the pumped well is represented mathematically as a face of constant discharge across the full width and depth of the aquifer. In practice the flow converges radially to the pumping well which is essentially a vertical line sink. Vandenberg (1977) showed that for observation wells further than one aquifer width distant from the pumping well the one-dimensional flow equations provide a good approximation of the drawdown. At smaller distances from the pumping well there is additional drawdown caused by the radial flow component. In this paper a slightly modified version of the type curves presented by Zhang (1992) is used, conforming to the commonly used "log-log" format for presenting drawdown data (Figure 1). Other mathematically equivalent forms of the type curves were described by Vandenberg (1977) and Motz (1991). The type curves (Figure 2) represent plots of dimensionless drawdown V as a function of dimensionless time t' and dimensionless distance x/L, which can be written in the form:

$$V(t', x/L) = \left(\frac{2T_A}{QL}\right) s(x, t) \tag{3}$$

$$t' = \left(\frac{tT_A}{S_A L^2}\right) = t/(Sb'/K_v') \tag{4}$$

V and t' are related to Vandenberg's F(u, x/L) and u by V = (x/L)F and $t' = (x^2/L^2)(1/4u)$. Values of V and t' have been tabulated and are available from the authors on request.

The type curve parameters are expressed in terms of T_A , the cross sectional conductance or transmissive capacity of the aquifer; S_A , the cross-sectional storativity of the aquifer; and L, the leakage factor, defined by:

$$T_A = TW' \tag{5}$$

$$S_A = SW' \tag{6}$$

$$L = \left(\frac{T_A b'}{W' K'_{v}}\right)^{\frac{1}{2}} \tag{7}$$

where T and S are the average values of transmissivity and storage coefficient of the aquifer, averaged over,

W', the width of the top of the aquifer (see Figure 2), b' is the thickness of the overlying aquitard, and $K'_{\rm V}$ is the vertical hydraulic conductivity of the aquitard. The width of the top of the aquifer, W', is used because it reflects the inflow from the overlying aquitard. These modified type curves are identical to the type curves presented by Zhang (1992, Figure 8, type A curves) with the proviso that here the cross-sectional conductance T_A and storativity S_A are used rather than T and S.

As suggested by Vandenberg (1977) use of the cross-sectional parameters T_A and S_A is appropriate for a narrow strip aquifer because the primary interest is usually with the total water transmitting and water storing capacity of the aquifer. For instance, the total rate of flow of water along the aquifer is simply the product of T_A and the hydraulic gradient along the aquifer. The use of these cross-sectional parameters avoids the need to determine the distributions of permeability and storage coefficient in the usually highly heterogeneous aquifers. However, the type curves can also be analyzed in terms of the parameters TW', S/T, and L, as indicated by Equations 1 and 2. Calculation of representative values of S and T for the entire cross-section of the aquifer then requires an independent determination of the aquifer width.

The analytical solution shows that the behavior of an ideal leaky strip aquifer is governed by the three aquifer parameters T_A , S_A , and L. These parameters can be determined by fitting measured drawdowns, plotted as a function of time, to the type curves. The procedure is the similar to the type curve fitting procedure used in the analysis of pumping test results for radial flow in sheet aquifers (Kruseman and de Ridder 1990). Ideally data from more than one observation well should be plotted together and then matched simultaneously to the type

curves, with values of x/L for each of the wells being proportional to the distance x for the various observation wells. The value of L is calculated from the type curve values of x/L for the observation wells at known distances x from the pumping well. T_A and S_A are then determined from the match point values of V, t', s, and t by means of Equations 3 and 4 which can be written:

$$T_A = \left(\frac{QLV_{\rm mp}}{2s_{\rm mp}}\right) \tag{8}$$

$$S_A = \left(\frac{t_{\rm mp} T_A}{t'_{\rm mp} L^2}\right) \tag{9}$$

 $V_{\rm mp}$, $s_{\rm mp}$, $t_{\rm mp}$, and $t'_{\rm mp}$ are the values of V, s, t, and t' corresponding to the match point. An example is given in the following section of this paper.

Case Study: Analysis of Pumping-Test Data for Estevan Valley Aquifer

The Estevan Valley Aquifer in southern Saskatchewan (Figure 3) is an extensive buried-valley aquifer system that has been evaluated for its groundwater resource potential in the process of several successive studies. The main features of the aquifer have been described in reports and papers (Meneley et al. 1957; Walton 1970, pp. 73–81; Beckie Hydrogeologists Ltd. 1984; van der Kamp 1985; Maathuis and van der Kamp 2003). The aquifer consists of sand and gravel within several intersecting buried channels, confined by 50 to 100 m of clay-rich till. The main buried-channel aquifer units are 1000 to 4000 m wide. The aquifer is up to 80 m thick and at most locations in the channels consists of

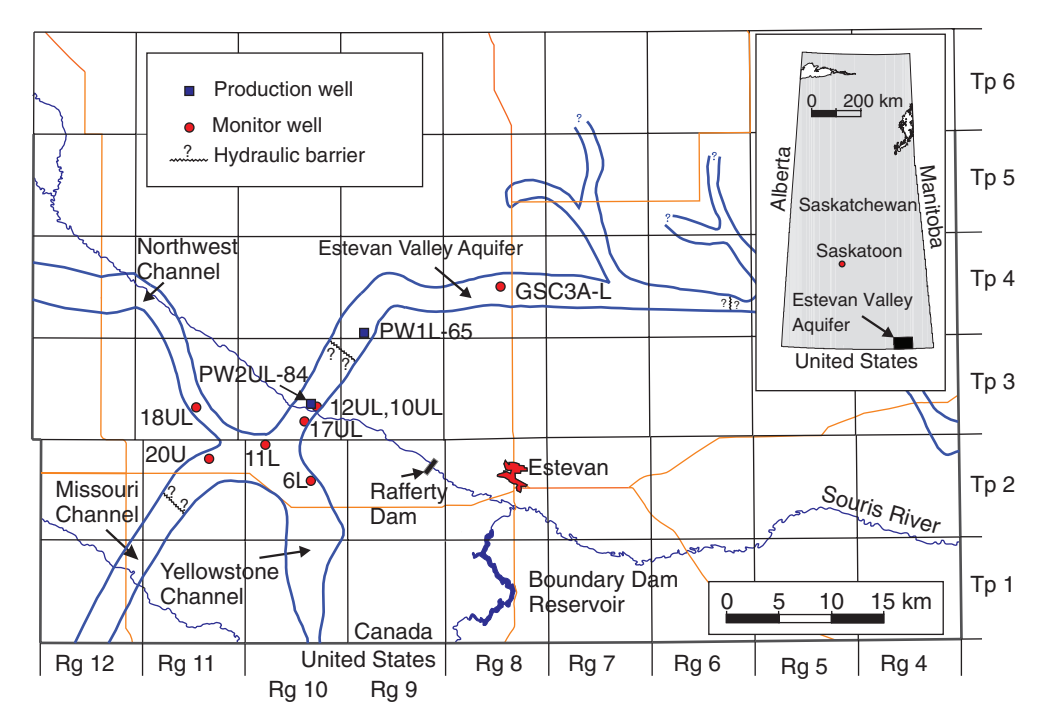


Figure 3. Plan view of the Estevan Valley Aquifer in southern Saskatchewan.

a lower and upper sand and gravel zone, separated by a clay and silt layer. The channels have been traced by means of geologic and geophysical logs for farm and oil wells and extensive test drilling over distances of up to 60 km. However, the static water levels and the pumping test data indicate that there are several transverse barriers across the aquifer channels that partially or completely eliminate hydraulic connection between different aquifer segments (Figure 3), similar to the barriers that have been described by Shaver and Pusc (1992) for buried-valley aguifers in North Dakota, USA. The well identifications shown in Figure 3 include "U," "L," or "UL" to indicate whether they are screened in the upper, lower, or both zones of the aguifer. The top of the buried valley aguifer lies well below the bottom of the Souris River valley and no effects of interaction with the overlying river could be detected in the hydraulic head data for the aguifer.

An 8-day pumping test, with a pumping rate of $0.035 \text{ m}^3/\text{s}$ was carried out in 1965 (Walton 1965) at PW1L-65 (Figure 3), with three observation wells at distances of 26, 76, and 222 m (84, 250, and 729 feet) that were decommissioned after the test. All wells were screened in the lower zone of the aquifer. Only the first 20 min of the drawdown data were used for analysis on the basis of the Theis confined-aquifer type curves, which gave $T = 0.032 \text{ m}^2/\text{s}$ (188,000 Igpd/ft) near the well and $S = 2.2 \times 10^{-4}$ (Figure 1). After the first 10 min

of pumping the observed drawdown increasingly exceeded the drawdown that would be expected for radial flow in a sheet aquifer, reflecting the influence of the channel boundaries. At the end of the test a drawdown of 0.20 m (0.59 feet) was measured for well GSC3A-L, 13,400 m east of the pumping well site (Figure 3), indicating that the drawdown effects could be far-reaching if pumping were continued for a longer time.

In 1984, a 29-day pumping test was conducted on pumping well PW2UL-84 screened in the upper and lower permeable zones of the Estevan Valley aguifer, at a point about 8600 m distant from the site of the 1965 test (Figure 3). The pumping rate was 0.0757 m³/s (van der Kamp 1985). Drawdown was measured in numerous observation wells at distances between 30.5 and 13,000 m from the pumping well, including well PW1L-65 that was pumped in 1965. The recovery after pumping was very slow and the residual drawdowns were measured for ten months after pumping ceased (Figure 4). The measured drawdowns in the observation wells follow a regular pattern of smaller drawdown with increasing distance, except for the drawdown in well PW1L-65 where the drawdown was much smaller. This smaller drawdown indicates the existence of a partial hydraulic barrier between the pumped well and PW1L-65, a hypothesis that was corroborated by a discontinuity in the static hydraulic gradient between the wells prior to pumping.

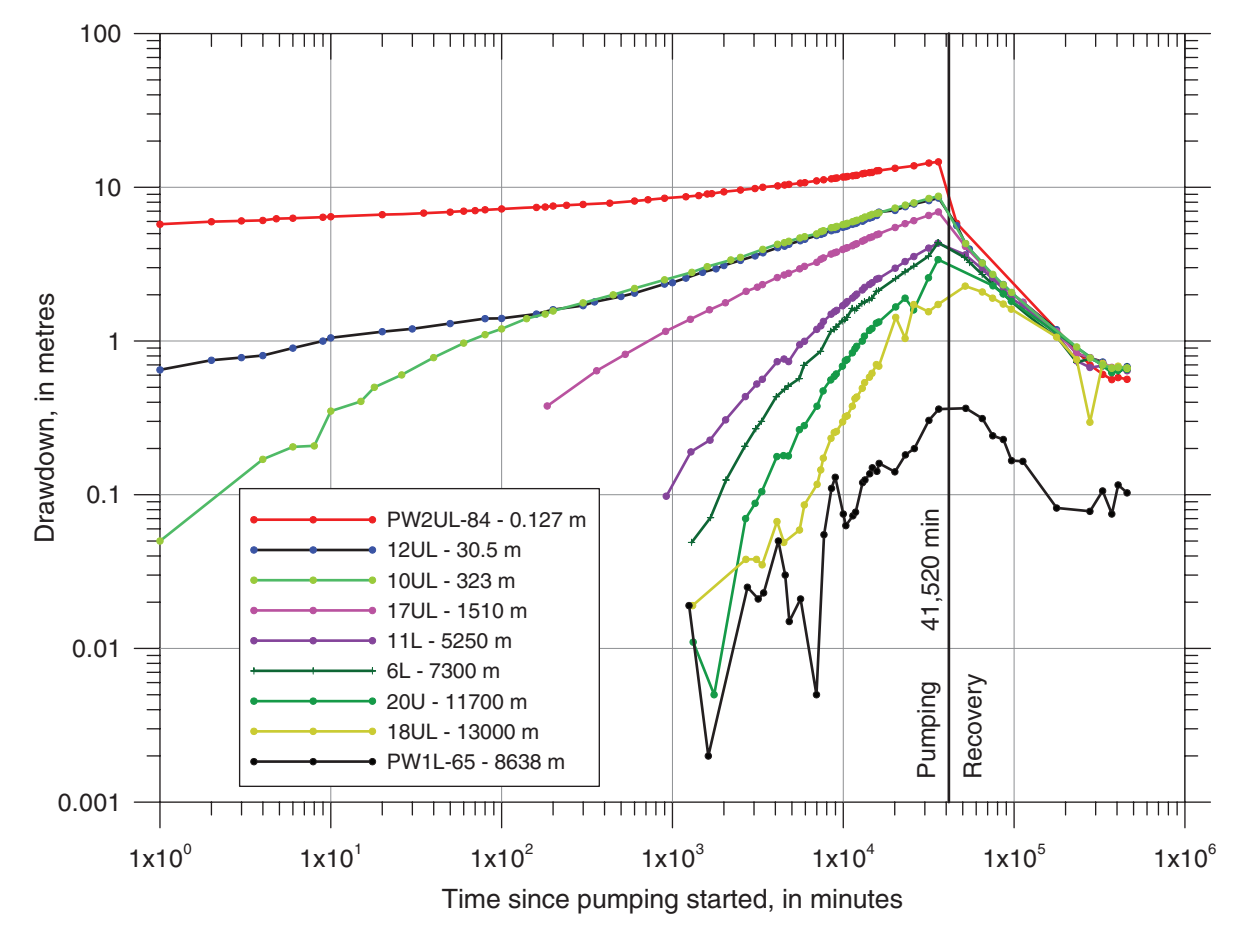


Figure 4. Drawdown data for the pumping and recovery phases of the 1984-85 pumping test on well PW2UL-84.

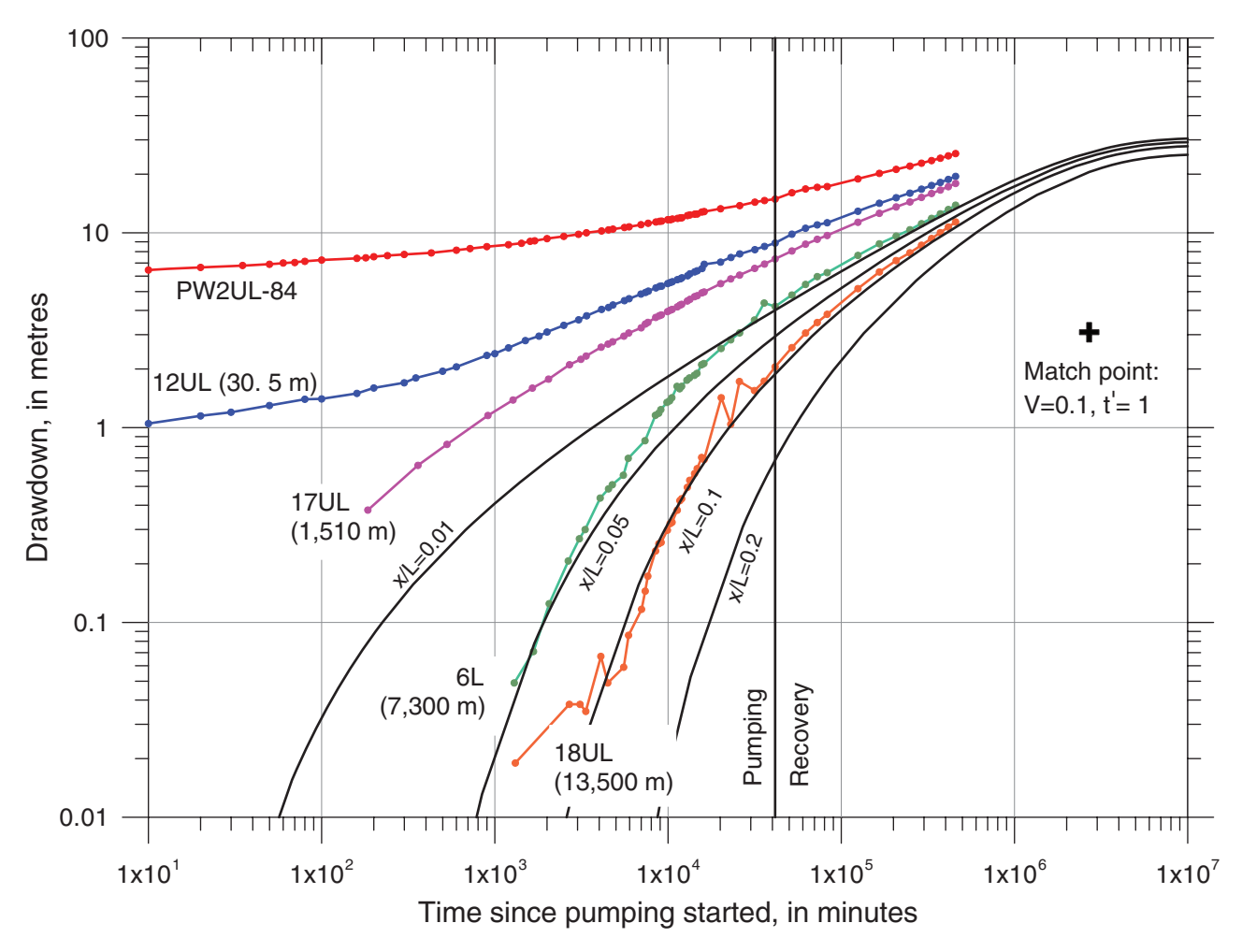


Figure 5. Extrapolated drawdown data for wells PW2UL-84, 12UL 17U, 6L, and 18UL compared with strip aquifer type curves matched to the data for 18UL. The match point is indicated for x/L = 0.1, x = 13,500 m (observation well 18UL).

The residual drawdowns were used to calculate the drawdowns that would have occurred had pumping continued, using the extrapolation method of van der Kamp (1989), thus extending he effective length of the test to almost 1 year. The extrapolation method is very general in its applicability, but it does accumulate the uncertainty in the residual drawdown during recovery because of uncertainty of the background "static water level," so that the possible error in the extrapolated drawdowns toward the end of the 11-month period is about ± 0.5 m. The late-time drawdown data for selected observation wells, including the extrapolated drawdown based on the recovery data, are plotted in Figure 5 as a log-log plot to facilitate matching to the type curves. As for the 1965 test on well PW1L-65 (Figure 1), the loglog plots of the drawdown curves for observation wells near the pumped well exhibited a "straight-line" behavior. The late-time drawdowns are likely to be influenced by transverse hydraulic barriers across the aguifer channels, the existence of which can be inferred from discontinuities in the hydraulic gradient along the various portions of the channels (Figure 3). Such barriers would be expected to lead to greater late-time drawdown then would be the case if the channels were continuous to very large distances (i.e., distances much greater than L).

To obtain aquifer parameters and an estimate of long-term yield for the aquifer, a type-curve match was made using the drawdown data for the far away well 18UL (x=13,000 m, greater than W'=4000 m) because it is the only distant observation well screened in both the top and bottom zones of the aquifer, corresponding to the pumped well. The drawdown curve for 18UL most closely matched the type curve for x/L=0.1 (Figure 5). The match point is shown, with values of $V_{\rm mp}=0.1$, $s_{\rm mp}=3.1$ m, $t_{\rm mp}=2.7\times10^6$ min and $t'_{\rm mp}=1.0$, resulting in values for the aquifer system properties of: L=130 km, $T_A=160$ m³/s, and $S_A=1.5$ m.

If the effective width of the aquifer, W', is taken to be 4000 m, these values give transmissivity and storage coefficient for the aquifer of 0.04 m²/s and 3.8×10^{-4} . Assuming an effective thickness of the aquitard of 75 m the vertical hydraulic conductivity of the aquitard K'_{ν} is then 1.8×10^{-10} m/s. The T and S values are comparable to the results of the 1965 pumping test which assessed only the lower zone of the aquifer. The K'_{ν} value of the glacial till aquitard corresponds to similar values obtained

at other sites in Saskatchewan (Keller et al. 1989; Shaw and Hendry 1998).

With x/L = 0.1 for well 18UL-84 at x = 13,000 m, the drawdown data for well 6L-82, at x = 7300 m would ideally match the type curve for x/L = 0.05. However, the drawdown data for well 6L-82 lie slightly above the x/L = 0.05 type curve. Considering the complexity of the aquifer geometry and taking into account that 6L is screened only in the upper aquifer zone, this lack of precise correspondence with the drawdown data for 18UL is not surprising. The drawdown curves show no obvious sign of a "leveling off" (indicating an approach to equilibrium) even for $t = 4.6 \times 10^5$ min, or almost 11 months (Figure 5), but the matched type curves suggest that full equilibrium would be approached after about 1×10^7 min, or about 20 years.

Within a few thousand meters of the pumped well the observed drawdowns (Figure 5) are influenced by radially convergent flow to the pumping well, causing the drawdown data at late time for well 12UL, 30.5 m from the pumped well, to lie above the type curve for x/L = 0.01 by about 6 m. The drawdown in the pumped well (diameter 0.254 m) was increased by about 11 m through a combination of radial flow and well losses.

Discussion

For late-time conditions (t' > 3, Figure 2), when steady-state conditions have been reached, the drawdown, s_0 , in the aquifer at distances greater than one aquifer width from the pumping well is given by (Vandenberg 1977):

$$s_0 = \left(\frac{QL}{2T_A}\right) e^{(-x/L)} \tag{10}$$

Equation 10 shows that the steady-state drawdowns decrease exponentially with distance away from the well, so that at x = L, 2L, and 3L the drawdowns are 0.37, 0.13, and 0.05 of the drawdown near the well (neglecting radial flow). The parameter L thus gives a useful measure of the extent of the drawdown "cone" when steady-state conditions are approached. For deep buried-valley aquifers, L values can be as large as 10 to 100 km or more and well interference can be significant even for production wells (or well fields) spaced tens of kilometers apart.

The peculiar properties of semiconfined strip aquifers as compared to semiconfined sheet aquifers are illustrated with the theoretical drawdown results given in Table 1 which summarizes the steady state drawdowns as a function of distance from the pumping well for a 1000 m wide strip aquifer and for a sheet aquifer with the same values of T and L. The steady-state drawdown in a semiconfined sheet aquifer is given by (Kruseman and de Ridder 1990):

$$s = \frac{Q}{2\pi T} K_0 \left(\frac{r}{L}\right) \tag{11}$$

Table 1

Theoretical Values of Steady-State Drawdown in a Semiconfined Strip Aquifer and a Semiconfined Sheet Aquifer with the Same Hydraulic Properties $(T=0.03 \text{ m}^2/\text{s}, L=35,000 \text{ m})$ and for the Same Pumping Rate $(0.040 \text{ m}^3/\text{s})$

	Drawdown (m)		
Distance x or r (m)	Strip aquifer	Sheet aquifer	
0.127	>23.3	2.68	
30	>23.3	1.52	
500	>23.01	0.93	
1000	22.7	0.78	
7000	19.1	0.37	
35,000	8.58	0.09	
70,000	3.16	0.02	

Note: The width of the strip aquifer is assumed to be 1000 m and the diameter of the pumping well is 0.254 m.

where r is the radial distance form the pumping well and K_0 is the modified second kind Bessel function of order zero.

These calculations show that the drawdowns caused by pumping from a strip aquifer can be at least an order of magnitude greater than for a sheet aquifer with the same hydraulic properties, especially at distances far from the pumped well. Clearly expectations about the hydraulic response to pumping for strip aquifers can be highly erroneous if they are based on experience with sheet aquifers.

The much larger drawdowns and much larger extent of the drawdown "cone" for strip aquifers have important implications for the design of pumping tests. Observation well distances of a few hundred meters, such as are typically used for sheet aquifers, can provide reasonable results for transmissivity and storage coefficient near the pumped well, but will not give useful results for the response of the strip aquifer at large distances from the pumped well. The response of the Estevan Valley Aquifer is a case in point. During the 1965 pumping test (Figure 1) with duration of 8 days, the focus was on the nearby observation wells up to 222 m distant, which provided useful data for only the first 20 min of the test. The 1984 to 1985 test (Figure 4) showed that after 8 days of pumping significant drawdowns extended out to at least 13,000 m. Observation well spacing for narrow strip aquifers should be much larger than the aquifer width and much greater than for sheet aquifers with similar hydraulic properties.

The transmissivity in the vicinity of the pumping well is an important parameter for well field design because it has a major bearing on the drawdown of the water level in the well. This transmissivity can be determined from the early-time drawdown data for nearby observation wells ($x \ll W'$) as was done for the 1965 test (Figure 1) or by means of a distance-drawdown analysis for radial

flow if data from more than one nearby observation well are available. For wide buried-valley aquifers, with width approaching or exceeding the leakage length L, the drawdown caused by pumping may be dominated by radial flow. For such cases sheet-aquifer type curves may be applicable, making use of image well methods.

When hydrogeologic data are sparse, it may not always be obvious that a particular aguifer will behave like a strip aquifer. "Straight-line" segments of the drawdown curves on log-log plots may be an indication that one is dealing with a strip aquifer or with an aquifer that has strip-like properties. The theoretical slope of the straight-line segment on a log-log plot would be 1/2 for observation wells near the pumped well in ideal strip aquifers, but radial flow drawdown will result in higher drawdown then predicted by the strip-aquifer type curves and straight-line behavior with a slope less than 1/2. Slopes somewhat less than 1/2 are commonly reported, in part because most reported pumping tests for buriedvalley aguifers only had observation wells located near the pumped well, as is routine for sheet aguifers. For example, Andersen and Haman (1970, Figure 6); Shaver and Pusc (1992, Figure 6) and Parks and Bentley (1996, Figures 6 and 9) each presented pumping test results that have typical "straight-line" strip aquifer behavior. The drawdown data for the Estevan Valley Aquifer (Figures 1 and 5) also illustrate such behavior.

Transverse low-permeability barriers are commonly encountered within buried-valley aguifers associated with glacial deposits (Shaver and Pusc 1992), but their origin is not well understood (Russell et al. 2004). Barriers of this type may not be identifiable on the basis of sparse geologic data, but a characteristic indication of their presence is the occurrence of "steps" in the hydraulic head profile along the aquifer. With respect to the drawdown caused by pumping, the possible presence of barriers means the aquifer should not be assumed to be of infinite extent. This restriction is particularly telling for buried strip aquifers in view of the large extent of the drawdown "cone." The presence of barriers, even at large distances from the pumped well may lead to additional drawdown at the well. Evaluations of flow in buried-valley aquifers typically need to take account of hydrogeological complications such as partially permeable transverse barriers within the aquifer, significant flow exchange with adjacent aquifers and complex buried-valley geometry. The type curves for an ideal leaky strip aquifer appear to be remarkably robust for simulating observations, judging by the example of the nonideal Estevan Aquifer. Nevertheless, their applicability is limited and more detailed numerical methods should be used as appropriate.

Conclusions

The type curves for semiconfined strip aquifers can be usefully employed in the understanding, prediction and analysis of drawdown caused by pumping from such aquifers. For narrow strip aquifers evaluations of groundwater resource availability based on the assumption of radial flow to the pumping well in a sheet aquifer can lead to underestimation of drawdowns and overestimation of the sustainable yields by as much as an order of magnitude.

The type curves for a strip aquifer are not applicable near the pumped well, but provide a useful theoretical model for drawdown far away from the pumping well caused by long-term pumping. Design of pumping tests for buried-valley aquifers should include placement of observation wells at distances from the pumped well greater than the width of the aquifers, and typically much further away then would be indicated by normal practice for sheet aquifers.

Log-log plots of drawdowns measured near the pumped well have a characteristic "straight-line" pattern which can serve as an indicator that a particular aquifer is behaving as a strip aquifer.

Many real-world strip aquifers, such as the buried-valley aquifers that are common in glacial deposits, have complex structures that challenge delineation by means such as test drilling or geophysical methods. Hence a pragmatic approach to dealing with groundwater flow in such aquifers is indicated, dealing with the aquifers as complex systems whose responses to pumping can only be determined and predicted by actual testing of the entire system. For important and complex cases numerical methods may be appropriate. However the strip-aquifer type curves allow useful estimates of how buried-valley aquifers respond to pumping.

Acknowledgments

An earlier version of this paper was published in conference proceedings (van der Kamp and Maathuis 2002). Many investigators have contributed to the information reviewed and summarized in this paper, among whom W.A. Meneley, W.C. Walton, and V.G. Beckie deserve particular mention. Most of the work on which this paper is based was carried out while the authors were employed by the Saskatchewan Research Council and with the financial support of the Saskatchewan Power Corporation and the Saskatchewan Watershed Authority.

References

Ahmad, J., D.R. Schmitt, C.D. Rokosh, and J.G. Pawlowicz. 2009. High-resolution seismic and resistivity profiling of a buried Quaternary subglacial valley: Northern Alberta, Canada. GSA Bulletin 121, no. 11/12: 1570–1583.

Andersen, L.J., and Z. Haman. 1970. Pumping tests and hydrogeological investigations of an artesian aquifer nears Horsens, Denmark. *Nordic Hydrology* 2: 69–110.

Beckie Hydrogeologists Ltd. 1984. Estevan Valley Aquifer System Exploration and Pump Test Program, Souris River Site. Regina: Beckie Hydrogeologists Ltd., 53 pp.

BurVal Working Group. 2006. Groundwater Resources in Buried Valleys—A Challenge for Geosciences. Hannover, Germany: Leibniz Institute for Applied Geosciences (GGA-Institut).

Butler, J.J., and W.Z. Liu. 1991. Pumping tests in non-uniform aquifers—the linear strip case. *Journal of Hydrology* 128: 69–99.

- Desbarats, A.J., M.J. Hinton, C.E. Logan, and D.R. Sharpe. 2001. Geostatistical mapping of leakance in a regional aquitard, Oak Ridges Moraine area, Ontario, Canada. *Hydrogeology Journal* 9: 79–96.
- Gill, M.A. 1992. Drawdowns for constant-discharge onedimensional leaky aquifer—discussion. ASCE Journal of Irrigation and Drainage Engineering 118, no. 2: 332–333.
- Hantush, M.S., and C.E. Jacob. 1955. Non-steady flow in an infinite leaky aquifer. *Transactions, American Geophysical Union* 36, no. 1: 95–100.
- Kehew, A.E., and W.M. Boettger. 1986. Depositional environments of the buried-valley aquifers in North Dakota. *Ground Water* 24, no. 6: 728–734.
- Keller, C.K., G. van der Kamp, and J.A. Cherry. 1989. A multiscale study of the permeability of a thick clayey till. *Water Resources Research* 25, no. 11: 2299–2317.
- Kruseman, G.P., and N.A. de Ridder. 1990. Analysis and Evaluation of Pumping Test Data, 2nd ed. Wageningen, The Netherlands: International Institute for Land Reclamation and Improvement.
- Maathuis, H., and G. van der Kamp. 2003. Groundwater resource evaluations of the Estevan Valley aquifer in south-eastern Saskatchewan: a 40-year historical perspective. *Proceedings (CD) of the 56th Canadian Geotechnical and 4th Joint IAH-CNC and CGS Conferences*, Winnipeg, MB, September 29—October 1, 4 p.
- Maathuis, H., and L.H. Thorleifson. 2000. Potential Impact of Climate Change on Prairie Groundwater Supplies: Review of Current Knowledge. Saskatoon: Saskatchewan Research Council, Publication No.11304-2E00.
- Meneley, W.A., E.A. Christiansen, and W.O. Kupsch. 1957. Preglacial Missouri river in Saskatchewan. *The Journal of Geology* 65, no. 4: 441–447.
- Motz, L.H. 1991. Aquifer parameters from constant discharge nonsteady-leaky type curves. *Ground Water* 29, no. 2: 181–185.
- Parks, K.P., and L.R. Bentley. 1996. Derivative-assisted evaluation of well yields in a heterogeneous aquifer. *Canadian Geotechnical Journal* 33, no. 3: 458–469.
- Russell, H.A.J., D.R. Sharpe, G. van der Kamp, and M.J. Hinton. 2004. A review of the architecture, sedimentology and hydrogeology of buried valley aquifers in Canada.

- Proceedings of the 57th Canadian Geotechnical conference and the 5th Joint IAH-CNC/CGS Groundwater Conference, Quebec, October 24–27, 2B26-2B33.
- Sandersen, P.B.E., and F. Jorgensen. 2003. 229-248.
- Seifert, D., T.O. Sonnenborg, P. Scharling, and K. Hinsby. 2008. Use of alternative conceptual models to assess the impact of a buried valley aquifer on groundwater vulnerability. *Hydrogeology Journal* 16, 659–674.
- Shaver, R.B., and S.W. Pusc. 1992. Hydraulic barriers in Pleistocene buried-valley aquifers. *Ground Water* 30, no. 1: 21–28.
- Shaw, J., and M.J. Hendry. 1998. Hydrogeology of a thick clay till and Cretaceous clay sequence, Saskatchewan, Canada. *Canadian Geotechnical Journal* 35, 1041–1052.
- Vandenberg, A. 1977. Type curves for analysis of pump tests in leaky strip aquifers. *Journal of Hydrology* 33, 15–26.
- Vandenberg, A. 1976. Tables and type curves for analysis of pump tests in leaky parallel-channel aquifers. *Environment Canada*, *Inland Waters Directorate*, *Technical Bulletin* 96, 28.
- van der Kamp, G. 1989. Calculation of constant-rate drawdowns from stepped-rate pumping tests. *Ground Water* 27, no. 2: 175–183.
- van der Kamp, G. 1985. *Yield Estimates for the Estevan Valley Aquifer System using a Finite-Element Model*. Saskatchewan Research Council Publication No. R-844-4-C-85.
- van der Kamp, G., and H. Maathuis. 2002. The peculiar groundwater hydraulics of buried-channel aquifers. *Proceedings* of the 55th Canadian Geotechnical and 3rd Joint IAH-CNC and CGS Conferences, Niagara Falls, Ontario, October 20–23.
- Walton, W.C. 1970. *Groundwater Resource Evaluation*. Toronto: McGraw-Hill Book Company.
- Walton, W.C. 1965. Potential yield of a sand and gravel aquifer in a buried valley near Estevan, Saskatchewan—results of aquifer and well production tests and evaluation of groundwater potential. Report prepared for the Saskatchewan Research Council.
- Zhang, W.Z. 1992. Transient groundwater flow in an aquiferaquitard system in response to water level changes in rivers or canals. *Journal of Hydrology* 133: 233–257.

TECHNICAL NOTE



A numerical investigation of pumping-test responses from contiguous aquifers

Silvain Rafini · Romain Chesnaux · Anouck Ferroud 1

Received: 3 December 2015 / Accepted: 20 February 2017 / Published online: 9 March 2017 © Springer-Verlag Berlin Heidelberg 2017

Abstract Adequate groundwater management requires models capable of representing the heterogeneous nature of aquifers. A key point is the theoretical knowledge of flow behaviour in various heterogeneous archetypal conditions, using analytically or numerically based models. This study numerically investigates transient pressure transfers between linearly contiguous homogeneous domains with non-equal hydraulic properties, optionally separated by a conductive fault. Responses to pumping are analysed in terms of time-variant flow dimension, n. Two radial stages are predicted (n: 2 - 2) with a positive or negative vertical offset depending of the transmissivity ratio between domains. A transitional n = 4segment occurs when the non-pumped domain is more transmissive (n: 2 - 4 - 2), and a fractional flow segment occurs when the interface is a fault (n: 2 - 4 - 1.5-2). The hydrodynamics are generally governed by the transmissivity ratio; the storativity ratio impact is limited. The drawdown log-derivative late stabilization, recorded at any well, does not tend to reflect the local transmissivity but rather the higher transmissivity region, possibly distant and blind, as it predominantly supplies groundwater to the well. This study provides insights on the behaviour of non-uniform aquifers and on theoretical responses that can aid practitioners to detect such conditions in nature.

Keywords Pumping tests · Heterogeneity · Hydraulic properties · Derivative analysis · Flow dimension

Introduction

Natural aquifers are essentially heterogeneous systems. Identifying hydraulic heterogeneities and anticipating their impact on groundwater flow is a fundamental and most important task given to hydrogeology researchers and practitioners. To this end, pumping tests constitute an adequate approach only if interpretative models are able to account for the heterogeneity of flow. Eighty years ago, the ground-breaking Theis (1935) model, later referred to as the infinite acting radial flow model, provided an analytical solution to the hyperbolic transient diffusivity problem by assuming a perfectly homogeneous flow configuration. By its very nature, this highest degree of idealization of aquifers is unable to render any heterogeneity of flow occurring in real aquifers. Critics of the model have cited its lack of realism, which leads to overly gross and approximate aquifer interpretations (Renard 2005; Renard et al. 2008; Pechstein et al. 2016). For practical and contextual reasons, this model has been the one most often used in hydrogeology applications without much assessment of the degree to which it diverges from reality. In contrast, decades of active research in the petroleum and hydrogeology fields have yielded several advances for modelling heterogeneous flow. The derivative analysis (Tiab and Kumar 1980; Bourdet et al. 1983, 1989; Spane 1993; Spane and Wurstner 1993; Beauheim et al. 2004; Samani et al. 2006; Dewandel et al. 2011; Avci et al. 2013; Xiao and Xu 2014; Sun et al. 2015) is frequently referred to as one of the most significant breakthroughs in pumping test analysis (e.g., Issaka and Ambastha 1999; Renard et al. 2008; Hammond and Field 2014). The central idea consists in deciphering the reservoir



Romain Chesnaux romain chesnaux@uqac.ca

Research Group R2Eau, Centre d'études sur les ressources minérales, Université du Québec à Chicoutimi, 555, boulevard de l'Université, Chicoutimi, Québec, Canada G7H 2B1

response to pumping tests by identifying the various types of flow regimes that are recorded, based on the shape of the drawdown log-derivative time series. Real data are compared to a reference panel of theoretical behaviors that have been established as corresponding to various conceptual flow models (Verweij 1995). These conceptual flow models are idealized models of aquifers which provide hydrogeologists with a range of archetypal frameworks used to interpret and describe real-world conditions that are more complex than basic idealized models. A first generation of these models is (semi-)analytical solutions of the diffusivity equation, assuming specific hydraulic and geometrical aquifer conditions. For mathematical suitability, strong postulates must commonly be made on the geometry of transient flow to reduce the diffusivity problem—a second-order partial differential equation, to a solvable form. Purely numerical approaches used in an experimental mode provide a second generation of conceptual models, predicting drawdown responses in two-dimensional (2D) or three-dimensional (3D), analytically unsolvable, heterogeneous flow configurations (e.g., Bourdet 2002). In such an approach, serial flow simulations into synthetic domains are processed to assess the sensitivity of the drawdown responses to every hydraulic and geometrical input parameter, into a given conceptual configuration (e.g., Rafini and Larocque 2009, 2012). A second breakthrough in pumping test analysis was the flow dimension theory (Barker 1988). It offered significant new perspectives in modelling hydraulic behavior by generalizing the conception of flow regimes to drawdown log-rates either increasing with time (flow dimension less than two) or decreasing with time (flow dimension greater than two), while previously published models accounted for drawdown log-rates constant or varying with time following specific coefficients 0.25, ± 0.5 or ± 1 . A constant drawdown log-rate such as described by Theis (1935), corresponds to the radial flow regime; such a regime is characterized by a flow dimension equal to two. Henceforth, to justify appropriate use of the Theis or Cooper-Jacob (1946) models, prior identification of such flow dimension conditions would theoretically be required; however, this is rarely if ever done in practice. Both the derivative and the flow dimension approaches have this in common, that they recognize the existence in nature of various types of flow regimes. Based on this recognition, and using recently developed approaches, it is now possible to select appropriate conceptual flow models by identifying the time-sequences of flow regimes observed during a pumping test. These concepts are the foundation for the interpretative framework proposed in this study.

The manner with which natural heterogeneities are hydraulically represented in commonly used conceptual models greatly depends on their size in relation to that of the investigated domain. In natural aquifers, heterogeneities governing hydraulic properties occur at various scales, from the very small (cm) grain or crystal arrangements, to commonly found

networks with characteristic metric fracture lengths, to largescale (km) features such as lithological spatial variations or regional structures where groundwater transfers occur primarily through faults, or to cross-connected aguifers (Chesnaux et al. 2012). It is of particular interest that in pumping-test conditions, the relative influence of micro-, meso-, and macro-scale heterogeneities on the drawdown response is time-variant as the scale of the investigation grows over time. Smaller-scale heterogeneities may typically be considered as fields, and may be adequately described using statistical functions; however when the investigation scale grows larger than the typical size of a single heterogeneity, usually after a very short pumping time, these fields tend to behave like homogenous media, with properties averaging the distribution function (e.g., Meier et al. 1998). Induced flow regimes will be radial, except when the distribution is scale-invariant (Cello et al. 2009). Such fields are typically well represented using stochastic hydraulic models. Conversely, larger heterogeneities that occur on a scale ranging from decameters to several kilometers must, in most pumping test cases, be represented as independent hydraulic domains influencing the macro-scale behavior during restricted time periods, i.e., when the investigation scale is of a magnitude which is comparable to the scale of the heterogeneity. These larger heterogeneities can often be modelled deterministically because only a small number of them may exert a significant impact on the flow field at any given time. Thus, the objective in this study is not to simulate stochastic heterogeneity fields but to deterministically investigate the hydrodynamic impact of specific types of large-scale heterogeneities, producing complex non-radial flow geometries. The evolving influence of such heterogeneities on the flow regime over time tends to generate convoluted responses to pumping tests, with time-variant flow regimes and inconstant drawdown log-rates.

Large-scale heterogeneous flow may result from the coexistence of several flow domains in the aguifer, each with different hydraulic properties. Indeed, in many real-life situations, the transmissivity and storativity may have different magnitudes in some domains (Rushton 2003). The assumption that hydraulic parameters are constant in the entire space located between the pumped borehole and the farthest limit of the field where pumping no longer exerts an influence may lead to false conceptual and quantitative interpretations. The hydrodynamic behavior of such composite systems has been studied analytically, assuming a radially symmetry of hydraulic domains (Barker and Herbert 1982; Bourdet et al. 1983; Butler 1988; Ambastha 1989; Oliver 1990, 1993; Roberts et al. 1996; Issaka and Ambastha 1999; Jordan and Mattar 2000). These models, referred to as patchy aguifers or composite domains, are intended to investigate pumping test responses when the local region in the vicinity of the pumped borehole is not representative of the reservoir's general hydraulic properties. For analytical suitability, the patch is



represented by a cylinder whose center is embodied by the pumping well. The predicted drawdown response of a linear interface between the two domains is more complex due to the fact that induced flow geometry is non-uniform in a 2D space. Such a configuration is also referred to as a linear strip or multi-strip reservoir. Guo et al. (2012) proposed an analytical solution for a three-region channel-aquifer combined with a dual porosity model. Flow restriction into a corridor makes it possible to process the interferences between flow domains as mathematically suitable one-dimensional (1D) problems. They obtained successive linear flow regimes before and after lateral domains were reached by the depressurization front. Ambastha et al. (1989) proposed an analytical solution for a "two-region reservoir" separated by a communicating fault, and for a strip aguifer, with emphasis on skin effects; however, the study focussed on the latter configuration with little development on the former, and the flow into the fault is not explicitly modeled. This nonintersecting finiteconductivity fault problem was later analytically approached by Abbaszadeh and Cinco-Ley (1995). These authors postulated that the problem could be reduced to three solvable problems, independent, radial and linear: (1) linear flow into the fault; (2) flows into the two embedding semi-infinite reservoirs are converted into infinite-acting flow problems by mirror-imaging them against the fault plane. The equality of pressure and fluxes is finally imposed at the domain interfaces in order to preserve hydraulic continuity. Butler and Liu (1991) developed a semi-analytical solution for a two-region aguifer split by a more transmissive strip which, under certain conditions (small transversal extent), tends to behave like a fault. Interestingly, although they used different modeling approaches, Abbaszadeh and Cinco-Ley (1995) and Butler and Liu (1991) arrived at conclusions that converge, in the sense that they predict a specific time-period where the aquifer response to pumping is predominantly governed by the properties of the nonintersecting fault or strip, namely where the flow dimension is equal to 1.5 (equivalent to the bilinear flow regime, see Rafini and Larocque 2009). Dewandel et al. (2014) submitted an analytical multi-domain model for "T" shape aquifers, which are formed by a deep and narrow region (representing a vertical fault) surrounded by two shallower and less transmissive domains. The interferences of transient depressurization into the fault and adjacent flow domains produce time-variant drawdown regimes that are analytically approximated as several infinite series of well-image functions.

This study numerically investigates the transient behaviour of aquifers composed of two laterally juxtaposed flow domains with differing hydraulic properties where the non-pumped domain may be either more transmissive or less transmissive then the pumped one. A method is proposed which predicts a singular theoretical response, in the form of a flow-dimension-sequence signature, which makes it possible to identify such aquifers in pumping test contexts. Classic

analytical solutions account for the flow behavior of juxtaposed hydraulic domains in extreme hydraulic conditions, including the impermeable barrier (i.e., nonconductive boundary) and constant-head boundary solutions (i.e., infinitely conductive). The numerical experiments described here investigate intermediate cases in which both domains have finite conductivities and the interface is nonimpermeable. The pressure transfers between both domains are deeply investigated as well as their time-variant relative contribution in supplying groundwater to the pumping well. Several cases are considered, with and without the occurrence of a fault at the interface between both domains. Cases where the non-pumped domain is respectively more transmissive and less transmissive than the pumped domain will hereafter be referred to as *leaky* and *non-leaky* cases. These two limiting cases deeply diverge from a hydrodynamic standpoint in that the domain which is predominantly supplying the well is the pumped domain or the non-pumped domain. The term *leaky* is borrowed from Hantush (1960) because the conceptual configuration to which this paper refers is a horizontal equivalent of the classic leaky aguifer model: in both cases, the pumped groundwater is supplied by a distant reservoir that is juxtaposed, either horizontally or vertically, to a less transmissive pumped aquifer; however, both problems are drastically different from a hydrodynamic perspective (i.e., geometry of leaky flow).

Materials and methods

The numerical simulations are performed using the HydroGeoSphere code, which is a three-dimensional finite-element code that has been used by numerous hydrogeology researchers (Brunner and Simmons 2012). Constitutive diffusion equations are solved using the control volume method with a fully implicit time discretization. The spatial discretization uses orthogonal tridimensional prisms of various sizes that are adjusted to anticipated drawdown variations. Hydraulic continuity between sub-domains (well/matrix or matrix/matrix) is implicitly ensured by superposing respective flow contributions at the interface nodes.

The inner boundary conditions are those of a pumping test. The wellbore is vertical, unidimensional and entirely crosscuts the aquifer. The source has no storage and a screen radius of 0.05 m. The pumping rate, Q, is equal to $4.17 \times 10^{-4} \, \mathrm{m^3 \, s^{-1}}$ or $1,500 \, \mathrm{L \, h^{-1}}$. The upper and lower boundaries are impermeable. The initial head is uniform over the entire domain and is equal to the constant-head values at the lateral boundaries. Time sampling is logarithmic and contains approximately $100 \, \mathrm{steps}$, beginning at $10^{-2} \, \mathrm{and}$ ending at approximately $10^9 \, \mathrm{seconds}$.

The flow domain is designed to be artificially large (4×10^5 by 4×10^5 by 42 m), the duration of the simulated pumping



tests is intentionally long (10⁹ and 10¹¹ s), while the distance, d, between the pumping well and the interface, is set at 2 m. These settings were designed for numerical experiment suitability, i.e., to "scan" a wide spectrum of parameter combinations to fully constrain the behavior of the system, without changing the model's geometry. Explicitly, to properly constrain the impact of a given parameter, it is necessary to perform numerous simulations while changing only this parameter, from the lower limiting case to the upper limiting case. Accordingly, the simulations were configured to optimize the visibility of successive flow regimes without changing other input parameters, even when covering a large panel of parameter combinations (e.g., aquifers transmissivities, $T_{\rm m}$, ratios). The implications of the modelling settings are addressed in the section 'Discussion', notably on the matter of using the results in real-world conditions. First, the technical note presents the case of laterally juxtaposed flow domains with no fault at the interface. Then, the effect of a finite-conductivity fault on transient flow interactions between the two domains is analysed. Such disposition of a fault between two distinct lithological domains is a widespread tectonic situation, since the fundamental characteristic of a fault is that it splits and offsets two contiguous units. The aquifer thicknesses, b, are set to 42 m. The interface between the two flow domains is vertical. Lateral boundaries oriented parallel to the Ov axis possess constant heads equal to 80 m, whereas those oriented parallel to the Ox axis are no-flow boundaries (Fig. 1). When present, the fault is vertical, 0.3 m wide and entirely crosscuts the aguifer. It is considered as a tabular vertical thin aguifer in itself, which allows for transient flow to be resolved in a similar fashion to a porous medium. Thus, the fault is viewed as a Darcian medium rather than a Poiseuille fracture. The Poiseuille model is considered inadequate to represent macro-scale faults, which are much thicker than infra-meterscale fractures and contain material-filled core rather than void space. The hydraulic properties are isotropic in the entire flow domain. The drawdown response examination focuses on time periods prior to reaching the lateral boundaries. The size of the mesh in the vicinity of the pumping well is 0.05 m, which progressively increases toward the boundaries. No vertical flows are generated from these configurations. Therefore, the vertical discretization is strongly restricted (three cells), for computing purposes. Only one flow domain is pumped (domain A); the non-pumped flow domain (domain B) can be variably conductive, and hence may or may not produce leakage from domain B to domain A. Finally, numerous simulations are performed to produce a systematic analysis of the effect of each hydraulic input parameter on the macroscopic response rendered at the pumping well. These series of simulations are designed to achieve a general flow behavior in which the sensitivity of every parameter is known.

Results from numerical simulations are analysed in terms of drawdown log-derivative ds/dlog(t) and of flow dimension

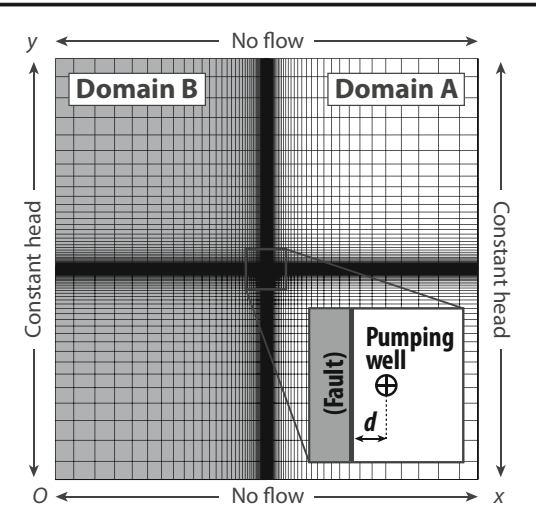


Fig. 1 Configuration used for the numerical flow simulations in laterally juxtaposed flow domains. The grid corresponds to the spatial discretization. Two cases are considered depending upon the occurrence of a fault at the interface between domains A and B

n that is calculated following the definition of Barker (1988), n = 2 - 2(p), where p is the slope of the log-derivative series. This equation of n postulates an asymptotic approximation that is, from a practical standpoint, valid after a very short pumping time at the pumping well.

Results

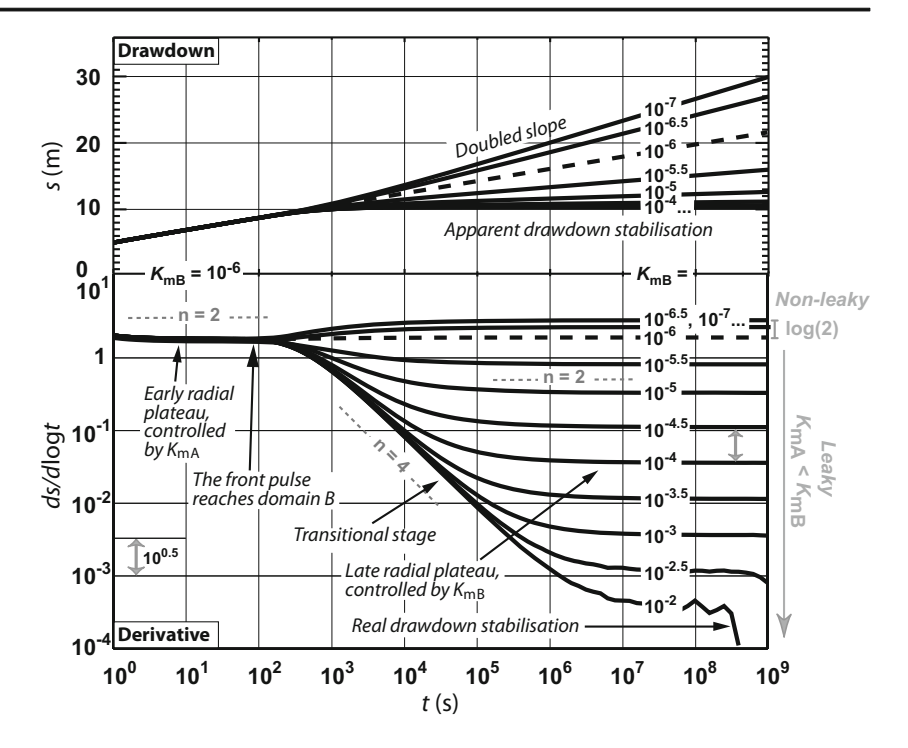
Contiguous aquifers with unfaulted interface

Influence of the conductivity ratio

The pumping well drawdown responses obtained from flow simulations with varying conductivity of the non-pumped domain, $K_{\rm mB}$, are presented in Fig. 2. A series of simulations was performed to assess the influence of $K_{\rm mB}$ being lower or higher than the pumped domain conductivity, K_{mA} , by incrementally changing K_{mB} , starting with $K_{\text{mA}} = K_{\text{mB}}$. The signals are composed of three successive flow regimes: (1) early radial flow corresponding to the normal diffusion into domain A before domain B is reached; (2) a transitional period marked by a characteristic derivative slope of p = -1 (n = 4); and (3) late radial flow corresponding to a simultaneous diffusion into both domains. The elevation, a, of the plateau formed during the radial flow regime is an inverse function of the conductivity. This function is simply derived using the Cooper-Jacob's model: $a = 2.3Q/4\pi T$, where T is the transmissivity and Q is the pumping rate. Here, the late radial plateau elevation, a_{r2} , displayed in Fig. 3, provides an apparent conductivity, K_{app} . The positive vertical offset of this plateau between the early and late radial stages is equal to log (2) when $K_{\rm mB} << K_{\rm mA}$ (i.e., the non-leaky case) because $K_{\rm app} = K_{\rm mA}/2$. This results in the classical impermeable boundary model (i.e., doubling the



Fig. 2 Simulated drawdown and drawdown log-derivative obtained from unfaulted laterally juxtaposed flow domains with different values of conductivity ratios. n indicates the successive flow dimensions. A series of simulations are performed with identical parameters except for the conductivity of the non-pumped domain B, $K_{\rm mB}$, which varies by increments of $10^{0.5}$ m s⁻¹, beginning with $K_{\rm mA} = K_{\rm mB}$ (dotted signal). Other parameters are $K_{\rm mA} = 10^{-6}$ m s⁻¹; $S_{\rm s_{\rm mB}} = 10^{-4}$ m⁻¹; d = 2 m; and $Q = 4.16 \times 10^{-4}$ m³ s⁻¹; and $Q = 4.16 \times 10^{-4}$



drawdown slope on conventional semi-log plots). However, when $K_{\rm mB} >> K_{\rm mA}$ (i.e., leaky cases), the vertical offset is negative and proportional to $K_{\rm mB}$ in such manner that $K_{\rm app} = K_{\rm mB}/2$; hence, when the non-pumped, more transmissive aquifer starts being depressurized, both the drawdown rate and its log-derivative drop. It is worth noting that, on a classic semi-log plot, this drop produces an apparent stabilization that is likely misinterpreted as the attainment of a recharge boundary (Fig. 2). Finally, these observations lead to the conclusion that the apparent conductivity is equal, in both configurations, to half the highest conductivity.

A series of simulations with varying $K_{\rm mB}$ and $K_{\rm mA}$ values achieved the relationship $K_{\rm app} = (K_{\rm mB} + K_{\rm mA})/2$, which is shown in Fig. 4. For each of the three lines shown in this figure, the zone in which both conductivities significantly

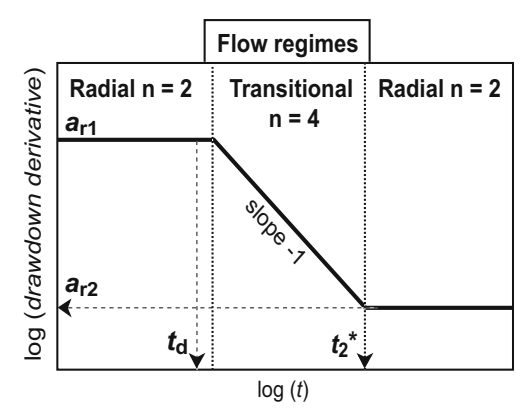


Fig. 3 Schematic illustration of the successive flow regimes predicted in the non-faulted leaky model, and their associated graphical features (see Table 1 for equations)

affect $K_{\rm app}$ is represented by the curved portion of the line between the straight portions that correspond to the dominance of either $K_{\rm mA}$ (horizontal straight portion, i.e., $K_{\rm mB}$ is negligible) or $K_{\rm mB}$ (unit slope straight portion, i.e., $K_{\rm mA}$ is negligible). This curved portion is nearly an order of magnitude wide along the $K_{\rm mB}$ axis, which means that the lower

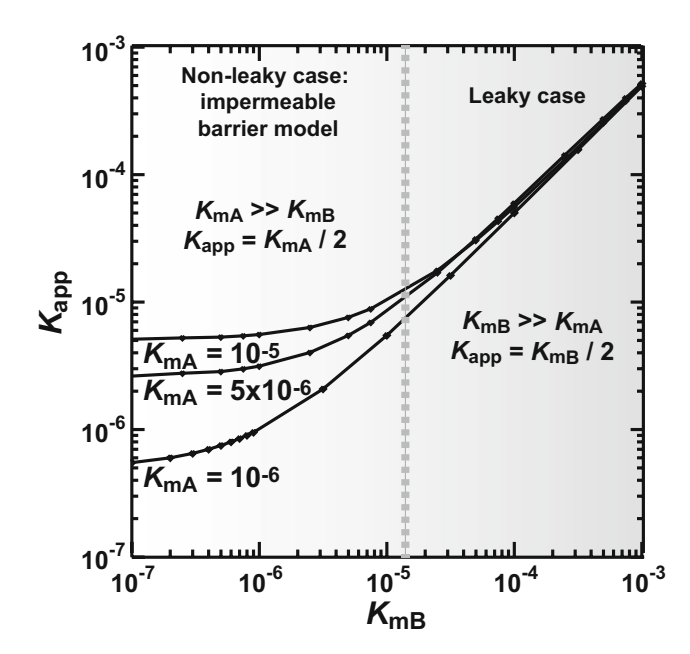


Fig. 4 K_{app} vs K_{mB} exhibiting the two models depending on the K_{mB}/K_{mA} ratio: laterally juxtaposed flow domains models with respectively high and low conductivity of the lateral flow domain (referred to as leaky and non-leaky cases in the text). The low conductivity case is similar to the impermeable barrier model. *Each point* corresponds to a numerical flow simulation



conductivity becomes practically negligible when the conductivity differences between both flow domains exceed half an order of magnitude (i.e., a factor of 3.16), all other parameters being equal.

During the second radial flow regime, the macroscopic behavior of the system, as given by the drawdown response at the pumping well, is controlled by the most conductive flow domain because drawdown propagation in the less conductive domain is slower $[r(t) \sim (K_{\rm m})^{0.5}]$. Thus, the portion of the cross-flow area (i.e., the surface of the front of depressurization) in this domain becomes negligible compared with the portion that propagates into the most conductive domain in such a manner that its depressurized volume becomes lower than that of the most conductive domain, as does its contribution to supplying water to the pumping well. This phenomenon is perfectly illustrated in Fig. 5 for the leaky case: the relative groundwater contributions from both domains to the pumping well becomes inverted over time, as the aquifer response becomes controlled by the properties of the nonpumped, and more transmissive, aquifer.

The outward propagation of drawdown into the two halfspaces forms two half front pulses growing at two different rates (Fig. 6). Only the half that propagates into the more conductive domain has a significant effect on the drawdown response at the pumping well during the late radial stage. The response is entirely controlled by the transient growth of the dominant front, whether or not this half front evolves into the flow domain that is directly pumped. In other words, if the non-pumped domain is the most conductive, the properties of the pumped domain have no influence on the drawdown response measured at the pumping well during this late radial stage. Finally, as the effective cross-flow surface growth is restricted to a half space, it takes the shape of a half cylinder, and the transmissive area is half that of an entire cylinder, which explains why the apparent conductivity is half the real conductivity of the most conductive domain.

In the leaky case, the significant portion of the domain supplying the well schematically forms a half cylinder in domain B (Fig. 6b), during the late radial stage; hence, from a hydrodynamic perspective, this can be regarded as an inverted impermeable boundary model (with the pumped domain playing the role of the barrier), albeit the less conductive domain is not actually impermeable. Analytically, the respective drawdown influences of both half fronts at the pumping well can be separately described. Based on the numerical simulation results, these drawdowns can be represented using the superposition of two impermeable-boundary radial solutions: one normal (domain B plays the role of barrier) and one inverted (domain A plays the role of barrier; see Fig. 6). These two solutions correspond to two half front pulses with unequal radii (approximate cylinders), one being largely dominant depending on the respective properties of both domains. The impermeable-boundary solution classically uses an

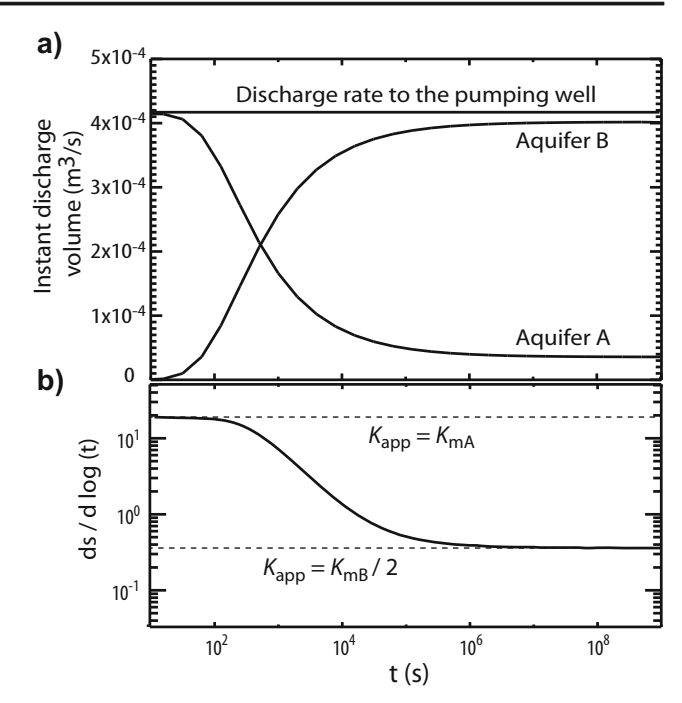


Fig. 5 a Evolution of the relative contribution of both domains to the pumping well discharge for the leaky case; **b** associated derivative response. Simulation input parameters are: $K_{\rm mA} = 10^{-7}$ m s⁻¹, $K_{\rm mB} = 10^{-5}$ m s⁻¹, $S_{\rm s_mA} = S_{\rm s_mB} = 10^{-5}$ m⁻¹; other conditions are identical to Fig. 2

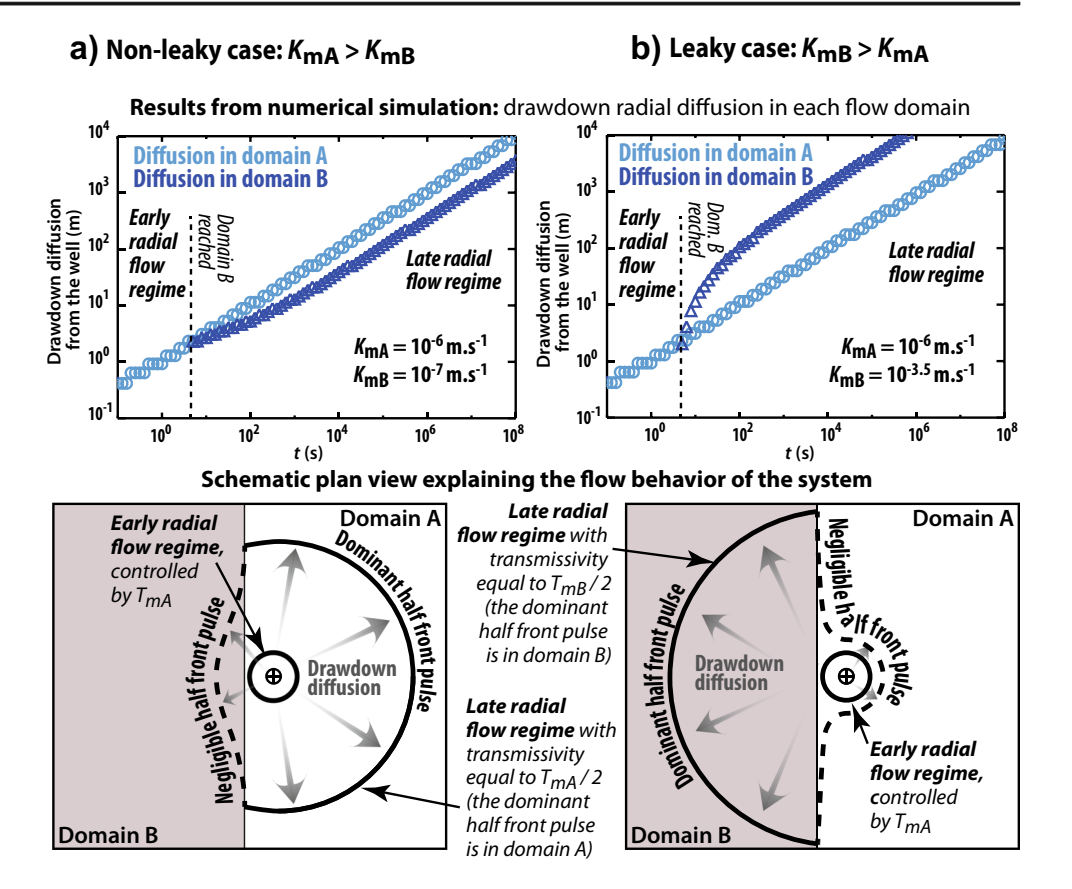
image-well analysis, which is based on the superposition of a fictitious well that is symmetrically opposite the true well, beyond the barrier. It is theoretically pumped at a rate equal to that of the true well in order to mimic the boundary effect (Ferris 1949; Fenske 1984); thus, the behavior of the system may be represented by four Theis functions: two with K_{mA} and $S_{\rm s~mA}$ properties (normal impermeable-boundary solution with real pumping in domain A and its image in domain B; S_S is specific storage) and two with $K_{\rm mB}$ and $S_{\rm s}$ mB properties (inverted impermeable-boundary solution with "false pumping" in domain B and its image in domain A). For each couple, one term (pumping or image) would have a distance equal to the well-casing radius and the other a distance equal to 2d; however, this assumption requires further validation. Separately, the two wells used in this solution can represent some of the flow regimes numerically achieved in this study, including early radial and late impermeable-boundary radial (non-leaky case) conditions; however, the late radial flow regime, or the leaky, inverted impermeable-boundary case (Fig. 6b), cannot be described by a trivial addition of these four terms, nor can a general solution be proposed that includes all flow stages. The reason is that this regime occurs in domain B, while in every case the early radial flow stage occurs in domain A; thus, an analytical solution to this problem requires further work.

Finally, it should be noted that the S_{s_mA}/S_{s_mB} ratio does not impact the shape of the derivative response, since it does



Hydrogeol J (2017) 25:877-894

Fig. 6 Top row: Drawdown diffusion vs elapsed pumping time obtained from simulations with (panel a) $K_{\text{mA}} > K_{\text{mB}}$ and (panel b) $K_{\text{mB}} > K_{\text{mA}}$. Other parameters are $S_{s_mA} = S_s$ $_{\rm mB} = 10^{-4} \text{ m}^{-1}; \ Q = 4.16 \ 10^{-4}$ $m^3.s^{-1}$; and d=2 m. Bottom row: Schematic views of the front pulse geometries for cases (panel a) and (panel b) during early and late radial flow stages. The small crossed circle in the middle is the pumping well. Dotted lines mark the portion of the depressurization front pulse that exerts a negligible influence on the macro-scale response. T_{mA} and T_{mB} are the transmissivities for domains A and B, respectively



not influence the elevations of the plateaus. It only slightly affects the shape of the transition n = 4 stage.

Calculation of hydraulic parameters

The diagnostic tool for the unfaulted leaky model is formalized in Fig. 3 and Table 1. The time, t_d , corresponds to the time it takes the front pulse to reach domain B. The solution of the set of three equations (Eqs. 1, 2 and 5 in Table 1) permits the estimation of $K_{\rm mA}$, $K_{\rm mB}$ and the distance, d, from the pumping well to domain B; however, this equation for t_d , which was proposed by Banton and Bangoy (1999), must be considered a first-order approximation. The form of the equation is correct because it is derived from the normal diffusion law $r^2 = C(K/V)$ S_s) t, but stating a diffusion coefficient, C, equal to 2.25 is based on the Cooper-Jacob solution (by posing drawdown equal to zero), which is not valid at early pumping times. During this time period, drawdowns are expected to diffuse in a strictly Theissian mode, which is faster due to a coefficient C equal to 4π based on the Theis solution, a value which falls much closer to, if not exactly on, the value derived from the numerical simulations of this study. Moreover, this equation does not account for any delay in the propagation of the front pulse caused by wellbore depressurization and/or skin effects; hence, Eq. (5) likely underestimates (strong wellbore storage or skin effect) or overestimates t_d (C greater than 2.25). This issue remains unresolved and requires further investigation, as it falls outside the scope of this article. In particular, it should be pondered that time-distance scaling relationships may vary with successive, radial and non-radial flow regimes. The formula published by Banton and Bangoy (1999) will be considered acceptable here as a first estimate.

Analysis of observation well data

Simulated drawdown behavior in synthetic observation wells (OW) at various distances from the pumping well are analysed. Specifically, this investigation focuses on the case of interest where the non-pumped domain B is the most conductive and hence predominantly supplies groundwater via the pumped domain A (leaky case). To this end, $K_{\rm mB}$ is set two orders of magnitude higher than $K_{\rm mA}$.

Figure 7 depicts the derivative responses obtained at OW at various distances from the pumping well. Only OWs located along the axis perpendicular to the interface are displayed, for illustrative purposes. At equal distance from the pumping well, OW located along other directional axes give derivative responses ranging between western and eastern OW along the *Ox* axis. Two plateaux are exhibited, corresponding to the successive predominance of radial flow regimes occurring



Table 1 Algebraic expressions of the graphical features of the models: segment intercepts and critical times

Eq. number	Expression	Graphical feature	Source
1	$a_{r1} = \frac{2.3Q}{4\pi b K_{mA}}$	Early radial plateau elevation	Modified from Cooper and Jacob (1946)
2	$a_{r2} = \frac{2.3Q}{4\pi b \left(\frac{K_{\text{mA}} + K_{\text{mB}}}{2}\right)}$	Late radial plateau elevation	This study (modified from Cooper and Jacob 1946)
2	$a_{\rm f} = \frac{2.8Q}{4\pi b T_{\rm f}^{0.5} \left(S_{\rm s-m} \frac{K_{\rm mA} + K_{\rm mB}}{2}\right)}$ 0.25	Intercept of the $n = 1.5$ segments	Modified from Rafini and Larocque (2009)
4	$a_{tr} = \frac{0.21d^2Q}{b\eta_{\text{mA}}K_{\text{mA}}}$	Intercept of the $n = 4$ segments	This study
5	$t_d = 0.44 \frac{d^2}{\eta_{\text{mA}}}$	Reaching of the interface	Cooper and Jacob (1946), Banton and Bangoy (1999)
6	$t_2^* = 0.58 \frac{d^2}{\eta_{\rm mA}} \frac{K_{\rm mB}}{K_{\rm mA}}$	Intersection time between segments $n = 4$ and late $n = 2$	This study
7	$t_{2AB} = \frac{0.44T_{f}^{2}S_{s_{m}}}{\left(\frac{K_{mA}+K_{mB}}{2}\right)^{3}}$	Intersection time between segments $n = 1.5$ and late $n = 2$	Modified from Rafini and Larocque (2009)
8	$t_1 = \frac{0.11S_{\rm f}^2}{K_{\rm m}S_{\rm s_m}}$	Beginning of the diffusion slow-down in the fault	Modified from Rafini and Larocque (2009)

Note t_2^* was obtained by assuming $K_{mB} >> K_{mA}$, and hence is exclusively valid for the leaky model. $S_{s,m}$ is the bulk specific storage coefficient, which encompasses $S_{s,mA}$ and $S_{s,mB}$. It is shown that $S_{s,m} \approx (S_{s,mA} + S_{s,mB})/2$. S_f is the fault's storage coefficient. Other parameters are introduced in the text

respectively in domains A and B as explained in the preceding. These two plateaux (early radial plateau and late radial plateau) are visible particularly well on the normalized t/r^2 plot. Due to the short distance (2 m) between the pumping well and the interface, the duration of the early radial plateau is short. OW located at distances less than 2 m behave similarly both on the west and east sides of the pumping well a

predictable result, since domain B has not yet been reached. At greater distances, the influence of an early radial flow regime is practically invisible on western OW, while eastern OW display a gradational transition to the late radial plateau elevation.

An unexpected result is that, among the eastern OW, i.e., those located on the side opposite to the interface, drawdown

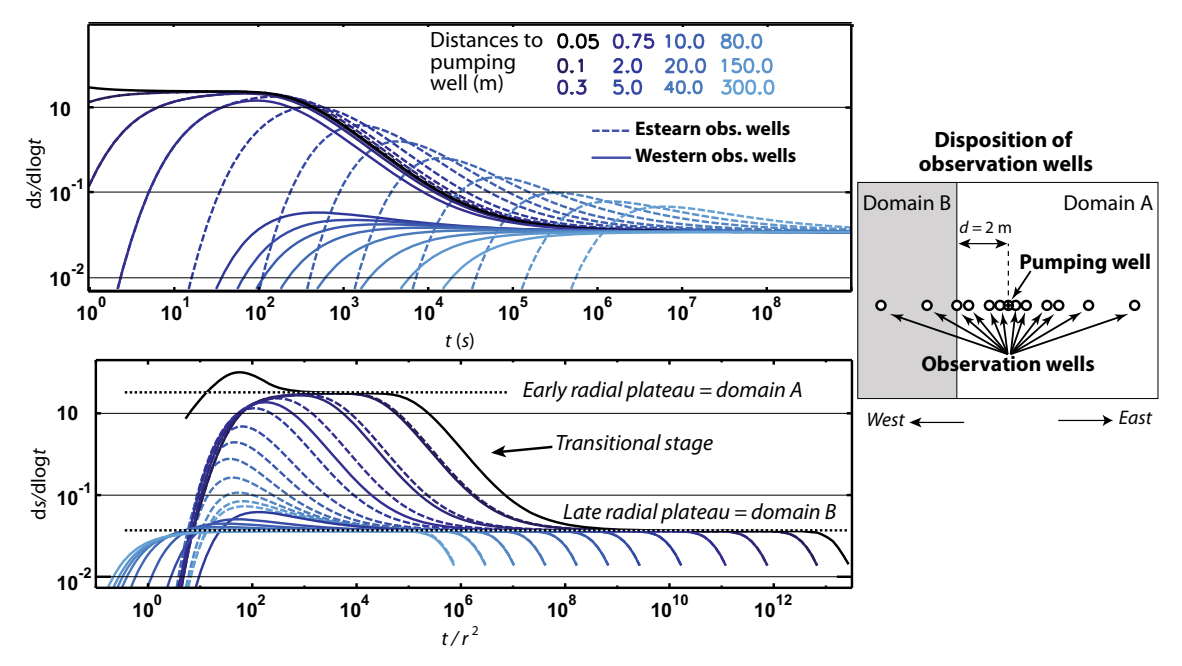


Fig. 7 Simulated drawdown log-derivative obtained from observation wells and the pumping well, in the unfaulted leaky case. The configuration is similar to Fig. 2 results. The pumping well response is

shown in *black color* (distance is equal to the casing radius, 0.05 m). Hydraulic parameters are $K_{\rm mA}=10^{-6}$ m s⁻¹; $K_{\rm mB}=10^{-4}$ m s⁻¹; $S_{\rm s_{-mA}}=S_{\rm s_{-mB}}=10^{-4}$ m⁻¹; $Q=4.16\times10^{-4}$ m³ s⁻¹



regimes do not rapidly adjust to the dominant aquifer behavior that is obtained at the pumping well and in the western OW. Indeed, at late time, when the pumping well response clearly shows that a late radial flow regime has settled into the aquifer and dominates its macro-scale hydrodynamics, the drawdown derivative in these distant eastern OW does not merge with this radial regime but rather displays a prolonged gradational transition. This implies that, while the drawdown regime tends to equilibrate over the entire aguifer, the attainment of such homogenous dynamic state is very slow in regions distant from the hydraulic heterogeneity governing the global behavior. This study's results suggest that, over the time scale of a pumping test, the state of equilibrium may not be obtained in distant OW. The greater the distance between the eastern OW and the pumping well and the contrast in conductivity between both aguifers, the later the late radial plateau settles after the transitional stage. This phenomenon may impede its proper identification in real pumping test conditions. This conclusion meets that of Ambastha et al. (1989).

After the transitional stage, drawdown behaviors in all OW are governed by the late radial flow regime. This regime is strictly controlled by the transmissivity of the non-pumped domain B, since domain B is more transmissive, as explained in previous sections. In other words, the transmissivity one would estimate by a classic Cooper-Jacob interpretation of the late radial regime measured in an OW located in domain A would actually correspond to the transmissivity of domain B (or more precisely, half of it as explained previously). This counteracts the general belief that the transmissivity measured at an OW is always a proxy to the *T*-field into the area between the OW and the pumping well. Instead, the results indicate that, after late-time stabilization of the derivative, the apparent *T* value actually corresponds to that of the more transmissive

region of the aquifer, regardless of its spatial disposition in relation to the OW.

A classic multi-well analysis in homogeneous media consists in plotting OW log-distances versus drawdown at a given pumping time. A straight line is obtained whose slope and vertical offset, respectively, allow estimating spatially averaged values of T and S, using the Cooper-Jacob model. In non-uniform or heterogeneous media, the points are not expected to form a straight line but rather several lines or curves expressing the successive flow regimes that occurred before the targeted time. The success of such analysis depends on the spatial equilibrium of the current drawdown regime over the entire aquifer. Any target time into transitional stages between two spatially homogenous drawdown regimes may not be likely to produce interpretable plots; hence, late-times are preferred, which more probably correspond to such equilibrium states, and investigate a larger volume of aquifer. Figure 8b displays the distance-drawdown plot for 100 OW placed around the well at distances ranging from 0.1 to 300 m, along eight directional axes (Fig. 8b). OW located along the Ox axis are symbolized by circles (east side) and crosses (west side). Drawdowns at these OW clearly exhibit two straight lines, with slopes changing abruptly (western OW) or gradually (eastern OW). Such responses are in accordance with the multi-well derivative analysis depicted above, where eastern OW flow regimes gradually evolve from the first to the second radial flow regime, while western ones display a short transition. These two straight lines depict the two successive flow regimes occurring during the well test, induced by the coexistence of two flow domains. Using the Cooper-Jacob equation $K = 2.3Q/2\pi p$, where p is the slope, one can estimate the apparent conductivity K_{app2} which is equal to $(K_{mA} +$ $K_{\rm mB}$)/2. OW located along other directional axes than Ox

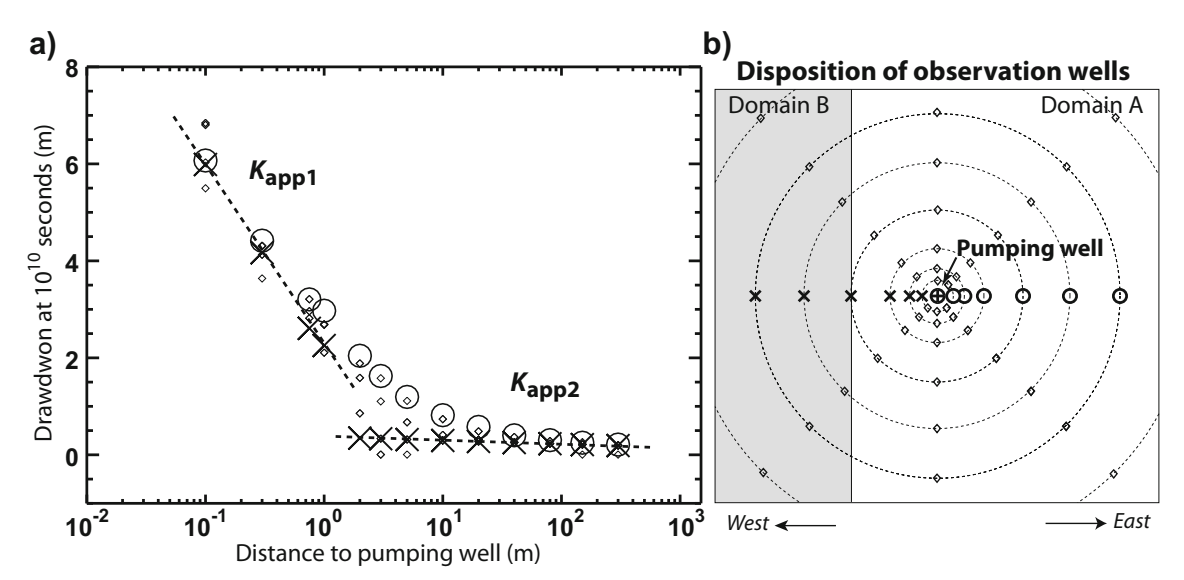


Fig. 8 a Distance-drawdown plot. Observation well drawdowns are obtained from flow simulation in the unfaulted leaky case. The simulation parameters are the same as those explained in Figure 6. b Spatial arrangement of observation wells



display drawdown levels with intermediate behaviours, i.e., ranging between the two lines formed by Ox-directed western and eastern OW drawdowns.

This distance-drawdown plot is a useful tool to diagnose the presence of two laterally contiguous flow domains, when two straight lines are exhibited either with a gradual or abrupt change. It provides valuable insight, along with the derivative and flow dimensional analysis, allowing for confident interpretation of this conceptual model.

Contiguous aquifers with faulted interface

Rafini and Larocque (2009) proposed an interpretative model for aguifers crosscut by a steeply inclined conductive fault that is not directly connected to the well. These results corroborated the analytical model proposed by Abbaszadeh and Cinco-Lev (1995) and provided the flow dimension diagnostic signature (2 -4-1.5-2). This signature indicates the following chronological succession of flow regimes: (1) an early radial flow before the fault is reached, with a plateau elevation equal to $2.3Q/4\pi T_{\rm m}$, where $T_{\rm m}$ is the embedding aquifer transmissivity; (2) a characteristic transitional regime n = 4; (3) the n = 1.5 typical fractional response of a conductive fault (also referred to as bilinear); and (4) a late radial flow regime that is identical to the early radial flow, during which the fault no longer influences the aquifer (Rafini and Larocque 2009). At this late radial stage, the aguifer response is controlled only by the hydraulic properties of the embedding aguifer, and the fault becomes transparent. In this model, the fact that early and late radial stages are identical (in other words, that their plateau elevations are equal) is a key point that indicates that flow domains on both sides of the fault are identical and that the fault does not juxtapose two distinct lithological units. Here, the study numerically investigates the case in which the fault embodies the interface between two distinct hydraulic blocks. The parameters of the numerical simulation are analogous to that described in the previous section in all aspects, except for the presence of a third hydraulic unit (the fault), which is much thinner and located between the two domains (Fig. 1). The simulation strategy is also analogous to the one explained previously, wherein a series of sensitivity analyses are performed to independently identify the respective impacts of each hydraulic parameter or combinations of parameters on the macroscopic response recorded at the pumping well.

The drawdown response obtained at the pumping well is presented in Fig. 9, in the form of a sensitivity analysis of coupled $K_{\rm mB}$ and $S_{\rm s~mB}$. These parameters are progressively modified by steps of half an order of magnitude, which increase and decrease from the equality to domain A properties (dotted curve). Modifying these parameters in the same way was set for illustrative purposes, to keep the domain B diffusivity $\eta_{\rm mB} = K_{\rm mB}/S_{\rm s_mB}$ constant and to optimize the visibility of the successive flow regimes. A succession of four flow regimes marked by flow dimension values 2, 4, 1.5, and 2 is obtained, which is analogous to the succession achieved by Rafini and Larocque (2009) for a single flow domain crosscut by a fault, except that in this case, the early and late radial flow regimes display unequal plateau elevations. These two early and late radial flow regimes are identical to that of the unfaulted model addressed in the previous section. Remarkably, the obtained sequence turns out to be a trivial combination of the respective signatures generated by, respectively, a single conductive fault embedded into an aguifer (n = 1.5), and contiguous aguifers with unfaulted interface (n sequence 2 - 4 - 2 with unequal plateau elevations).

Similar to the unfaulted cases, the apparent conductivity calculated from the late radial plateau elevation corresponds to the arithmetic mean of the conductivities for

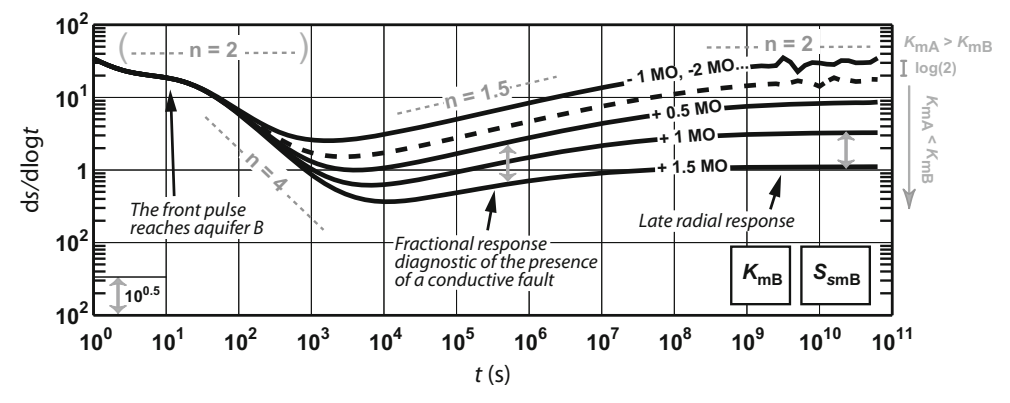


Fig. 9 Drawdown log-derivative response and flow dimension (n) analysis for flow simulations in faulted laterally juxtaposed flow domains. A series of simulations are performed with identical parameters except for the conductivity and specific capacity of the non-pumped domain $(K_{\text{mB}} \text{ and } S_{\text{s_mB}}, \text{ respectively})$, which vary by the quantity indicated on each signal (MO magnitude order), compared

with the case in which both domains have equal properties (dotted signal). Other parameters are $K_{\rm mA}=10^{-7}~{\rm m~s^{-1}}$; $S_{\rm s_mA}=10^{-6}~{\rm m^{-1}}$; $b_{\rm m}=42~{\rm m}$; $K_{\rm f}=10^{-3}~{\rm m~s^{-1}}$; $S_{\rm s_f}=10^{-5}~{\rm m^{-1}}$; $b_{\rm f}=0.34~{\rm m}$; and $Q=4.16\times10^{-4}~{\rm m^{3}~s^{-1}}$. Noise occurrence in late time is due to numerical instability



domains A and B. Figure 9 illustrates that this elevation inversely and linearly evolves with K_{mB} (as indicated by the gray arrow; the vertical offset is a factor that is equal and inverse to the variation of $K_{\rm mB}$), when $K_{\rm mB}$ exceeds $K_{\rm mA}$. When $K_{\rm mB}$ is less than $K_{\rm mA}$, the elevation of the late radial plateau tends to remain equal to twice the early radial plateau elevation, mimicking the behavior of nonleaky cases described in the previous section. Moreover, the simulations demonstrate that during the preceding n = 1.5 flow regime, the vertical offset, a_f , of the logderivative straight-line response (a_f strictly equals ds/dlog(t) at log(t) = 0, see Fig. 10) evolves as an inverse square root function of $K_{\rm mB}$ $S_{\rm s_mB}$ when $K_{\rm mB} > K_{\rm mA}$, as visible in Fig. 9. Hence, $a_{\rm f} \sim (K_{\rm mB}~S_{\rm s_mB})^{-0.25}$. The effects of other hydraulic parameters, such as $K_{\rm mA}$, $S_{\rm s}$ $_{\rm mA}$, $T_{\rm f}$, $S_{\rm f}$, b and Q, on a_f were analysed, leading to Eq. (3) (Table 1). The simulations are also designed to identify eventual non-independent factors, which would express in the equation through the presence of additive or subtractive operators. The only additive operator is $K_{\rm mB}$ + $K_{\rm mA}$. This factor does not modify the effect of other parameters because it is situated at the downstream end of the hierarchical structure of the equation. Finally, this equation is analogous in its form to the general equation of aquifers crosscut by a steeply inclined conductive fault (Rafini and Larocque 2009, 2012).

The time, $t_{\rm 2AB}$, which marks the transition between the fractional and late radial flow regimes (Fig. 10), can be derived using the a_{r2} and $a_{\rm f}$ equations displayed in Table 1 (Eqs. 2 and 3). Thus, a graphical interpretation of $a_{\rm f}$ and $t_{\rm 2AB}$ makes it possible to calculate the fault transmissivity, $T_{\rm f}$, and the apparent specific storage of the embedding aquifer, $S_{\rm s_m}$, using Eqs. (3) and (7), after having previously derived the apparent transmissivity of the embedding aquifer, 0.5 ($T_{\rm mA} + T_{\rm mB}$) from the interpretation of a_{r2} using Eq. (2).

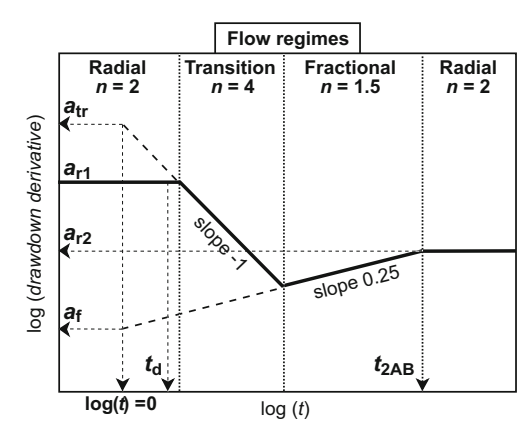


Fig. 10 Schematic illustration of the successive flow regimes predicted in the faulted leaky model, and their associated graphical features (see Table 1 for equations)

Discussion

Summary of the conceptual models

The flow dimension sequences obtained are summarized in Fig. 11. The (2-2) sequence with non-equal plateau elevations can be interpreted as the presence of two contiguous hydraulic domains with non-equal properties. The positive or negative vertical offset between both plateau elevations indicates whether or not the juxtaposed non-pumped domain is more transmissive than the pumped one. The apparent transmissivity as derived from the late plateau's elevation (Eq. 2) is the arithmetic mean of both aquifers. This result corroborates Barker and Herbert (1982) for "patchy" aquifers, Butler and Liu (1991) for the strip aguifer, and Guo et al. (2012) for linear aguifers. The n = 1.5 segment between the two plateaus indicates that the interface between aquifers is a conductive fault. A graph of various segments' intercepts and intersection times leads to the estimation of the hydraulic properties of the fault and aquifers, using equations displayed in Table 1.

The results interestingly imply that when the non-pumped domain is more transmissive than the pumped domain by one or more orders of magnitude, the large-time response at the pumping well is independent of the pumped domain's hydraulic properties. This also aligns with the conclusions of Barker and Herbert (1982) regarding radial "patchy" aquifers. It is a common belief in applied hydrogeology that "bulk" aquifer properties are obtained by analysing the late rather than early time straight line on drawdown semi-log plots when several straight segments are present with non-equal slopes. Although in a first approach, such bulk properties appear to be representative of reality because they are averaged over an extended volume of depressurized aguifer, in fact, these results show that the bulk properties may actually not describe the targeted aguifer but rather may correspond to a blind, more transmissive hydraulic region which is not intercepted by the borehole. The obtained apparent transmissivity is in actual fact half the real transmissivity of this region.

The contour maps displayed in Fig. 12 make it possible to represent the transient diffusion of the front pulse during the early and mid-time of a pumping test, before and during the non-pumped domain and when the fault begins to exert a significant influence on the general hydrodynamics of the aquifer. For the leaky models (Fig. 12a,b), the non-pumped aquifer predominantly supplying groundwater to the well is visible as the front pulse becomes larger than that of the pumped aquifer, because it diffuses faster. Predictably, in non-leaky models, the non-pumped domain is practically non-depressurized. In both hydraulic configurations, the presence of a conductive fault at the interface leads to a longitudinal drastic extension of the area of influence of the pumping, in such a manner that regions far afield are likely depressurized. If a more greatly transmissive remote area is



888 Hydrogeol J (2017) 25:877–894

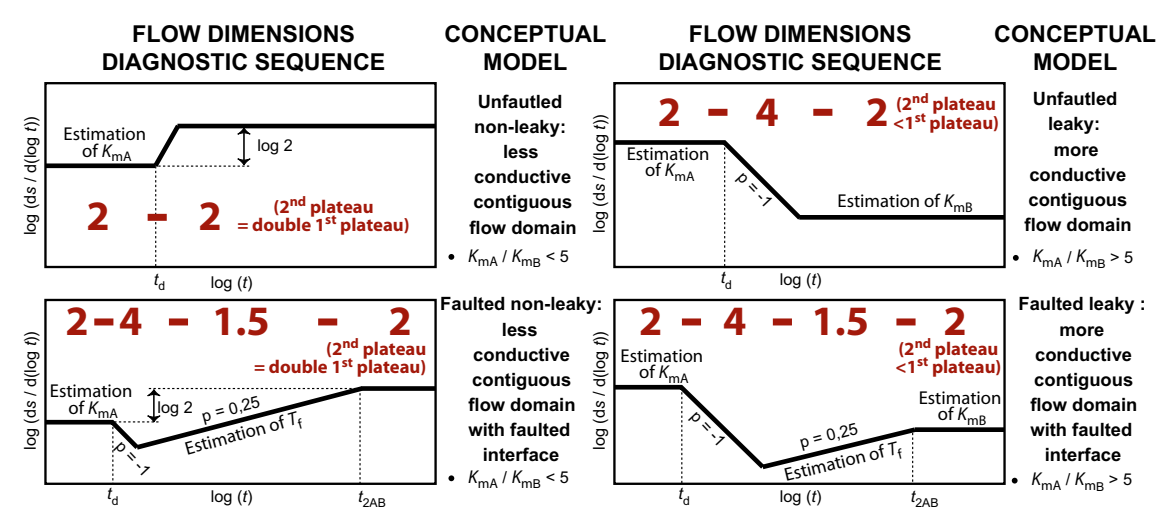
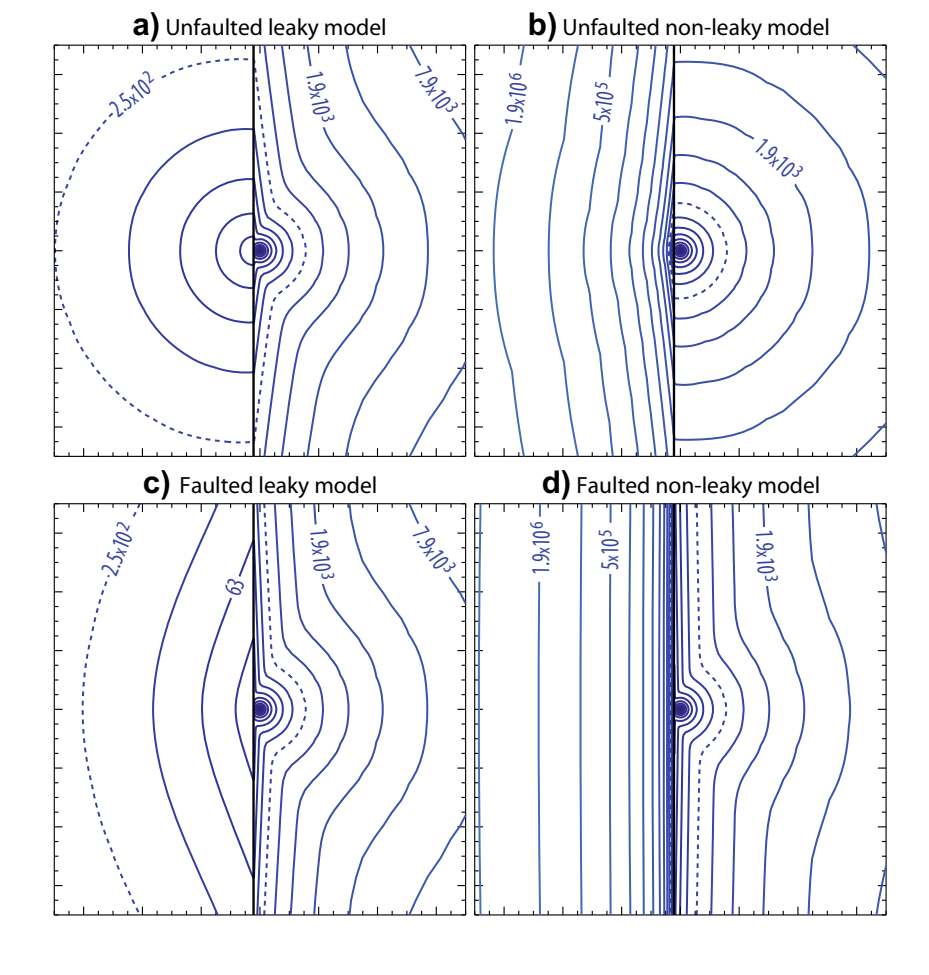


Fig. 11 Summary of the diagnostic flow dimension sequences analyzed in this study (the successive values of flow dimension are indicated in *large bold numbers*) and the associated conceptual models achieved by numerical investigations. Time, t_d , corresponds to the time needed to reach the lateral aquifer

reached by such means, into which the front pulse expands rapidly and becomes dominant, it is likely that the pumping well response will reflect the hydraulic properties of this distant region.

As a general statement, the results indicate that the aquifer response is governed by the region with the highest transmissivity rather than the lowest, contrary to what may be apprehended intuitively. The reason is that the response at the pumping well reflects the expansion of the front pulse. The apparent transmissivity obtained at a given pumping time reflects the region into which the front pulse is currently and predominantly expanding, i.e., the most transmissive region,

Fig. 12 Front pulse propagation contour maps obtained from simulations. Labels are elapsed pumping time in seconds. The represented area is zoomed in (lateral length is 140 m) on the center of the larger simulated domain; hydraulic boundaries effects are invisible here. The dotted contour corresponds to the same time in the four images $(2.51 \times 10^2 \text{ s})$. Simulations input values are: $d = 2 \text{ m}, K_{\text{mA}} = 10^{-}$ m s⁻¹; $S_{\text{mA}} = S_{\text{mB}} = 10^{-5} \text{ m}^{-1}$; $S_{\rm f} = 3.16 \times 10^{-5} \,\mathrm{m}^{-1}$; **a** and **c** $K_{\rm mB} = 10^{-5} \text{ m s}^{-1}$; **b** and **d** $K_{\rm mB} = 10^{-9} \text{ m s}^{-1}$; **c** and **d** $K_{\rm f} = 3.16 \times 10^{-3} \text{ m s}^{-1}$; $b_{\rm f} = 0.34 \, {\rm m}$





even if that region is not connected to the pumping well, rather than to regions that were previously spanned by the front pulse.

Practical use of the models

Duration and visibility of the segments

The duration of simulations was intentionally set to be extremely long and the distance between the pumping well and the interface very short, for experimental and illustration purposes. A large number of numerical simulations were performed in order to constrain the models that are presented in Figs. 3 and 10 and in Table 1; the curves displayed in Figs. 2 and 9 are only illustrative examples. Since the influence of each input parameter on the general response has been strictly deciphered, it is very easy to understand the manner with which the resulting theoretical responses are not restricted to the singular combinations of hydraulic parameters of the presented simulation cases. For instance, changing d to 20 m and $K_{\rm mA}$ to 10^{-4} m s⁻¹ would produce a strictly identical result to that presented in Fig. 2, for equal $K_{\rm mA}/K_{\rm mB}$ ratios (except, of course, that the early radial plateau would be two log-cycles lower). Similarly, a decrease of T_f by a half order of magnitude causes the late radial plateau to begin one log-cycle earlier, according to the definition of t_{2AB} (see Eq. 7 in Table 1).

The critical duration of one log-cycle has been recommended by Beauheim et al. (2004) for a proper identification of a derivative straight segment prior to the estimation of the associated flow dimension. Using this criterion, it can be seen in Fig. 2 that, for a 3-day-long pumping test, the complete (2-4-2) sequence is visible for any $K_{\rm mA}/K_{\rm mB}$ ratio greater than 10^{-2} . For a 2-week-long test, this critical ratio is practically 10^{-3} . For shorter tests, or lower $K_{\rm mA}/K_{\rm mB}$ ratios, the late radial stage will not have time to settle before the end of pumping. Similarly, Fig. 9 shows that a two-week long pumping test is necessary to allow for the entire combination of sequences (2-4-1.5-2) to be observed in optimal conditions. This is for the specific combinations of hydraulic parameters shown Figs. 2 and 9; a generalization is provided into the next sections.

The early radial stage will be lacking in cases where a fast diffusion into the pumped aquifer – high $\eta_{\rm mA}$ – is conjugated with a short distance d between the interface and the pumping well: $d^2/\eta_{\rm mA}$ is the controlling factor, according to the definition of t_d (see Eq. 5 in Table 1). In real-world conditions where a buffer period of 10^2 s might be considered reasonable to cover pumping rate stabilization and wellbore storage effects, i.e., before the drawdown response actually reflects real aquifer conditions, the settlement of the early radial stage during one log-cycle requires that $t_d = 10^3$ s. Referring to $t_d = (d^2/\eta_{\rm mA})/2.25$, in order for the early radial stage to be visible, the criterion is $d^2/\eta_{\rm mA} \ge 2,250$ s. If the pumped aquifer has conductivity $K_{\rm mA}$ as low as 10^{-8} m s⁻¹, and assuming $S_{\rm s_mA} = 10^{-6}$ (two realistic lower limiting values for confined

hard-rock aquifers, e.g., Batu 1998), this brings the minimum distance d_{\min} to 4.7 m, while to the contrary, the upper limiting values $K_{\text{mA}} = 10^{-3} \text{ m s}^{-1}$ and $S_{\text{s_mA}} = 10^{-5} \text{ m}^{-1}$ give $d_{\min} = 474 \text{ m}$. These constitute realistic distance ranges for real-world settings.

For the unfaulted leaky model, the minimum $K_{\rm mA}/K_{\rm mB}$ ratio for late radial stage to settle one log-cycle during a given pumping test duration, t_{pump} , can be estimated by posing t- $_2* \le t_{\text{pump}}/10$, where t_2* is the approximated beginning of this radial stage. Following the equation of t_2 * (see Eq. 6 in Table 1), this gives 0.21 $(d^2/\eta_{mA}) (K_{mB}/K_{mA}) \le t_{pump}/10$. By considering $d^2/\eta_{\rm mA} = 2{,}250$ s, it can hence be determined that the full (2-4-2) sequence will be visible for 3-day, 2-week and 3-month-long pumping tests, for any $K_{\rm mA}/K_{\rm mB}$ ratio higher than, respectively, $10^{-1.74}$, $10^{-2.4}$ and $10^{-3.22}$. For non-optimal values of $d^2/\eta_{\rm mA}$, these limiting ratios will increase by a factor equal to $d^2/(2,250 \eta_{\rm mA})$. To conclude, the full exhibition of the (2-4-2) sequence is a realistic forecast in hard-rock aguifer contexts where the conductivity contrast does not exceed two to three orders of magnitude depending of the pump test duration (3 days to 3 months), for optimal values of $d^2/\eta_{\rm mA}$. However, the latter ratio may constitute a more restrictive control on the full observation of the sequence. A valuable insight is that, for tests that last 3 days or less, the response (2-4) is predicted where $K_{\rm mA}$ is low and d is high, for almost all conductivity log-ratios greater than 1.5. These results cause one to question the universal interpretation of the (2-4) sequence as a recharge boundary in short- and medium-term pump tests.

For the faulted leaky model, the experiment revealed that the starting time, t_{2AB} , of the late radial stage evolves with the ratio $T_{\rm f}^2/(K_{\rm mA}+K_{\rm mB})^3$, as depicted in Eq. (7) (Table 1). A consequence is that a very high conductivity of the fault or a low conductivity of embedding aguifers will tend to delay the settlement of this radial stage. It will be exhibited over one log-cycle at the end of a pumping test of duration t_{pump} if $t_{2AB} < t_{pump}/10$, hence $T_f^2/K_m^3 \le 5.6 \times 10^{-2} t_{pump}/S_s$ m, according to Eq. (7). For the sake of simplicity, the terms $K_{\rm m}$ and $S_{\rm s\ m}$ are used, which are the properties of the most conductive embedding aquifers (an acceptable first-order approximation thus is $K_{\rm m} = 2 \times K_{\rm app}$). Assuming $S_{\rm s~m} = 10^{-5}~{\rm m}^{-1}$ and t $p_{\text{ump}} = 1.2 \times 10^{61} \text{s}$ (2 weeks), this leads to T_{f}^2 $K_{\rm m}^{-3} \le 6.7 \times 10^9$. In other words, the late radial stage will be visible within 2 weeks in real-world cases where the contrast between the fault transmissivity and the conductivity of the most conductive embedding aquifer is not drastic, namely if $\log~(T_{\rm f}/K_{\rm m}^{-1.5})\!\leq\!2.4+0.5~\log~(S_{\rm s~m}).$ Moreover, according to previous results (Rafini 2008; Rafini and Larocque 2009), the occurrence of n = 1.5 fractional flow is directly governed by the diffusivity ratios η_f/η_m : it is forecast for any value of this ratio greater than 1 and a first-order approximation of its logduration is given by the square of this ratio. Furthermore, these authors achieved Eq. (8) (Table 1) for the beginning time, t_1 ,



representing the diffusion slow-down into the fault, a necessary condition for the n = 1.5 flow regime to occur. Hence, this regime will exhibit over one log-cycle if the two following conditions are met: (1) the regime begins before $t_{\text{pump}}/10^2$; i.e., $t_1 \le t_{\text{pump}}/10^2$ which gives $11 S_f^2/(K_m S_{\text{s m}}) \le t_{\text{pump}}$, and hence $K_{\rm m} \ge (11/t_{\rm pump}) (S_{\rm f}^2/S_{\rm s~m})$; and (2) the regime lasts at least one log-cycle, i.e., $\eta_f/\eta_m \ge 10^{0.5}$, hence $T_f/K_m \ge 10^{0.5} S_f/S_{s}$ m. To set ideas, assuming $S_{s,m} = 10^{-5} \text{ m}^{-1}$, $S_f = 5 \times 10^{-5}$ (as fault-rock typically is slightly more compressible than sound rock) and $t_{\text{pump}} = 1.2 \times 10^6 \text{ s}$ (2 weeks), the n = 1.5 stage will be visible if $K_{\rm m} \ge 2.3 \times 10^{-9} \text{ m s}^{-1}$ and $T_{\rm f}/K_{\rm m} \ge 15.8$, both of which are highly plausible conditions. Going further, combining these criterions with that depicted above for the occurrence of the late radial stage leads to the following conditions of exhibition for the (1.5 – 2) sequence: $K_{\rm m} \ge 2.3 \times 10^{-10} \text{ m s}^{-1}$, $T_{\rm f}/K_{\rm m} \ge 15.8$ and $T_{\rm f}^2/K_{\rm m}^3 \le 6.8 \times 10^9$. These constitute nonrestrictive conditions towards the model's validity in the real world. Ultimately, for the complete (2-4-1.5-2) sequence, all these criterions must be verified, along with some temporal constraints on the distribution and visibility of the four successive segments into realistic pump test timelines. Taking the minimum, $t_d = 1,000$ s, for the early radial stage to settle (see the preceding), plus one log-cycle for each segment, gives 10' s (3.7 months). Adding the transition time-periods leads to unrealistically long times. A consequence is that this sequence will likely occur in real-world conditions in a truncated form: the early and/or the late radial stage will be partially visible or even lacking. Also, the n = 4 or n = 1.5 segments will atrophy under some combinations of hydraulic parameters for instance, it is shown here that the log-duration of the n = 4segment is a condition of the ratio $K_{\rm mB}^{-0.2}/K_{\rm mA}^{-0.6}$, as well as the product $(K_{\rm mB} T_{\rm f})^{0.2}$. In contrast, the n=1.5 segment's logduration is a function of $(\eta_f/\eta_m)^2$, as obtained by posing t_{2AB} / t_1 , where the subscript m refers to the most conductive aquifer (which must be $K_{\rm mB}$ concerning the 4 – 1.5 sequence). The n = 1.5 segment's duration is thus independent of the ratios between aquifers properties, and rapidly decreases with $K_{\rm mB}$, in contrast with the n = 4 segment. Hence, the respective durations of the mid-time segments n = 4 and n = 1.5 both increase with $T_{\rm f}$ but exhibit opposite relationships on $K_{\rm mB}$.

To conclude, these considerations demonstrate that the submitted models are plausible and suitable to the timelines of real-world pumping tests under wide and realistic ranges of hydraulic properties, except the full four-segment sequence that rather likely occurs in truncated form as explained. However, where only partial sequences are obtained that are (2-4-1.5), (1.5-2), (4-1.5-2), (2-4), (4-2), or eventually (4-1.5), incomplete, yet highly valuable, interpretations may still be conducted. The (1.5-2) sequence by itself makes it possible to interpret a conductive fault embedded into an aquifer, and the calculation of the hydraulic properties of both the aquifer and the fault. The (4-1.5) sequence alone makes it possible to qualitatively identify that such a

conductive fault is not directly connected to the wellbore, yet $T_{\rm mB}$ and $T_{\rm f}$ can be quantified only if the late radial plateau is visible, leading to the sequence (4-1.5-2). The sequence (4-2) is sufficient to interpret the presence of a non-pumped, blind and highly transmissive flow domain, and $T_{\rm mB}$ can be quantified. The (2-4) sequence points to the presence of a more transmissive, non-pumped aquifer, unless a recharge boundary is observed in the environment.

Impact of the geometrical assumptions

Where the model's basic postulates are verified in nature, pumping tests will render the predicted responses, under the conditions depicted in the previous section; however, the model is geometrically idealized. This section deciphers the impact of the two main geometrical assumptions of the model: (1) the interface's verticality, and (2) the equality of lower boundaries for the fault and surrounding aquifers. Before everything else, it should be noted that these are classical assumptions of fault-aquifer flow models (Gringarten et al. 1974; Cinco-Ley and Samaniego 1981; Abbaszadeh and Cinco-Ley 1995; Rafini and Larocque 2009). Both a slight inclination of the interface, either faulted or not, and a fault whose bottom is significantly deeper than embedding aquifers, would be reflected by an additional time-period during which the diffusion into the fault and/or aquifer B is not strictly horizontal, that is, before the front pulse diffusion reaches the top and bottom boundaries and practically reverts to the horizontal. For a faulted interface, Rafini and Larocque (2012) demonstrated that the drawdown response associated with such a flow regime is a fault-related radial stage prior to settlement of the n = 1.5 flow regime. For the non-faulted leaky model, a spherical regime prior to the late radial stage is expected. In both cases, this would tend to delay the beginning of the subsequent flow regimes. However, this delay is only significant if: (1) the interface's inclination is low (which is outside the scope of this study); (2) the root of the fault is greatly deeper than the substratum of surrounding aquifers; or (3) the diffusivity of the fault or of aquifer B is very low, leading to the late radial stage being controlled by aquifer A properties only, since the interface acts as a no-flow boundary. To conclude, the submitted models remain valid when the assumption of the interface's verticality is only partially verified or when the fault's thickness is moderately greater than the thickness of the aguifer. The models are not intended to be applied to configurations with highly inclined interfaces or high contrasts between fault and aquifer thickness. Such cases generate 3D flow with flow regimes that are not accounted for in this study, namely fault-related radial flow and spherical flow. Finally, cases where the transmissivity change between both flow domains is gradual have been assessed by Levitan and Crawford (1995) for radially symmetric systems. This



essentially results in a more progressive and prolonged transitional stage between both plateaux.

Data quality

It is a common statement that the quality and objectivity of derivative analysis are highly dependent on data quality. In the real world, the derivative diagnostic sequence may be only partly visible or too noisy, making it difficult to properly interpret the conceptual model. Noise may be due either to a significant diffuse random heterogeneity field, or to human errors such as pumping rate instabilities or imprecise measurement. Gaussian noise may be substantially reduced by using specifically designed differentiation algorithms (e.g., Bourdet et al. 1989; Spane and Wurstner 1993). Conversely, sudden changes in pumping rate will be increased by differentiation process since it will be felt over the entire smoothing interval. producing a signal distortion. To conclude, it is recommended that the time-segmentation into successive flow regimes should be performed manually, by simultaneously fitting semi-log drawdown plots, derivative bilog plots and differentiated derivative bilog plots. This makes it possible to properly discriminate between the signal and various forms of noise, and to distinguish between transitional stages and settled flow regimes—a particularly sensitive task. In a second methodological step, the estimation of the flow dimension (or slope) in each segment can be optimized using automated linear regression functions. The use of any polynomial regression function, by its very nature, is not suitable to the approach promoted by this study.

Uniqueness of interpretations

It is well recognized that derivative data are much more sensitive to hydraulic conditions than drawdown only (e.g., Issaka and Ambastha 1999; Samani et al. 2006), allowing for finer and more objective aquifer interpretations. Still, in some cases, the differences between theoretical responses may be very subtle and hardly visible from real data, in such manner that several conceptual models may be attributed to a single dataset. This long-debated issue of non-uniqueness remains the largest difficulty in interpreting pumping tests. It may be overcome by providing subsidiary, often geological, inputs on hydraulic conditions. A great advantage of hydrogeological analysis over petroleum research still lies in the common use of observation-well responses. The numerical experiment reported here demonstrates that multi-well analysis provides spatial insights that may be highly valuable in adequately identifying the proposed conceptual model. Two plots proved useful in doing so: derivative responses of observation wells versus time, eventually using a standard Cooper-Jacob time-normalization by r^2 , and distance-drawdown plots where the interpretation of two distinct straight segments is indicative of two successive radial flow regimes.

Derivative data displaying two successive radial plateaux have been predicted by other conceptual models: dual porosity (Warren and Root 1963; Boulton and Streltsova 1977; Moench 1984), unconfined aguifer (Moench 1997), and "T" shape aguifers (Dewandel et al. 2014). It is worth noting that the differences between these theoretical responses lie in the shape of the transitional stage between the plateaux. The dual porosity derivative response forms a characteristic "V" depression between both plateaux, which is deeper in models with a pseudopermanent rather than transient transfer function between matrix and fractured continua (e.g., Bourdet et al. 1989). Such a feature is totally absent from predicted responses produced by juxtaposed flow domains, providing a means of discrimination between these conceptual models. The "T" shape aquifer described by Dewandel et al. (2014) addresses cases where two symmetrical lateral domains are less conductive and shallower than a central and deep pumped domain, representing a vertical, deep-rooted, fault-unit crosscutting a more surficial hardrock aquifer. Such a configuration exhibits a close analogy to the non-leaky case analysed in the present study. The present study's results corroborate the Dewandel et al. model, in that two successive radial plateaux are obtained, the late being systematically higher than the early plateau, their respective elevations being governed by the transmissivities of flow domains, and the storativity ratio exerting a more limited influence and essentially impacting the transitional stage. However, one submits that, since the late-time apparent transmissivity is an average of the transmissivities of both domains, transmissivity ratios of ten or greater produce drawdown regimes at the pumping well that are practically not impacted by the lower transmissivity value, whether this value originates from the pumped or the non-pumped domain (Figs. 2, 3 and 4). It is therefore observed that (1) when the non-pumped aguifer is less transmissive by a factor of 10 or more than the pumped one, it has an influence on the pumping well response similar to that of an impermeable barrier (i.e., doubling the drawdown rate); and (2) the impermeable barrier constitutes a limiting case and thus the elevation of the second plateau must theoretically not exceed double that of the first plateau, under any conditions. Finally, the "T" shape model postulates that the faults generate a radial stabilization rather than an n = 1.5-fractional-flow regime. From a conceptual standpoint, this may relate to the wide transversal extent of the fault, and to the highly contrasted depth ratio between the pumped domain (in this case, the fault) and non-pumped domains—a statement whose validation would require 3D simulation. These two criteria could hence be adjustment variables between the two conceptual models of faulted aquifers.

Finally, the conclusions corroborate those of Butler and Liu (1991) in that a segmented response is predicted with the early radial flow regime relating to the flow domain which is directly connected to the pumping well, while later regimes, radial



892 Hydrogeol J (2017) 25:877–894

and non-radial, mark the predominant influence of successive juxtaposed flow domains on the aquifer's response, as the front pulse propagates. Similar to the numerical results with faulted aguifers found for this study, the semi-analytical approach of Butler and Liu predicts a fractional n = 1.5 stage when the strip is drastically more transmissive than surrounding domains. The strip indeed begins behaving like a fault when the pressure diffusion inside it is linear and exerts a dominant control over the geometry of the depressurization front into the adjacent matrix domain (see Rafini and Larocque 2009). In other words, the strip must be depressurized over its entire transversal extent, which implies an additional transitional time-period that delays the settlement of the fractional regime. Such a strip must therefore have a very short transversal extent and be extremely diffusive for the fractional stage to occur, unless it is situated very close to a pumping well.

Conclusions

This technical note numerically investigates the transient hydraulic behavior of the archetype aquifer model composed of two laterally juxtaposed flow domains with non-equal properties, with or without a conductive fault at the interface. The study focussed specifically on the flow-dimensional sequence occurring during constant-rate pumping tests. An interpretative framework is developed that provides valuable insights into the identification of such heterogeneous flow conditions. A critical emphasis was placed on the real-world conditions of application of the model, and on its unicity. It is also explained how multi-well datasets may be used to interpret the proposed model with greater confidence.

Key results are:

- 1. Two radial flow stages are predicted that correspond to the periods before and after the moment when the non-pumped aquifer is reached; with an optional transitional stage marked by a flow dimension equal to 4 (negative unit slope of the derivative signal).
- 2. The apparent transmissivity calculated from the second radial plateau is equal to the arithmetic mean of the transmissivity of both aquifers. Hence, for transmissivity ratios practically greater than ten, the least transmissive aquifer does not exert a significant influence on the drawdown response at the pumping well, however the apparent transmissivity is half the higher one.
- 3. When the non-pumped aquifer is less transmissive than the pumped aquifer, its influence tends to be similar to that of an impermeable barrier (the drawdown rate is doubled), a limiting behavior that occurs beyond transmissivity ratios as small as ten.

- 4. In contrast, when the non-pumped domain is more transmissive than the pumped domain (practically, more than ten times), the aquifer's general late-time response is exclusively controlled by the depressurization of the non-pumped domain.
- 5. This implies a counterintuitive observation to the effect that when two straight segments are visible on timedrawdown semi-log plots, the apparent transmissivity given by the late segment does not correspond to a bulk transmissivity of the region that is physically investigated but rather to that of a distant, blind, non-pumped region.
- 6. In such a case, the depressurization of the non-pumped aquifer induces a sudden decrease of the drawdown rate at the pumping well that may be misinterpreted as a recharge frontier when using an inappropriate interpretative methodology.
- 7. A valuable input for confidently interpreting the promoted conceptual model lies in multi-well distance-draw-down plots that characteristically exhibit two straight lines with either an abrupt or a gradual transition, depending on the orientation of the observation well in relation to the interface.
- 8. Going further, transmissivity values measured from late-time stabilizations of the drawdown log-derivative at observation wells (OW) likely corresponds to that of the most transmissive region of the aquifer, whether or not it encompasses the OW; this invalidates the common postulate that OW strictly investigates the hydraulic properties of the area between the OW and the pumping well.
- 9. The existence of a conductive fault at the interface between both flow domains produces a characteristic intermediate segment with flow dimension equal to 1.5, whose duration is proportional to the square diffusivity ratio between the fault and the most transmissive embedding aquifer.
- 10. Because a conductive fault induces fast and expanded pressure diffusion along its longitudinal axis, it is capable of provoking the depressurization of remote transmissive regions in such manner that the aquifer which predominantly supplies groundwater to the pumping well—and which governs the late radial flow regime—is distant from the targeted site of investigation.
- 11. It is shown that the obtained responses are predicted for a wide range of realistic combinations of hydraulic parameters; however, where the flow dimension sequence is longer than the pump test, even a partial exhibition that leads to an incomplete analysis may yet be valuable. In particular, a partial exhibition is forecast in the case of a transmissive non-pumped aquifer, where the contrast in transmissivity exceeds three orders of magnitude due to an extended-duration transition segment n = 4, and where the interface is a conductive fault, as the predicted full sequence is very long (2 4 1.5 2).



From a practical standpoint, this study proposes several recommendations for the interpretation of pumping tests where drawdown responses display several straight segments on semi-log plots. This work provides a general methodological framework to understand such responses, by deciphering the relationships between the apparent hydraulic properties calculated from respective segments, and the real properties of distinct hydraulic regions of the heterogeneous aquifer. In addition, the method proposed in this study makes it possible to identify the existence of a conductive fault at the interface between two regions with non-equal transmissivities, based on the analysis of the drawdown response at the pumping well and, optionally, at observation wells.

When appropriately applied, the methodology described in this technical note can be used to better interpret aquifer responses to pumping. It is hoped that this method be considered when testing heterogeneous aquifers that exhibit various and unfamiliar hydraulic behaviors, which will avoid errors caused by the use of conventional methods, provide a better diagnostic of the pumping test and improve heterogeneous aquifer assessments.

Acknowledgements The authors would like to thank the National Sciences and Engineering Research Council of Canada (NSERC - individual discovery grants program) and the Fonds de recherche du Québec - Nature et technologies (FRQNT- new university researchers start-up program) grant programs held by Prof. Romain Chesnaux for their financial contribution in supporting this study. The manuscript benefited from fruitful review by R. Beauheim and an anonymous associate editor. The manuscript was kindly checked by Josée Kaufmann.

References

- Abbaszadeh M, Cinco-Ley H (1995) Pressure-transient behavior in a reservoir with a finite-conductivity fault. SPE Form Eval 10:26– 32. doi:10.2118/24704-PA
- Avci CB, Şahin AU, Çiftçi E (2013) A new method for aquifer system identification and parameter estimation. Hydrol Process 27:2485– 2497. doi:10.1002/hyp.9352
- Ambastha AK (1989) Pressure transient analysis for composite systems. DOE/BC/14126-11, SUPRI TR 68, US Department of Energy, Washington, DC, 178 pp
- Ambastha AK, McLeroy PG, Sageev A (1989) Effects of a partially communicating fault in a composite reservoir on transient pressure testing. SPE Form Eval 4(2):210–218
- Batu V (1998) Aquifer hydraulics: a comprehensive guide to hydrogeologic data analysis. Wiley, New York, 727 pp
- Banton O, Bangoy L (1999) Hydrogeologie: multiscience environnementale des eaux souterraines [Hydrogeology: environmental multidisciplinary study of groundwater]. Presse de l'Université du Québec, AUPELF-UREF, Sainte-Foy, QB
- Barker J (1988) A generalized radial flow model for hydraulic tests in fractured rock. Water Resour Res 24:1796–1804. doi:10.1029/WR024i010p01796
- Barker JA, Herbert R (1982) Pumping tests in patchy aquifers. Groundwater 12(2):150–155

- Beauheim RL, Roberts RM, Avis JD (2004) Well testing in fractured media: flow dimensions and diagnostic plots. J Hydraul Res 42: 69–76. doi:10.1080/00221680409500049
- Boulton NS, Streltsova TD (1977) Unsteady flow to a pumped well in a two-layered water-bearing formation. J Hydrol 35(3–4):245–256
- Bourdet D (2002) Well test analysis: the use of advanced interpretation models, In: Handbook of petroleum exploration and production, Elsevier, Amsterdam, 439 pp
- Bourdet D, Ayoub JA, Pirard YM (1989) Use of pressure derivative in well test interpretation. SPE Form Eval 4:293–302. doi:10.2118/12777-PA
- Bourdet D, Whittle T, Douglas A, Picard Y (1983) A new set of types curves simplifies well test analysis. World Oil 196:95–106
- Brunner P, Simmons CT (2012) HydroGeoSphere: a fully integrated, physically based hydrological model. Groundwater 50(2):170–176
- Butler JJ Jr (1988) Pumping tests in nonuniform aquifers: the radially symmetric case. J Hydrol 101:15–30
- Butler JJ, Liu WZ (1991) Pumping tests in non-uniform aquifers: the linear strip case. J Hydrol 128:69–99
- Cello PA, Walker DD, Valocchi AJ, Loftis B (2009) Flow dimension and anomalous diffusion of aquifer tests in fracture Networks. Vadose Zone J 8(1):258–268. doi:10.2136/vzj2008.0040
- Chesnaux R, Rafini S, Elliott AP (2012) A numerical investigation to illustrate the consequences of hydraulic connections between granular and fractured-rock aquifers. Hydrogeol J 20:1669–1680. doi: 10.1007/s10040-012-0912-9
- Cooper HH Jr, Jacob CE (1946) A generalized graphical method for evaluating formation constants and summarizing well-field history. Trans Am Geophys Union 27:526–534. doi:10.1029/TR027i004p00526
- Cinco-Ley H, Samaniego F (1981) Transient pressure analysis for fractured wells. J Petrol Techn 33:1749–1766
- Dewandel B, Lachassagne P, Zaidi FK, Chandra S (2011) A conceptual hydrodynamic model of a geological discontinuity in hard rock aquifers: example of a quartz reef in granitic terrain in South India. J Hydrol 405:474–487. doi:10.1016/j.jhydrol.2011.05.050
- Dewandel B, Aunay B, Maréchal JC, Roques C, Bour O, Mougin B (2014) Aquilina C (2014) Analytical solutions for analysing pumping tests in a sub-vertical and anisotropic fault zone draining shallow aquifers. J Hydrol 509:115–131
- Fenske PR (1984) Unsteady drawdown in the presence of a linear discontinuity. In: Rosenshein JS, Bennett GD (eds) Water Resources Monograph. American Geophysical Union, Washington, DC, pp 125–145
- Ferris J (1949) Ground water. In: Hydrology. Wiley, New York, pp 198–272 Gringarten AC, Henry J, Ramey HJ, Raghavan R (1974) Unsteady state pressure distributions created by a well in a well with single infinite conductivity vertical fracture. SPE J 14:347–360
- Guo JJ, Zhang LH, Wang HT, Qi-Guo L (2012) Well responses in threezone linear composite dual-porosity reservoirs, In: Zheng J-H (ed) Hydrodynamics: theory and model. InTech, Rijeka, Croatia
- Hammond PA, Field MS (2014) A reinterpretation of historic aquifer tests of two hydraulically fractured wells by application of inverse analysis, derivative analysis, and diagnostic plots. J Water Resour Prot 06:481–506. doi:10.4236/jwarp.2014.65048
- Hantush MS (1960) Modification of the theory of leaky aquifers. J Geophys Res 65:3713–3725. doi:10.1029/JZ065i011p03713
- Issaka MB, Ambastha AK (1999) A generalized pressure derivative analysis for composite reservoirs. J Can Pet Technol 38(16):96–115
- Jordan CL, Mattar L (2000) Comparison of pressure transient behaviour of composite and multi-layer reservoirs. Paper 2000-45, Canadian International Petroleum Conference, Calgary, AB, 4–8 June 2000
- Levitan MM, Crawford GF (1995) General heterogeneous radial and linear models for well test analysis. SPE paper 30554, 70th Annual Fall Meeting, Dallas, TX, Oct 1995



894 Hydrogeol J (2017) 25:877–894

Meier PM, Carrera J, Sanchez-Vila X (1998) An evaluation of Jacob's method for the interpretation of pumping tests in heterogeneous formations. Water Resour Res 34(5):1011–1025

- Moench AF (1997) Flow to a well of finite diameter in a homogeneous, anisotropic water table aquifer. Water Resour Res 33:1397–1407. doi:10.1029/97WR00651
- Moench AF (1984) Double-porosity models for a fissured ground-water reservoir with fracture skin. Water Resour Res 20:831–846. doi:10.1029/WR020i007p00831
- Oliver DS (1990) The averaging process in permeability estimation from well-test data. SPE paper 19845. SPE Form Eval 5(3):319–324
- Oliver DS (1993) The influence of nonuniform transmissivity and storativity on drawdown. Water Resour Res 29(1):169–178
- Pechstein A, Attinger S, Krieg R, Copty NK (2016) Estimating transmissivity from single-well pumping tests in heterogeneous aquifers. Water Resour Res 52:495–510. doi:10.1002/2015WR017845
- Rafini S (2008) Comportement hydraulique des milieux faillés [The hydraulic behaviour of faulted media]. PhD Thesis, Université du Québec à Montréal, Canada
- Rafini S, Larocque M (2009) Insights from numerical modeling on the hydrodynamics of non-radial flow in faulted media. Adv Water Resour 32:1170–1179. doi:10.1016/j.advwatres.2009.03.009
- Rafini S, Larocque M (2012) Numerical modeling of the hydraulic signatures of horizontal and inclined faults. Hydrogeol J 20:337–350. doi:10.1007/s10040-011-0812-4
- Renard P (2005) The future of hydraulic tests. Hydrogeol J 13:259–262. doi:10.1007/s10040-004-0406-5
- Renard P, Glenz D, Mejias M (2008) Understanding diagnostic plots for well-test interpretation. Hydrogeol J 17:589–600. doi:10.1007/s10040-008-0392-0

- Roberts RM, Ruskauff GJ, Avis JD (1996) A generalized method for analyzing well tests in complex flow systems. SPE-36023, Petroleum Computer Conference, Dallas, TX, 2–5 June 1996
- Rushton KR (2003) Groundwater hydrology: conceptual and computational models. Wiley, Chichester, UK, 433 pp
- Samani N, Pasandi M, Barry D (2006) Characterizing a heterogeneous aquifer by derivative analysis of pumping and recovery test data. J Geol Soc Iran 1:29–41
- Spane FA (1993) Selected hydraulic test analysis techniques for constantrate discharge tests. PNL-8539, Pacific Northwest Laboratory, Richland, WA
- Spane FA, Wurstner SK (1993) DERIV: a computer program for calculating pressure derivatives for use in hydraulic test analysis. Ground Water 31:814–822. doi:10.1111/j.1745-6584.1993.tb00855.x
- Sun X, Xu Y, Lin L (2015) The diagnostic plot analysis of artesian aquifers with case studies in Table Mountain Group of South Africa. Hydrogeol J 23:567–579. doi:10.1007/s10040-014-1203-4
- Theis CV (1935) The relation between the lowering of the piezometric surface and the rate and duration of discharge of a well using ground-water storage. Trans Am Geophys Union 16:519–524. doi: 10.1029/TR016i002p00519
- Tiab D, Kumar A (1980) Application of the p'D function to interference analysis. J Pet Technol 32:1465–1470. doi:10.2118/6053-PA
- Verweij JM (1995) Analysis of pumping test data from hard rock aquifers. Report GG R-95-39(A), TNO Institute of Applied Geoscience, Delft, The Netherlands, 62 pp
- Warren JE, Root PJ (1963) The behavior of naturally fractured reservoirs. Soc Pet Eng J 3:245–255. doi:10.2118/426-PA
- Xiao L, Xu Y (2014) Diagnostic analysis of pumping tests using derivative of dlgs/dlgt with case study. Groundwater. doi:10.1111/gwat.12175

